Simulation-Guided DNA Probe Design for Consistently Ultraspecific Hybridization Supporting Materials

J. Sherry Wang[1,2] and David Yu Zhang[1,2]

[1]*Systems, Synthetic, and Physical Biology, Rice University, Houston, TX*
[2]*Department of Bioengineering, Rice University, Houston, TX*

Extended Methods Description

Universal Region Sequence Design. The sequences of the universal regions of the X-Probe (dark blue), namely regions 1, 2, 6, 7, 10, 11, 12, and 13 (See Fig. S2-2), were rationally designed to minimize the likelihood that these universal regions will interact nonspecifically with coding DNA or transcript mRNA from any biological samples. Subsequently, these sequences were then subject to minor adjustment to reduce secondary structure of the F and Q strands, remove undesirable hybridization between regions 10 and 12 (or 11 and 13), and adjust the values of $\Delta G^\circ_{\text{10-11}}$ and $\Delta G^\circ_{\text{12-13}}$ to our desired values. For all 44 COSMIC mutations tested here, the universal regions did not appear to exhibit any undesirable interactions with the target sequences.

Target, P, and C Sequence Selection. The COSMIC database provided the sequence of the WT and SNV for the 44 mutations we performed experiments on. Modern synthesis of oligonucleotides is still limited in fidelity for longer oligonucleotides, so we decided to design all P and C strands to be less than 50 nt. This resulted in an upper bound of 27 nt on the target-specific region of the C strand. Given that, on average, a random 16 nt sequence will be observed exactly once in the human genome, and standard PCR primers range from 18 to 22 nt, we designed our X-probe target-specific regions to be between 22 and 25 nt.

Consequently, we needed to select target subsequences with length between 22 and 25 nt that contains the polymorphic nucleotide of interest. For a given length subsequence (e.g. 24 nt), there are as many choices for "frames" as the length (i.e. the polymorphic nucleotide could reside as any nucleotide in the length). We arbitrarily picked target subsequences with the polymorphic nucleotide at different positions, in order to show that the X-Probes are robust to the exact location of the rare allele.

Given the target subsequence and the universal region sequences, the C sequence is absolutely determined, and the P sequence has only one other design parameter left – the length of the toehold region 4. We selected the length of region 4 based on having $\Delta G^\circ_{\text{9-4}} \approx -9$ kcal/mol, in order to maximize kinetics [1].

In order to observe the effects of dangling overhang regions on the target, as would be the case in targeting a biologically derived RNA or a PCR-amplicon, our target sequences sometimes had a few $5'$ and/or $3'$ overhang bases. We did not observe any significant effect on β due to overhang bases, although we expect that for very long overhangs (e.g. mRNA) secondary structure may result in reduced kinetics.

Oligonucleotide Ordering and Storage. Oligonucleotides used for studies were ordered from Integrated DNA Technologies; their sequences are given in Section S12. Oligonucleotides were analytically checked by IDT for purity by capillary electrophoresis and for identity by electrospray ionization mass spectrometry. All functionalized strands (F and Q) were post-synthesis HPLC purified by IDT; all other strands (P, C, WT, SNV) were ordered with standard desalt and not purified. All oligonucleotides were ordered in "Lab-Ready" format if allowed, pre-suspended by Integrated DNA Techologies in Tris·EDTA buffer at roughly 100 μM concentration. Large scale fluorophore and quencher strands were ordered in dry format, and suspended by either JSW or DYZ in Tris·EDTA buffer. These stock oligonucleotides were stored at 4 °C. Serial dilutions were made based on this primary stock at 10-fold dilution each.

X-Probe Formulation and Preparation. To formulate the X-Probes, we mixed together the Q, P, C, and F strands in a 5:3:1.5:1 ratio, respectively, in a solution that was finally 1 μM in the limiting reagent (F) and 5x Phosphate Buffered Saline (5x PBS), diluted from 10x PBS purchased commercially from Sigma-Aldrich. The X-Probe mixtures were then thermally annealed using one of three Eppendorf MasterCycler Personal PCR machines, following a process of initial heating to 95 °C for 5 minutes, and subsequent uniform cooling to 20 °C over the course of 75 minutes. Formulated X-Probe solutions were then stored in 4 °C until use.

Sink Design and Formulation. The sequence design of our Sink complexes was based on achieving a $\Delta G^\circ_{\text{rxn2}}$ value that would yield good β based on the ordinary differential equation simulation presented in Section S6. Additionally, we considered heuristics described in ref. [2] to design nonhomologous regions (brown in Fig. 4d), and subsequently the P_S and C_S strands.

To formulate the Sinks for Competitive Composition at experiments 0.1%VAF, we mixed together the P_S and C_S strands in a 1.2:1 ratio, respectively, in a solution that was finally 25 μM in the limiting reagent (C_S) and 5x Phosphate Buffered Saline (5x PBS), diluted from 10x PBS purchased commercially from Sigma-Aldrich. Sink formations for other experiments are listed in Table 2. The Sink mixtures were then thermally annealed using one of three Eppendorf MasterCycler Personal PCR machines, following a process of initial heating to 95 °C for 5 minutes, and subsequent uniform cooling to 20 °C over the course of 15 minutes. Formulated Sink solutions were then stored in 4 °C until use.

Competitive Composition experiment	P_S to C_S ratio	Final stock concentration
VAF $\geq$ 0.033%	1.2:1	25 μM
VAF = 0.01%	1.2:1	40 μM
Various SNV concentration (0.1-300 nM)	1.2:1	15 μM
Labeled Sink	1.2:1	15 μM
Post PCR (SMAD7-C)	2:1	1 μM
Post PCR (SMAD7-T)	5:1	1 μM

TABLE 1: Sink mixtures for Competitive Composition experiments.

X-Probe Only Reaction Setup. To achieve final concentration of roughly 10 nM X-Probe, 12 μL of the 1 μM X-Probe solution is mixed with 1200 μL of the appropriate buffer (typically 5x PBS) in the cuvette. This buffer/X-Probe solution is incubated in the cuvette in the machine for 20 minutes to 1 hour to allow temperature equilibration before the start of data acquisition. The buffer and X-Probe are further incubated in the cuvette for an additional 5 to 20 minutes after fluorescence data acquisition begins in order to establish the f_B background fluorescence.

Subsequently, the cuvettes are removed from the machine; 24 μL of 1 μM WT or SNV solution, 60 μL of 10 μM WT solution, and optionally 6 μL of 1 μM SNV solution are added to four separate cuvettes. Each cuvette is then capped with a fitted Teflon stopper, and the solution is mixed by inverting the cuvette roughly 10 times. During this reagent addition and mixing process, the data acquisition continues, resulting in a low fluorescence level that is indicative of the cuvettes being removed from the machine. Upon completion of mixing, the cuvettes are replaced into the machine ($t = 0$). Note that the cuvettes tend to cool somewhat while out of the machine, so that initial fluorescence data after $t = 0$ may show inaccuracies due to temperature fluctuations.

Probe formulation and reaction setup were performed by either JSW or DYZ; our internal calibration experiments show no significant operator bias in experimental results. Note that true concentrations of species in reactions were slightly less than the nominal concentrations given, due to the slight dilution of the species caused by the added volume of WT or SNV solution.

Competitive Composition Reaction Setup. To achieve a desired final concentration, appropriate amount of X-Probe and Sink solution is mixed with appropriate amount of 5$\times$ PBS buffer in the cuvette. At the time of reagent addition, the appropriate volume of WT solution and SNV solution are added to the cuvette. The concentrations and amount of X-Probe, Sink, SNV, and WT solutions added for different Competitive Composition experiments are listed in Table 2.

Probe and Sink concentrations were chosen to be comparable and sightly in excess of that of SNV and WT, respectively. High Probe concentrations cause increased background fluorescence due to incomplete quenching, while low Probe concentrations slow down reaction kinetics. High Sink concentrations increase non-specific fluorescence loss (false-negatives) due to SNV bound to Sink, while low Sink concentration increases WT interference with the Probe (false-positives).

Upon the addition of WT or SNV target, Competitive Composition experiments generally tended to show higher initial fluorescence variability than X-Probe only experiments. We believe this is in large part due to the high stoichiometric ratios of WT added; immediately after pipetting in the target solution, there is a high local concentration of WT, which quickly reacts with Sink and X-Probe before the solution is mixed. WT targets that have reacted with the X-Probe must then slowly dissociate before the X-Probe can react with SNV that was not initially locally present. Because the spread of the target solution pipetted in is variable, as well as the amount of time before mixing, fluorescence readings for Competitive Compositions can be decreasing for up to 30 minutes after addition of reagents.

Temperature Control and Calibration. Reactions were performed in Hellma 114F cuvettes in one of two different Horiba Fluoromax-4 instruments in our group. Each instrument used an external water bath (Thermo Fisher) to control cuvette and reaction temperature. Using a thermocouple sensor, we calibrated the water bath temperature against the true temperature inside the cuvettes, and constructed a linear correction formula for the temperature control (e.g. to maintain 37.0 °C cuvette temperature, we set the water bath to 38.3 °C). The correlation coefficient r^2 for the regression line was over 0.98, and we believe all temperatures were accurately controlled to within 0.2 °C.

Time-based Fluorescence Data Acquisition. Time-based fluorescence data were acquired using one of two

Experiment	Species	Solution conc.	Addition volume (μL)	Nominal final conc.
VAF = 0.1%	Buffer	5×	1200	5×
	X-Probe	667 nM	4.5	2.5 nM
	Sink	25 μM	108	2250 nM
	WT	100 μM	18	1500 nM
	SNV	100 nM	18	1.5 nM
VAF = 0.033%	Buffer	5×	1100	5×
	X-Probe	66.7 nM	45	2.5 nM
	Sink	25 μM	108	2250 nM
	WT	100 μM	18	1500 nM
	SNV	100 nM	6	0.5 nM
VAF = 0.01%	Buffer	5×	1100	5×
	X-Probe	66.7 nM	27	1.5 nM
	Sink	40 μM	225	7.5 μM
	WT	100 μM	60	5 μM
	SNV	100 nM	6	0.5 nM
Post PCR	Buffer	5×	1200	5×
	X-Probe	50 nM	12	0.5 nM
	Sink	1 μM	12	10 nM
	PCR product	–	40	–
Labeled Sink	Buffer	5×	1200	5×
	X-Probe	50 nM	12	0.5 nM
	Sink	15 μM	12	150 nM
	WT	10 μM	12	100 nM
	SNV	200 nM	6	1 nM
Various SNV concentration (10 - 300 nM)	Buffer	5×	1200	5×
	X-Probe	2 μM	12	20 nM
	Sink	15 μM	12	150 nM
	WT	10 μM	12	100 nM
	SNV	2 | 2 | 2 | 10 μM	6 | 18 | 60 | 36	10 | 30 | 100 | 300 nM
Various SNV concentration (0.1 - 3 nM)	Buffer	5×	1200	5×
	X-Probe	50 nM	12	0.5 nM
	Sink	15 μM	12	150 nM
	WT	10 μM	12	100 nM
	SNV	10 | 60 | 200 | 200 nM	12 | 6 | 6 | 18	0.1 | 0.3 | 1 | 3 nM

TABLE 2: Formulation of Competitive Composition reactions.

different Horiba Fluoromax-4 instruments in our group. Data taken on the two machines yielded consistent differences of around 10% in fluorescence intensity, possibly due to lamp intensity and cuvette positioning. To minimize the effects of machine-to-machine variability, all experiments on one target and plotted into the same subfigure are performed on the same instrument. Observed background-constrained discrimination factor β is consistent between the two machines, exhibiting less than 5% error.

From initial calibration experiments, we determined optimal excitation wavelength of 582 nm and optimal emission wavelength of 600 nm for ROX fluorophore that we used on X-Probe. For Competitive Composition experiments with labeled Sink (Section S7), we additionally used excitation wavelength of 685 nm and emission wavelength of 710 nm for Alexa 647 fluorophore (on the Sink), instead of using its optimal excitation/emission wavelength (646 nm/663 nm). This offsetting of excitation and emission wavelength from the optimal was intentional, because the fluorescence signal at optimal excitation/emission wavelengths would have caused an overwhelmingly large signal that would have resulted in photodetector saturation.

Competitive Composition experiment	Slit sizes (ex/em)
VAF = 1%	4nm/4nm
VAF $\leq$ 0.1%	8nm/8nm
Various SNV concentration (0.1-3 nM)	8nm/8nm
Various SNV concentration (10-300 nM)	3nm/3nm
Labeled Sink	8nm/8nm
Post PCR	8nm/8nm

TABLE 3: Slit sizes of Competitive Composition experiments.

For experiments involving only X-Probes, monochromator slit sizes were set at 4 nm for both excitation and

emission, and integration time was set to 10 s (per cuvette) for each 60 s time point. For experiments involving Competitive Compositions, the monochromator slit sizes for excitation and emission are listed in Table 3, and the integration time was set to 10 s (per cuvette) for each 60 s time point. In the FluorEssence software provided by Horiba, fluorescence data saved was "S1/R1" data, which corrects for fluctuations in lamp output.

The duration of fluorescence acquisition varied. Typically, we set a maximum acquisition duration of 4 hours, but terminate the experiment early if it appears that the reaction has roughly reached equilibrium (in order to facilitate more rapid collection of data). Based on our simulations (Section S6), we know that equilibration could potentially be very slow. In the interest of practical application, however, we were primarily interested in seeing the performance of the X-Probes and Competitive Compositions at reasonable assay durations, even if the reaction has not reached equilibrium.

On rare occasions (less than 1 per 100 experiments), the cuvette mount fixing the position of the cuvettes to the rotating 4-sample changer became loose, and fluorescence data acquired was erratic. It was apparent to us that this is due to physical movement of the cuvette itself, and this data would be discarded and re-acquired after adjusting the mechanical mount. As one example, Fig. S10-10b (Competitive Composition, PIK3CA>E545K, 0.033% SNV load) shows example erratic behavior observed due to the loose mount problem. In that particular case, the data was judged to be still reasonably representative, and the experiment was not repeated.

Fluorescence Data Analysis. Data acquired by the FluorEssence software was exported to a tab-delimited text file, which was subsequently imported, analyzed, and plotted using MATLAB scripts. Time was linearly adjusted so that $t = 0$ corresponds to the first data point acquired after the cuvettes were replaced into the machine after addition of reagents and mixing. No additional adjustments are made to data for the raw fluorescence kinetics plots shown in the Supplementary materials.

Background-constrained discrimination factor β values reported in Fig. 3-5 were calculated by dividing the average of the last five data points for the WT+SNV traces by the average of the last five data points for the WT only traces. β values reported in Fig. 6 were calculated similarly but only based on the last data points.

Protocol Differences for RNA Targets. RNA oligonucleotides were diluted using DEPC-treated RNAse-free water (Fisher Scientific); furthermore, 0.1% RNAse-Zap (Life Technologies) were introduced into each RNA solution. The RNAse-Zap solution caused the RNA solution to be "soapy" and somewhat reduced pipetting accuracy. All RNA solutions were stored separately in an RNAse-free refridgerator, which was periodically scrubbed with RNAse-Zap. We did not notice any significant degradation of RNA.

Asymmetric PCR. We first quantitate the concentrations of the repository human genomic DNA samples NA18537 (SMAD7-T homozygote) and NA18546 (SMAD7-C homozygote) (Coriell) by Nanodrop 2000c spectrophotometer (Thermo Fisher). Then, sample solutions of certain concentrations were diluted in 1× Tris·EDTA buffer, prepared by diluting 100× Tris·EDTA buffer (Sigma-Aldrich) in DEPC-treated Nuclease-free water (Fisher Scientific). We mixed the two samples at 1:9 and 1:99 concentration ratio to prepare low allele frequency template solutions.

All template solutions were at a total concentration of 10 ng/μl, and 10 μL of the template solutions were added into the corresponding reaction solutions to achieve a final template concentration of 2 ng/μl (50 μL). Thus, the amount of rare allele template in 1:9 reaction mixture was 10 ng/50 μl, and that in 1:99 reaction mixture was 1 ng/50 μl.

Reagent	Final Concentration
10× PCR buffer	1x
dNTP (each)	200 μM
Forward Primer	2 μM
Reverse Primer	0.2 μM
Taq Polymerase	0.05 Unit/μL
Mixed gDNA	2 ng/μL
Nuclease-free Water	Fill to 50 μL

TABLE 4: Asymmetric PCR reaction protocol

To achieve desired final concentrations for each species, appropriate amount of 10× PCR buffer (with Mg^{2+} included, Sigma-Aldrich), dNTP (each, Sigma-Aldrich), non-allele specific forward primer, non-allele specific reverse primer, Taq polymerase (Mg^{2+} free, Sigma-Aldrich), template solution, and nuclease-free water were mixed to 50 μL in a 200 μL Eppendorf PCR tube, according to Table 4.

We use asymmetric PCR, with forward primer being 10× of the concentration of the reverse primer, to generate single-stranded amplicons that can directly hybridize to our Probes and Sinks. The mixed PCR reaction solutions were then incubated into an Eppendorf MasterCycler Personal PCR machine with pre-heated lid to 95 °C. The following program steps are listed in Table 5.

Step	Temperature	Duration
0. Preheat Lid to 95 °C		
1. Initial Denaturation	95 °C	2 min
2. Denaturation	95 °C	30 s
3. Annealing	55 °C	30 s
4. Extension	72 °C	30 s
Repeat Steps 2 to 4 for 60 times		
5. Final Extension	72 °C	5 min
6. Hold	10 °C	

TABLE 5: Thermocycler program.

After reaction, 40μL of the PCR products were directly pipetted into the cuvette containing pre-mixed X-Probe and Sink (Table 2, see also Competitive Composition Reaction Setup), and the fluorescence responses were collected.

Text S1: Analysis and Simulations of Generic Competitive Compositions

Statistical Mechanics Model and Analysis

We first present a simple statistical mechanics model of the equilibrium between Competitive Composition and a sample comprising SNV and WT. Both Probe and Sink react with SNV and WT reversibly, and the 4 reactions that simultaneously occur in the system are illustrated in Fig. S1-1a.

Here we assume that there is a large excess reservoir of the Probes and the Sinks, such that the binding of any number of SNV or WT molecules are practically independent. Then the reaction system can be divided into 4 subsystems. Ignoring short-lived intermediates, each SNV or WT molecule can exist in one of three states: unbound, bound to the Probe, or bound to the Sink; molecules in the bound to the Probe states can contribute to either direct or indirect detectable signals.

For convenience, we define the state energy E of each reaction product as the "concentration-adjusted standard free energy" of the reaction, and the state energy of free SNV and WT to be zero. Concentration-adjusted standard free energy is defined such that when it equals 0, the reaction yield is 50%. The exact expression is determined by the reaction schemes of Probe and Sink upon binding to a target, and thus varies among different Probe and Sink architectures.

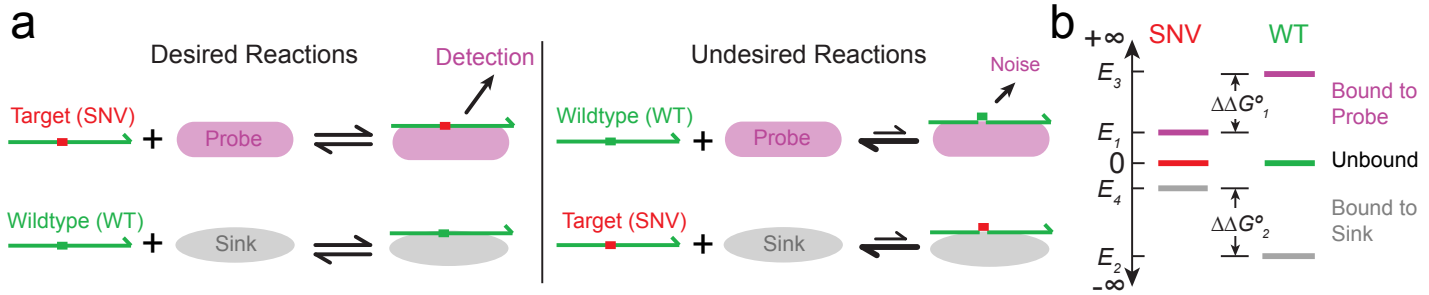

FIG. S1-1: Competitive Compositions: **(a)** reactions and **(b)** energy level diagram.

For standard(non-dissociative) Probe and Sink architectures (Fig. 2a), such as standard single-stranded probes, Molecular Beacons, hairpin probes, etc., the four relevant reactions between a sample mixture and the Competitive Composition are:

$$\begin{aligned} \mathrm{SNV} + \mathrm{Probe} &\rightleftharpoons \mathrm{SNV}\cdot\mathrm{Probe} \quad E_1 \\ \mathrm{WT} + \mathrm{Sink} &\rightleftharpoons \mathrm{WT}\cdot\mathrm{Sink} \quad E_2 \\ \mathrm{WT} + \mathrm{Probe} &\rightleftharpoons \mathrm{WT}\cdot\mathrm{Probe} \quad E_3 \\ \mathrm{SNV} + \mathrm{Sink} &\rightleftharpoons \mathrm{SNV}\cdot\mathrm{Sink} \quad E_4 \end{aligned}$$

E_1 and E_2 are defined as:

$$\begin{aligned} E_1 &= \Delta G^\circ_{\mathrm{rxn1}} - R\tau\ln([\mathrm{Probe}]_0) \\ E_2 &= \Delta G^\circ_{\mathrm{rxn2}} - R\tau\ln([\mathrm{Sink}]_0) \end{aligned}$$

where $\Delta G^\circ_{\mathrm{rxn1}}$ and $\Delta G^\circ_{\mathrm{rxn2}}$ are the reaction standard free energies, R is the ideal gas constant, τ is the temperature in Kelvin, and $[\mathrm{Probe}]_0$ and $[\mathrm{Sink}]_0$ are the initial concentrations of the Probe and Sink. E_3 and E_4 can be similarly defined. Additionally, we introduce $\Delta\Delta G^\circ_1$ and $\Delta\Delta G^\circ_2$ to represent the thermodynamic penalties of undesired reactions as compare to the corresponding desired reactions (Section S6). Thus $E_3 = E_1 + \Delta\Delta G^\circ_1$ and $E_4 = E_2 + \Delta\Delta G^\circ_2$.

Let's take the reaction between Probe and SNV as an example. Given $\Delta G^\circ_{\mathrm{rxn}} = -R\tau\ln(K_{\mathrm{eq}})$, if $E_1 = 0$, then $K_{\mathrm{eq}} = \frac{1}{[\mathrm{Probe}]_0}$. When Probe is in large excess of the SNV, the equilibrium Probe concentration [Probe] is approximately equal to $[\mathrm{Probe}]_0$. Then there is:

$$\begin{aligned} \frac{1}{[\mathrm{Probe}]_0} = K_{\mathrm{eq}} &\equiv \frac{[\mathrm{SNV}\cdot\mathrm{Probe}]}{[\mathrm{SNV}][\mathrm{Probe}]} \\ &\approx \frac{[\mathrm{SNV}\cdot\mathrm{Probe}]}{[\mathrm{SNV}][\mathrm{Probe}]_0} \end{aligned}$$

so that $[\mathrm{SNV} \cdot \mathrm{Probe}] \approx [\mathrm{SNV}]$, and thus 50% of the SNV will be bound to the Probe at equilibrium, consistent with state energy definition.

For dissociative Probe and Sink (Fig. 2c), such as toehold probe, Yin-Yang probe, and X-probe, the four relevant reactions between sample and the Competitive Composition are:

$$\begin{aligned}
\mathrm{SNV} + \mathrm{P_P C_P} &\rightleftharpoons \mathrm{SNV} \cdot \mathrm{C_P} + \mathrm{P_P} \qquad E_1 \\
\mathrm{WT} + \mathrm{P_S C_S} &\rightleftharpoons \mathrm{WT} \cdot \mathrm{C_S} + \mathrm{P_S} \qquad E_2 \\
\mathrm{WT} + \mathrm{P_P C_P} &\rightleftharpoons \mathrm{WT} \cdot \mathrm{C_P} + \mathrm{P_P} \qquad E_3 \\
\mathrm{SNV} + \mathrm{P_S C_S} &\rightleftharpoons \mathrm{SNV} \cdot \mathrm{C_S} + \mathrm{P_S} \qquad E_4
\end{aligned}$$

E_1 and E_2 are defined as:

$$\begin{aligned}
E_1 &= \Delta G^\circ_{\mathrm{rxn1}} - R\tau \ln\left(\frac{[\mathrm{P_P}]_0}{[\mathrm{P_P C_P}]_0}\right) \\
E_2 &= \Delta G^\circ_{\mathrm{rxn2}} - R\tau \ln\left(\frac{[\mathrm{P_S}]_0}{[\mathrm{P_S C_S}]_0}\right)
\end{aligned}$$

where $[\mathrm{P}]_0$ is the excess concentration of the auxiliary species initially present in solution,and $[\mathrm{PC}]_0$ is the initial concentration of Probe or Sink, with subscription "P" indicating Probe and "S" indicating Sink. E_3 and E_4 can be similarly defined. Likewise, when $E_1 = 0$, $K_{\mathrm{eq}} = \frac{[\mathrm{P_P}]_0}{[\mathrm{P_P C_P}]_0}$. When Probe is in large excess of the SNV, there is $[\mathrm{SNV} \cdot \mathrm{C_P}] \approx [\mathrm{SNV}]$, so that 50% of the SNV will be bound to the Probe at equilibrium.

Ordinary Differential Equation Simulations

To factor in the effects of Probe and Sink concentrations on the distribution of species in the system, and to consider the dynamic feature of such distribution, we construct an ordinary differential equation (ODE) model of two example systems: Competitive Composition consists of non-dissociative components and Competitive Composition consists of dissociative components.

For non-dissociative Competitive Composition, the chemical reactions between the Competitive Composition and a sample mixture, not including short-lived intermediates, are:

$$\begin{aligned}
\mathrm{SNV} + \mathrm{Probe} &\underset{k_{1-}}{\overset{k_{1+}}{\rightleftharpoons}} \mathrm{SNV} \cdot \mathrm{Probe} \qquad \Delta G^\circ_{\mathrm{rxn1}} \\
\mathrm{WT} + \mathrm{Sink} &\underset{k_{2-}}{\overset{k_{2+}}{\rightleftharpoons}} \mathrm{WT} \cdot \mathrm{Sink} \qquad \Delta G^\circ_{\mathrm{rxn2}} \\
\mathrm{WT} + \mathrm{Probe} &\underset{k_{3-}}{\overset{k_{3+}}{\rightleftharpoons}} \mathrm{WT} \cdot \mathrm{Probe} \qquad \Delta G^\circ_{\mathrm{rxn3}} \\
\mathrm{SNV} + \mathrm{Sink} &\underset{k_{4-}}{\overset{k_{4+}}{\rightleftharpoons}} \mathrm{SNV} \cdot \mathrm{Sink} \qquad \Delta G^\circ_{\mathrm{rxn4}}
\end{aligned}$$

wherein k_+ and k_- represent the forward and the reverse rate constants. The values of all forward reaction rate constants k_+ are assumed to be 3×10^5 $\mathrm{M^{-1}s^{-1}}$; this is estimated based on previous studies [2] and our own calibration experiments (data not shown). The reverse rate constants can be calculated as

$$k_- = \frac{k_+}{K_{\mathrm{eq}}} = k_+ e^{\Delta G^\circ_{\mathrm{rxn}}/R\tau}$$

where $\Delta G^\circ_{\mathrm{rxn}}$ denotes the standard free energy of the relevant reaction. For convenience, we abbreviate SNV to S

and WT to W. The corresponding ordinary differential equations are:

$$\begin{aligned}
\frac{d[\mathrm{S}]}{dt} &= -k_{1+}[\mathrm{S}][\mathrm{Probe}] + k_{1-}[\mathrm{S}\cdot\mathrm{Probe}] - k_{4+}[\mathrm{S}][\mathrm{Sink}] + k_{4-}[\mathrm{S}\cdot\mathrm{Sink}] \\
\frac{d[\mathrm{W}]}{dt} &= -k_{3+}[\mathrm{W}][\mathrm{Probe}] + k_{3-}[\mathrm{W}\cdot\mathrm{Probe}] - k_{2+}[\mathrm{W}][\mathrm{Sink}] + k_{2-}[\mathrm{W}\cdot\mathrm{Sink}] \\
\frac{d[\mathrm{Probe}]}{dt} &= -k_{1+}[\mathrm{S}][\mathrm{Probe}] + k_{1-}[\mathrm{S}\cdot\mathrm{Probe}] - k_{3+}[\mathrm{W}][\mathrm{Probe}] + k_{3-}[\mathrm{W}\cdot\mathrm{Probe}] \\
\frac{d[\mathrm{Sink}]}{dt} &= -k_{4+}[\mathrm{S}][\mathrm{Sink}] + k_{4-}[\mathrm{S}\cdot\mathrm{Sink}] - k_{2+}[\mathrm{W}][\mathrm{Sink}] + k_{2-}[\mathrm{W}\cdot\mathrm{Sink}] \\
\frac{d[\mathrm{S}\cdot\mathrm{Probe}]}{dt} &= k_{1+}[\mathrm{S}][\mathrm{Probe}] - k_{1-}[\mathrm{S}\cdot\mathrm{Probe}] \\
\frac{d[\mathrm{W}\cdot\mathrm{Probe}]}{dt} &= k_{3+}[\mathrm{W}][\mathrm{Probe}] - k_{3-}[\mathrm{W}\cdot\mathrm{Probe}] \\
\frac{d[\mathrm{S}\cdot\mathrm{Sink}]}{dt} &= k_{4+}[\mathrm{S}][\mathrm{Sink}] - k_{4-}[\mathrm{S}\cdot\mathrm{Sink}] \\
\frac{d[\mathrm{W}\cdot\mathrm{Sink}]}{dt} &= k_{2+}[\mathrm{W}][\mathrm{Sink}] - k_{2-}[\mathrm{W}\cdot\mathrm{Sink}]
\end{aligned}$$

These ordinary differential equations are simulated using MATLAB's stiff "ode23s" solver, using relative tolerance of 10^{-4} and absolute tolerance of 10^{-20}. For simulations shown in the main text, $\Delta\Delta G^\circ_1 = +3$ kcal/mol, $\Delta\Delta G^\circ_2 = +4$ kcal/mol, and initial concentrations are [S] = 0.5 nM, [W] = 1500 nM, [Probe] = 2.5 nM, [Sink] = 2250 nM.

For dissociative Probe/Sink that releases an auxiliary species upon reacting with a target, the chemical reactions of the Competitive Composition and a sample mixture, not including short-lived intermediates, are:

$$\begin{aligned}
\mathrm{SNV} + \mathrm{P_P}\cdot\mathrm{C_P} &\underset{k_{1-}}{\overset{k_{1+}}{\rightleftharpoons}} \mathrm{SNV}\cdot\mathrm{C_P} + \mathrm{P_P} \qquad \Delta G^\circ_{\mathrm{rxn1}} \\
\mathrm{WT} + \mathrm{P_S}\cdot\mathrm{C_S} &\underset{k_{2-}}{\overset{k_{2+}}{\rightleftharpoons}} \mathrm{WT}\cdot\mathrm{C_S} + \mathrm{P_S} \qquad \Delta G^\circ_{\mathrm{rxn2}} \\
\mathrm{WT} + \mathrm{P_P}\cdot\mathrm{C_P} &\underset{k_{3-}}{\overset{k_{3+}}{\rightleftharpoons}} \mathrm{WT}\cdot\mathrm{C_P} + \mathrm{P_P} \qquad \Delta G^\circ_{\mathrm{rxn3}} \\
\mathrm{SNV} + \mathrm{P_S}\cdot\mathrm{C_S} &\underset{k_{4-}}{\overset{k_{4+}}{\rightleftharpoons}} \mathrm{SNV}\cdot\mathrm{C_S} + \mathrm{P_S} \qquad \Delta G^\circ_{\mathrm{rxn4}}
\end{aligned}$$

wherein the value and calculation method of k_+ and k_- are the same as Competitive Compositions with non-dissociative components.

The corresponding ordinary differential equations are:

$$\begin{aligned}
\frac{d[\mathrm{S}]}{dt} &= -k_{1+}[\mathrm{S}][\mathrm{P_PC_P}] + k_{1-}[\mathrm{S}\cdot\mathrm{C_P}][\mathrm{P_P}] - k_{4+}[\mathrm{S}][\mathrm{P_SC_S}] + k_{4-}[\mathrm{S}\cdot\mathrm{C_S}][\mathrm{P_S}] \\
\frac{d[\mathrm{W}]}{dt} &= -k_{3+}[\mathrm{W}][\mathrm{P_PC_P}] + k2-[\mathrm{W}\cdot\mathrm{C_P}][\mathrm{P_P}] - k_{2+}[\mathrm{W}][\mathrm{P_SC_S}] + k_{2+}[\mathrm{W}\cdot\mathrm{C_S}][\mathrm{P_S}] \\
\frac{d[\mathrm{P_P}]}{dt} &= k_{1+}[\mathrm{S}][\mathrm{P_PC_P}] - k_{1-}[\mathrm{S}\cdot\mathrm{C_P}][\mathrm{P_P}] + k_{3+}[\mathrm{W}][\mathrm{P_PC_P}] - k2-[\mathrm{W}\cdot\mathrm{C_P}][\mathrm{P_P}] \\
\frac{d[\mathrm{P_PC_P}]}{dt} &= -k_{1+}[\mathrm{S}][\mathrm{P_PC_P}] + k_{1-}[\mathrm{S}\cdot\mathrm{C_P}][\mathrm{P_P}] - k_{3+}[\mathrm{W}][\mathrm{P_PC_P}] + k2-[\mathrm{W}\cdot\mathrm{C_P}][\mathrm{P_P}] \\
\frac{d[\mathrm{P_S}]}{dt} &= k_{4+}[\mathrm{S}][\mathrm{P_SC_S}] - k_{4-}[\mathrm{S}\cdot\mathrm{C_S}][\mathrm{P_S}] + k_{2+}[\mathrm{W}][\mathrm{P_SC_S}] - k_{2+}[\mathrm{W}\cdot\mathrm{C_S}][\mathrm{P_S}] \\
\frac{d[\mathrm{P_SC_S}]}{dt} &= -k_{4+}[\mathrm{S}][\mathrm{P_SC_S}] + k_{4-}[\mathrm{S}\cdot\mathrm{C_S}][\mathrm{P_S}] - k_{2+}[\mathrm{W}][\mathrm{P_SC_S}] + k_{2+}[\mathrm{W}\cdot\mathrm{C_S}][\mathrm{P_S}] \\
\frac{d[\mathrm{S}\cdot\mathrm{C_P}]}{dt} &= k_{1+}[\mathrm{S}][\mathrm{P_PC_P}] - k_{1-}[\mathrm{S}\cdot\mathrm{C_P}][\mathrm{P_P}] \\
\frac{d[\mathrm{W}\cdot\mathrm{C_P}]}{dt} &= k_{3+}[\mathrm{W}][\mathrm{P_PC_P}] - k_{2-}[\mathrm{W}\cdot\mathrm{C_P}][\mathrm{P_P}] \\
\frac{d[\mathrm{S}\cdot\mathrm{C_S}]}{dt} &= k_{4+}[\mathrm{S}][\mathrm{P_SC_S}] - k_{4-}[\mathrm{S}\cdot\mathrm{C_S}][\mathrm{P_S}] \\
\frac{d[\mathrm{W}\cdot\mathrm{C_S}]}{dt} &= k_{2+}[\mathrm{W}][\mathrm{P_SC_S}] - k_{2+}[\mathrm{W}\cdot\mathrm{C_S}][\mathrm{P_S}]
\end{aligned}$$

These ordinary differential equations are simulated using MATLAB's stiff "ode23s" solver, using relative tolerance of 10^{-4} and absolute tolerance of 10^{-20}. For simulations shown in this manuscript, $\Delta\Delta G^\circ_1 = +3$ kcal/mol,

$\Delta\Delta G_2^\circ$ = +4 kcal/mol, and initial concentrations are $[S]$ = 0.5 nM, $[W]$ = 1500 nM, $[P_PC_P]$ = 2.5 nM, $[P_P]$ = 3.75 nM, $[P_SC_S]$ = 2250 nM, $[P_S]$ = 2250 nM.

The ordinary differential equation model of Competitive Compositions with combined dissociative and non-dissociative components can be constructed and simulated similarly based on the techniques presented here.

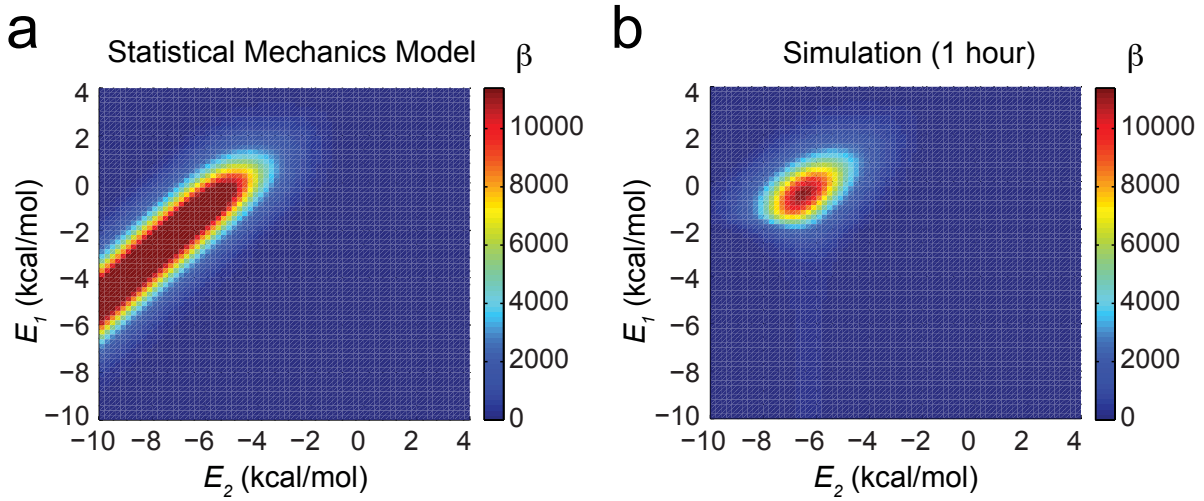

FIG. S1-2: Comparison between optimal E values predicted by statistical mechanics model and by simulation, assuming $\Delta\Delta G_1^\circ$ = 2 kcal/mol, and $\Delta\Delta G_2^\circ$ = 5.5 kcal/mol at 37 °C. **(a)** Equilibrium analysis of background-constrained discrimination factor β dependence on optimal E values, assuming [SNV] = 0.5 nM, [WT] = 1500 nM, and Background = 0.04 nM. **(b)** Simulation predicted β at 1 hour of reaction time, using dissociative Probe and Sink, assuming $[P_PC_P]$ = 2.5 nM, $[P_P]$ = 2.5 nM, $[P_SC_S]$ = 2250 nM, $[P_S]$ = 2250 nM and the rest to be consistent with (a).

Limitations of Statistical Mechanics Model and Analysis

The statistical mechanics model simplifies the reaction system and only provides qualitative insight to the system behavior. Although for some $\Delta\Delta G^\circ$ values as well as certain SNV and WT concentrations, optimal E values predicted by equilibrium analysis and simulation maybe similar. However, this is not generally true.

Fig. S1-2 shows the heat-map of background-constrained discrimination factor β predicted by the two approaches, using $\Delta\Delta G_1^\circ = 2$ kcal/mol and $\Delta\Delta G_2^\circ = 5.5$ kcal/mol. In the simulation, we arbitrarily chose dissociative Probe and Sink. According to statistical mechanics model, the top-right-most deep red point indicated E values

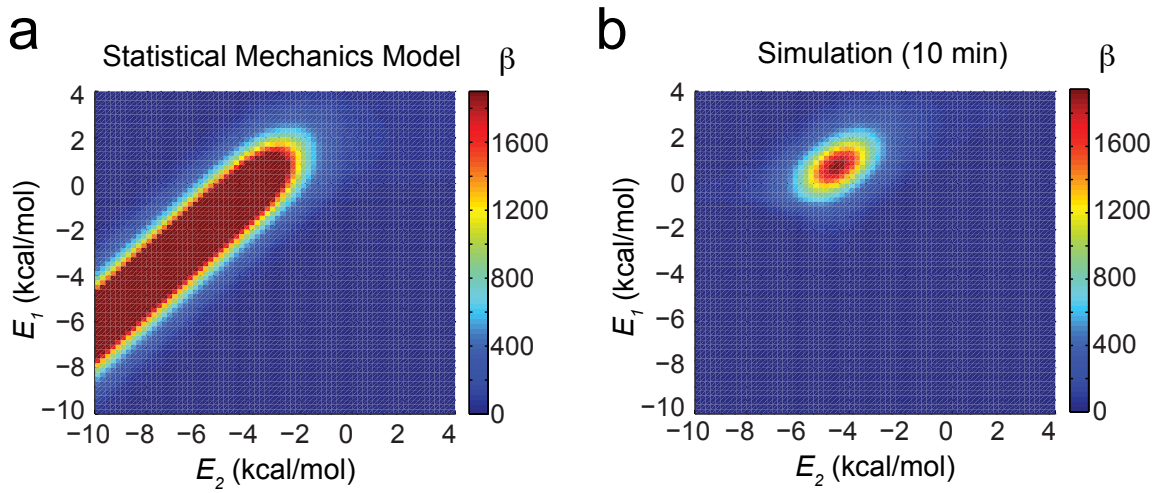

FIG. S1-3: Comparison between optimal E values predicted by statistical mechanics model and by simulation for short reactions, assuming $\Delta\Delta G_1^\circ = 2.5$ kcal/mol, and $\Delta\Delta G_2^\circ = 3.5$ kcal/mol at 37 °C. **(a)** Equilibrium analysis of background-constrained discrimination factor β dependence on optimal E values, assuming [SNV] = 0.5 nM, [WT] = 1500 nM, and Background = 0.04 nM. **(b)** Simulation predicted β at 10 minutes of reaction time, using dissociative Probe and Sink, assuming $[P_PC_P]$ = 2.5 nM, $[P_P]$ = 2.5 nM, $[P_SC_S]$ = 2250 nM, $[P_S]$ = 2250 nM and the rest to be consistent with (a).

are (-4.8, 0) kcal/mol for (E_1, E_2), which deviates as large as 2 kcal/mol in E_1 from the simulation predicted optimal values (-6.6, -0.6) kcal/mol.

Fig. S1-3 shows comparison of β for short reactions. The optimal E values predicted by simulation are (-4.6, 0.6) kcal/mol. In contrast, almost all the parameter space within (-4.6 $\pm$ 2, 0.6 $\pm$ 1) kcal/mol will result in optimal β according to statistical mechanics model. This indicate that, for shorter reactions, simulation is superior than statistical mechanics model, because the latter cannot provide accurate guidance to the Probe and Sink design.

Because statistical mechanics model simply assumes Probe and Sink are in large excess and does not consider the exact values of the concentrations, different concentration combinations may result in even larger differences.

Text S2: X-Probe Structure and Reaction Mechanism

The X-Probe (FQPC) is a conditionally fluorescent probe comprising four pre-hybridized components: a universal quencher strand Q, a universal fluorophore strand F, a specific protector strand P, and a specific complement strand C (Fig. S2-1).

Each strand can be subdivided into various regions as denoted by numbers (Fig. S2-2a). Each region represents a number of contiguous nucleotides that act as a functional unit in hybridization. Polymorphic nucleotide that distinguishes the SNV from the wildtype (dominant allele) sequence is shown in red. In this diagram, the polymorphic nucleotide exists in the double-stranded region of the specific arms, but it may also exist in the single-stranded region as shown in Fig. 3a.

The hybridization between region 10 region 11 results in the fluorophore being in close proximity to the quencher, so that the X-Probe is natively dark. Initiated by region 4 (known as a toehold), the reaction between X-Probe and its target proceeds through a branch migration process, and is completed via the dissociation of regions 12 and 10 to release the PQ complex. The fluorescence increases when the quencher diffuses away with PQ. Similar to other dissociative probes, such as the toehold probe [3] , the number of different species is conserved during the reaction (Fig. S2-2bc).

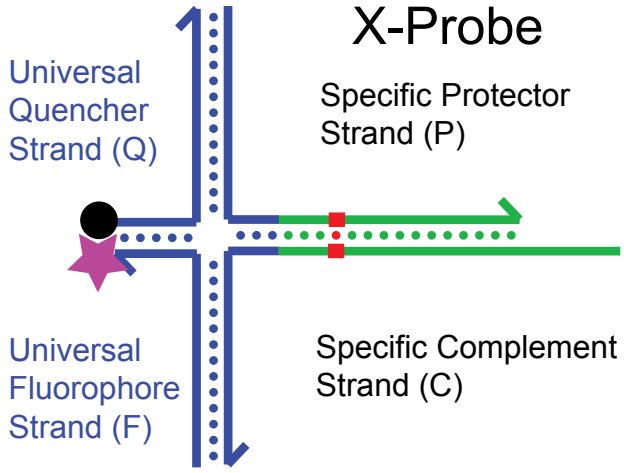

FIG. S2-1: X-Probe structure. The X-Probe is a 4-stranded complex; the specific protector strand P and the specific complement strand C depend on the rare allele (SNV) sequence, but the same universal quencher strand Q and universal fluorophore strand F can be used for X-Probes targeting any number of different sequences.

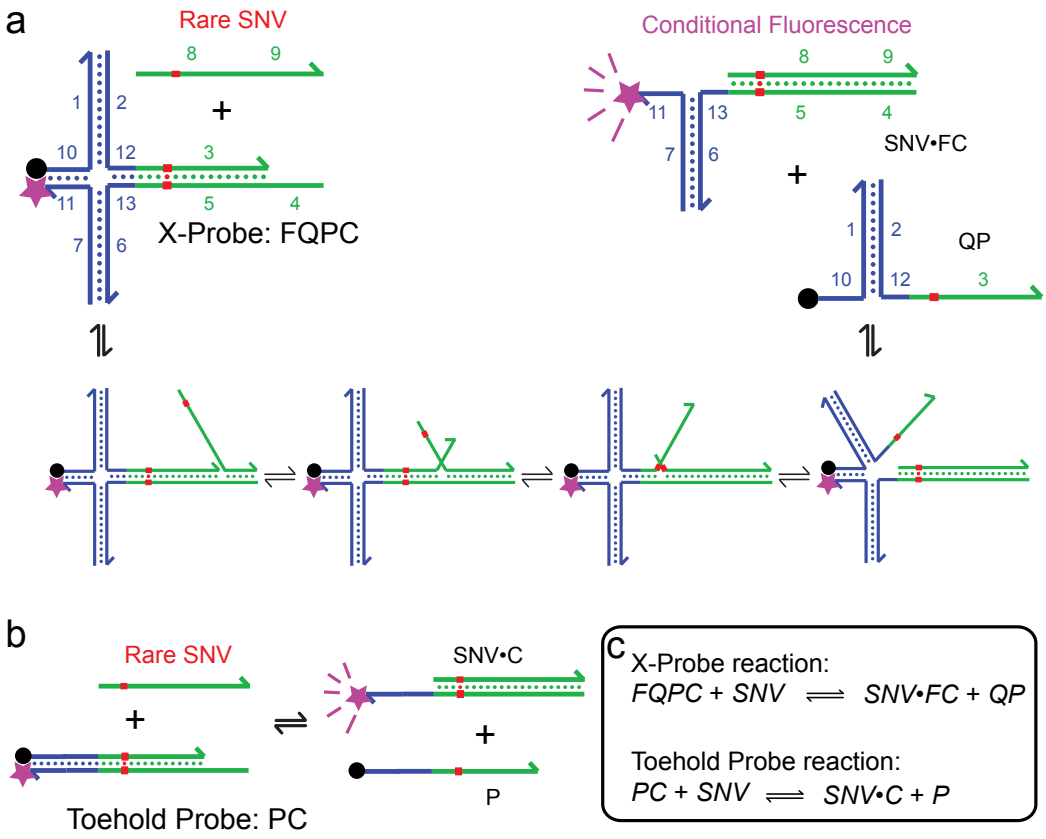

FIG. S2-2: Reaction mechanism of the X-Probe. **(a)** The reaction is initiated by the hybridization between regions 9 and 4. The 5-stranded intermediate then progresses in random-walk fashion through a number of roughly isoenergetic states in a process known as branch migration [1, 2], before the nonhomologous regions 10 and 12 dissociate from their complements, regions 11 and 13. The resulting product fluorescents because the quencher is no longer colocalized to the fluorophore. **(b)** Net reaction of toehold probe [3]. **(c)** Comparison of chemical reactions of X-Probe and toehold probe.

Text S3: Thermodynamics-Guided Design of X-Probe sequences.

We design X-Probe to react with the intended target with optimal $\Delta G^\circ_{\text{rxn1}}$ informed by ordinary differential equation simulation. By adjusting the lengths and sequences of the regions on each strand, X-Probes were first designed computationally, and finalized by hand.

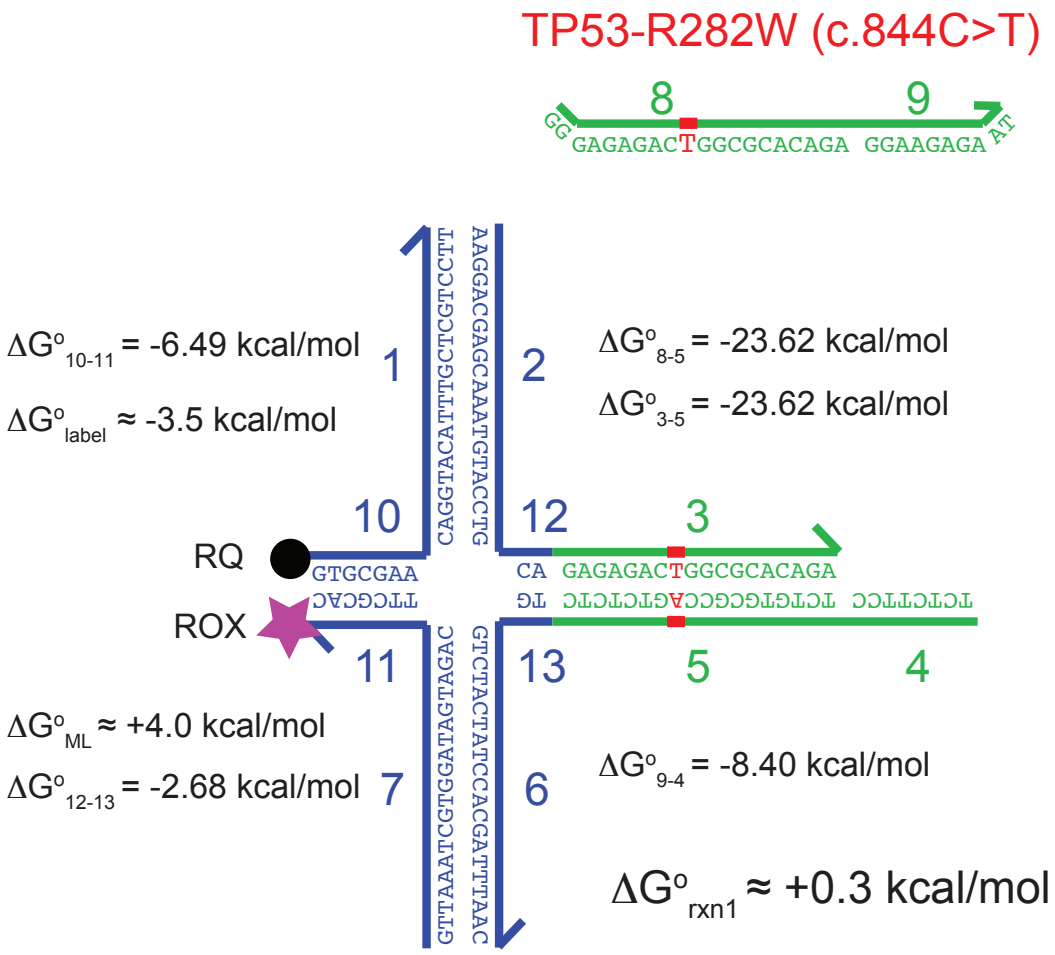

FIG. S3: Example of $\Delta G^\circ_{\text{rxn1}}$ calculation.

Specifically, $\Delta G^\circ_{\text{rxn1}}$ can be decomposed as the following:

$$\Delta G^\circ_{\text{rxn1}} = \Delta G^\circ_{9-4} - (\Delta G^\circ_{10-11} + \Delta G^\circ_{12-13} + \Delta G^\circ_{\text{ML}} + \Delta G^\circ_{\text{label}}) + (\Delta G^\circ_{8-5} - \Delta G^\circ_{3-5}) \quad (1)$$

wherein ΔG°_{9-4} is the standard free energy of the hybridization between regions 4 and 9, ΔG°_{10-11} is the standard free energy of the hybridization between regions 10 and 11, ΔG°_{12-13} is the standard free energy of the hybridization between regions 12 and 13, ΔG°_{8-5} is the standard free energy of the hybridization between regions 5 and 8, ΔG°_{3-5} is the standard free energy of the hybridization between regions 3 and 5, $\Delta G^\circ_{\text{ML}}$ is the standard free energy of the multi-loop formed at the four-arm junction, and $\Delta G^\circ_{\text{label}}$ is the standard free energy of fluorophore and quencher interaction when they are in close proximity. The value of $\Delta G^\circ_{\text{ML}}$ is somewhat poorly characterized; for our sequences, we estimated this to be roughly $+4.0 \pm 0.5$ kcal/mol, based on MFold predictions [5]. As far as we are aware, the value of $\Delta G^\circ_{\text{label}}$ is has not been reported for any fluorophore/quencher pairs; for our sequences and our usual fluorophore/quencher pair (ROX and Iowa Black RQ), we estimated this to be roughly -3.5 ± 0.5 kcal/mol, based on our unpublished experimental results.

Then, the standard free energies of hybridization between regions are calculated based on the nearest neighbor model as described in the literature [4]. In nearest neighbor model, two adjacent base pairs compose one stack, which has a defined enthalpy (ΔH°) and entropy (ΔS°) value. The standard free energy of each stack (ΔG°) at a particular temperature τ (in Kelvin) can be calculated based on $\Delta G^\circ = \Delta H^\circ - \tau \Delta S^\circ$. Then, standard free energy of a hybridization region can be calculated by summing up the energies of all the stacks.

For example, the ΔG° of a '5′-CTC-3′' region pairing to a '5′-GAG-3′' region is the sum of the ΔG° of stack 'CT/GA' and the ΔG° of stack 'TC/AG'. At 37 °C, the ΔG° of stack 'CT/GA' is -1.28 kcal/mol and the ΔG° of stack 'TC/AG' is -1.30 kcal/mol, so the ΔG° of 'CTC' pairing to 'GAG' is -2.58 kcal/mol. ΔG°_{8-5} and ΔG°_{3-5} can be calculated similarly.

In addition to including the stack energies as calculated above, calculation of ΔG°_{12-13} and ΔG°_{9-4} also requires to add an additional stack at the boundary between domain 12 and 3, and between 8 and 9, respectively.

The calculation of ΔG°_{10-11} and ΔG°_{9-4} further includes an initiation standard free energy $\Delta G^\circ_{\text{init}}$, with a reported value of +1.96 kcal/mol at 37 ° for DNA-DNA hybridization, and +3.11 kcal/mol for DNA-RNA hybridization [4]. This term represents the additional entropy lost for colocalizing and orienting two complementary nucleic acid strands for Watson-Crick hybridization.

Fig. S3 shows the ΔG° break down of an X-Probe targeting the TP53-R282W (c.844C>T) mutation.

Design Thermodynamics Inaccuracies.

The above decomposition and design of $\Delta G^\circ_{\text{rxn1}}$ contain a number of simplifying assumptions. To be accurate, the true species-level decomposition of $\Delta G^\circ_{\text{rxn1}}$ is:

$$\Delta G^\circ_{\text{rxn1}} \;=\; \Delta G^\circ(\text{FC}\cdot\text{SNV}) + \Delta G^\circ(\text{PQ}) - \Delta G^\circ(\text{FQPC}) - \Delta G^\circ(\text{SNV}) \tag{2}$$

where FC·SNV, PQ, FQPC, and SNV denote SNV bound to FC complex, PQ complex, X-Probe, and free SNV (Fig. S2-2). The decomposition in eqn. (1) captures most but not all of the factors in eqn. (2); the two terms missing are ΔG°(SNV) and the interactions between regions 10, 12, and 3 in the PQ species. In equation (1), because regions 8 and 3 have the same sequence, and are significantly longer than regions 10, 12, and 9, we generally expect that there is minimal difference between ΔG°(SNV) and the interactions between regions 10, 12, and 3 in PQ, so that the two unaccounted terms cancel each other out. This is not necessarily true for all sequences, but there is enough uncertainty in the calculation of the ΔG° terms in eqn. (1) that the total amount of error is not significantly worsened. In our experience, the difference between our designed $\Delta G^\circ_{\text{rxn1}}$ and experimentally observed $\Delta G^\circ_{\text{rxn1}}$ has a standard deviation of slightly less than 1 kcal/mol.

Text S4: Kinetic traces for 44 X-Probes to DNA targets

Shown in this section are the experimental results of 44 different X-Probes as summarized in Fig. S4-1, each designed against one frequently observed point mutation (Fig. S4-2 through S4-13). For all experiments, the concentration of X-Probe is 10 nM. Each X-Probe was designed based on the method Section S3, aiming to achieve optimal $\Delta G^{\circ}_{\mathrm{rxn1}}$ informed by simulation. However, because of inaccuracies in literature-reported values for different DNA thermodynamics motifs, some X-Probes possessed $\Delta G^{\circ}_{\mathrm{rxn}}$ that was either significantly negative (resulting in very low α values due to saturated fluorescence signal by WT alone, or significantly positive (resulting in very low fluorescence values).

We believe that the variations in the performance of the X-Probe can be primarily attributed to (1) differences in $\Delta\Delta G^{\circ}$ for different base mismatches, and (2) imperfect thermodynamic design of X-Probes as described above.

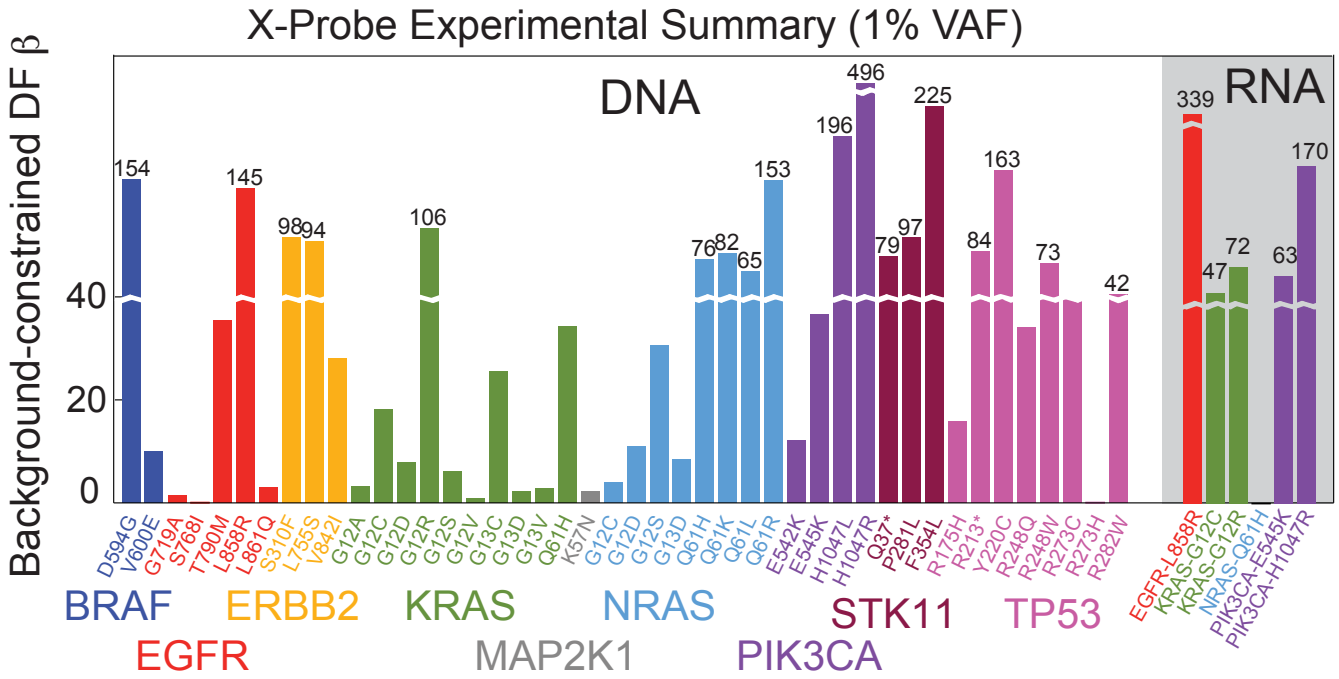

FIG. S4-1: Summary of background-constrained discrimination factor β observed for X-Probes designed to 44 different frequently observed cancer mutation sequences across 9 genes. To facilitate display of the observed β distribution, β values above 40 were plotted nonlinearly and β values are displayed above the bar. 6 of the 44 sequences were additionally tested using RNA SNV and WT targets.

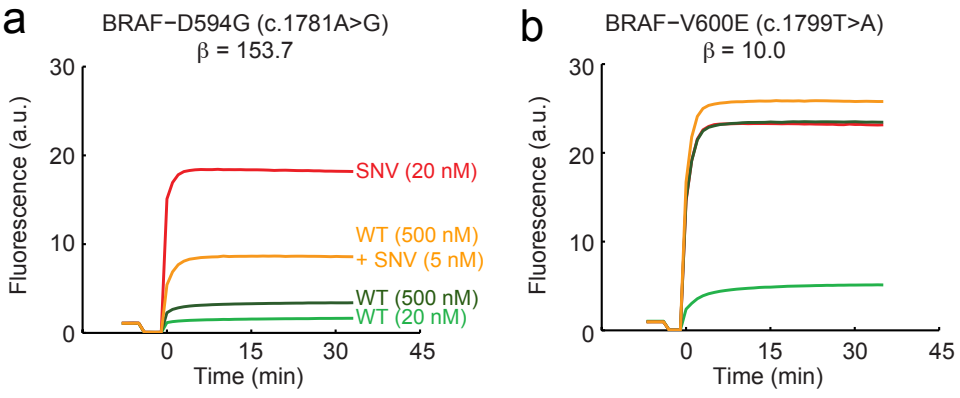

FIG. S4-2: Kinetic responses of X-Probes targeting BRAF mutations.

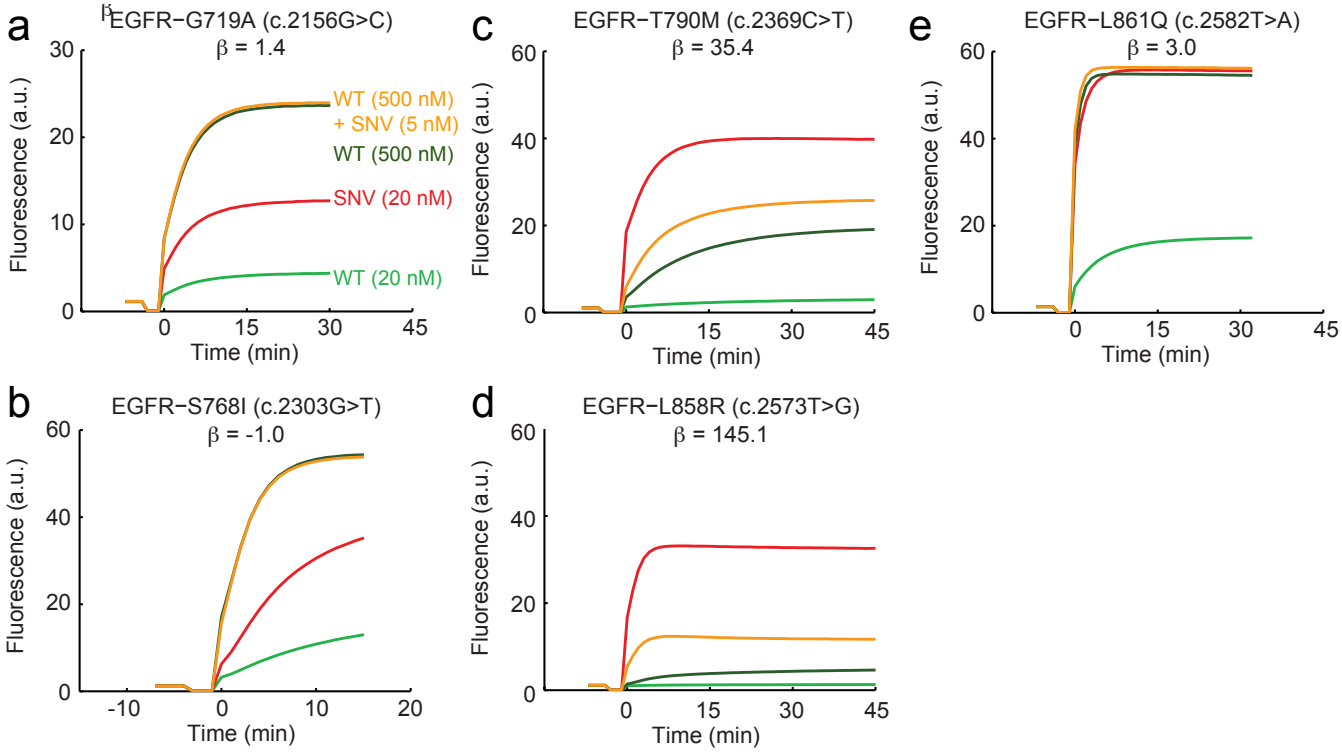

FIG. S4-3: Kinetic responses of X-Probes targeting EGFR mutations.

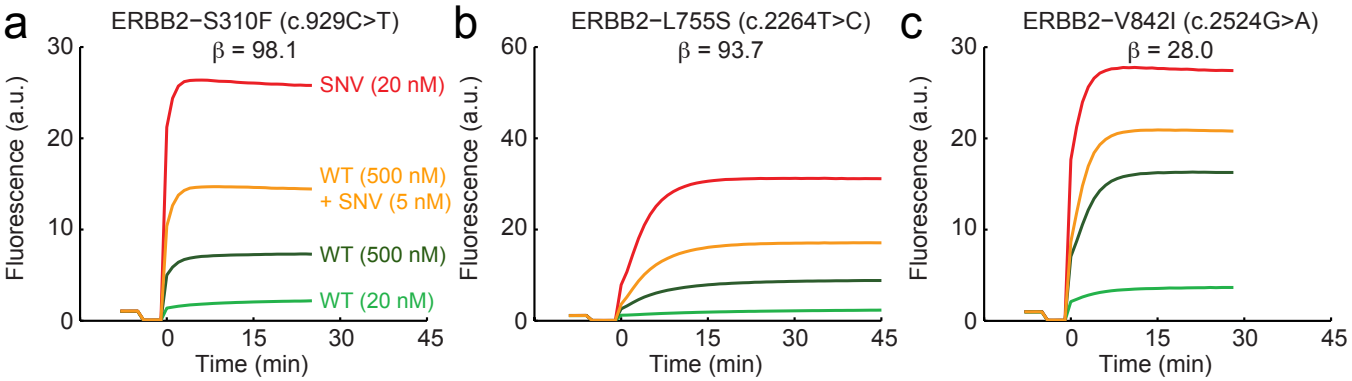

FIG. S4-4: Kinetic responses of X-Probes targeting ERBB2 mutations.

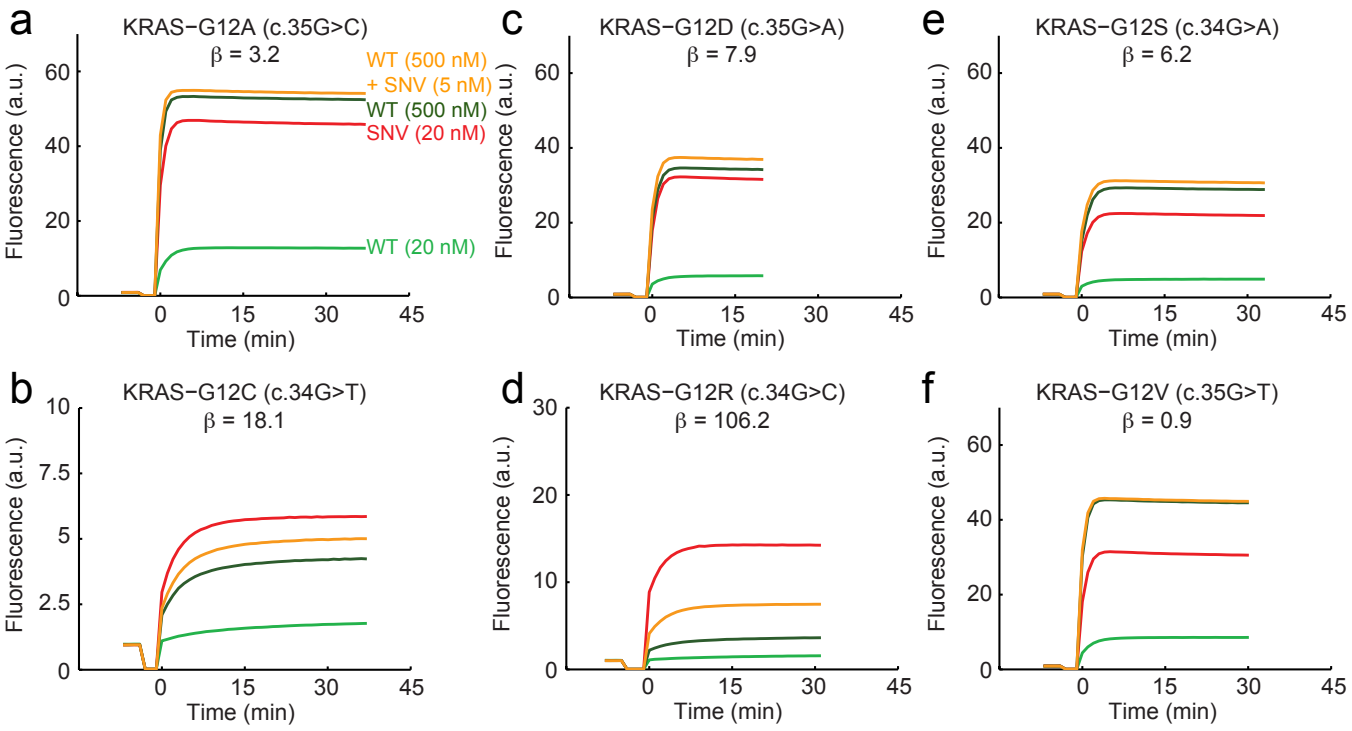

FIG. S4-5: Kinetic responses of X-Probes targeting KRAS mutations.

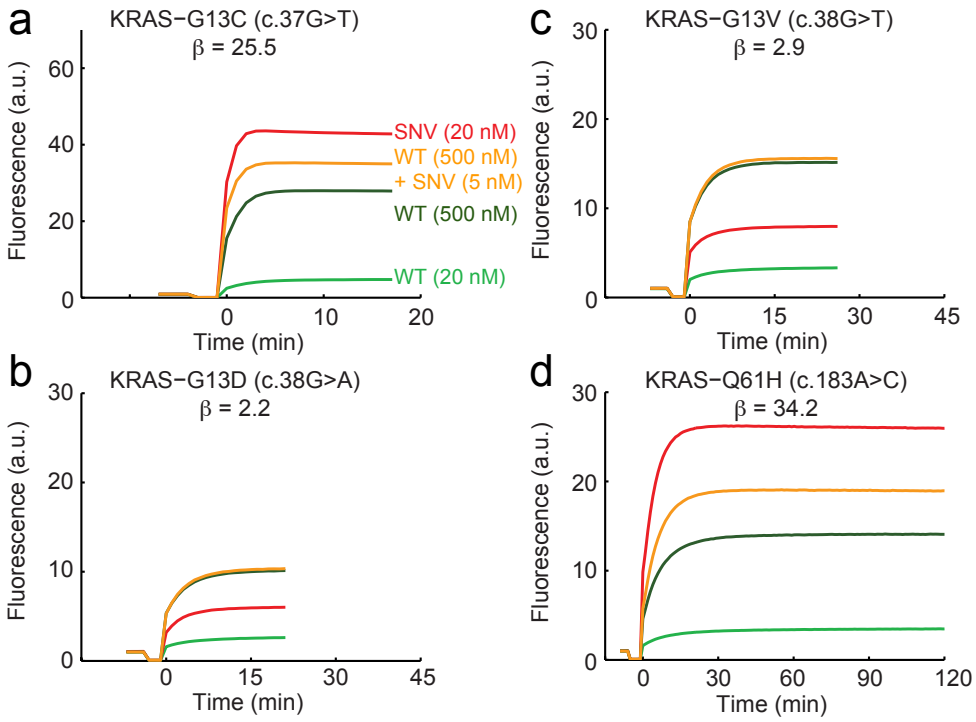

FIG. S4-6: Kinetic responses of X-Probes targeting KRAS mutations.

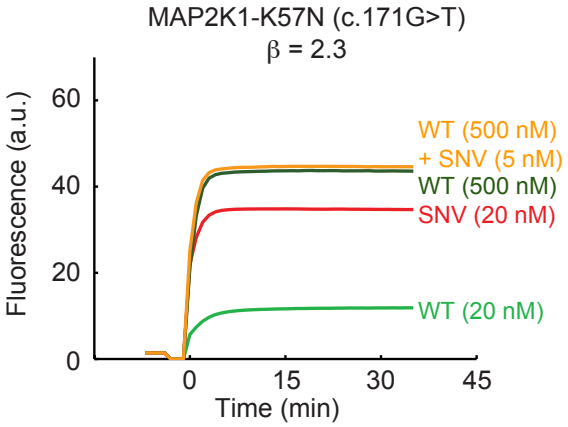

FIG. S4-7: Kinetic responses of X-Probes targeting a MAP2K mutation.

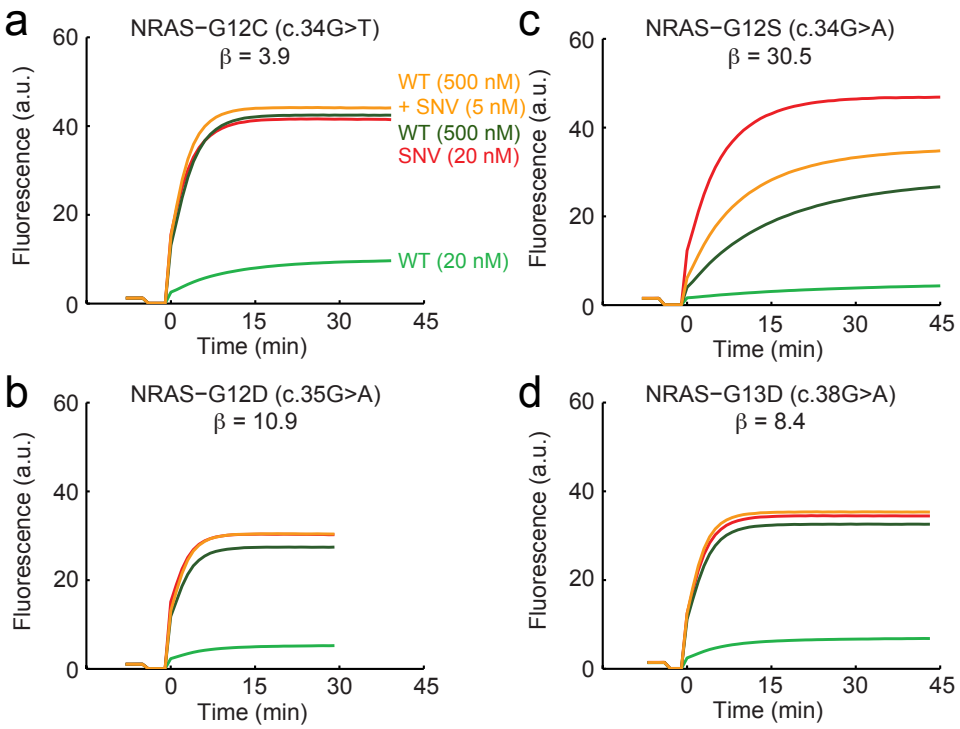

FIG. S4-8: Kinetic responses of X-Probes targeting NRAS mutations.

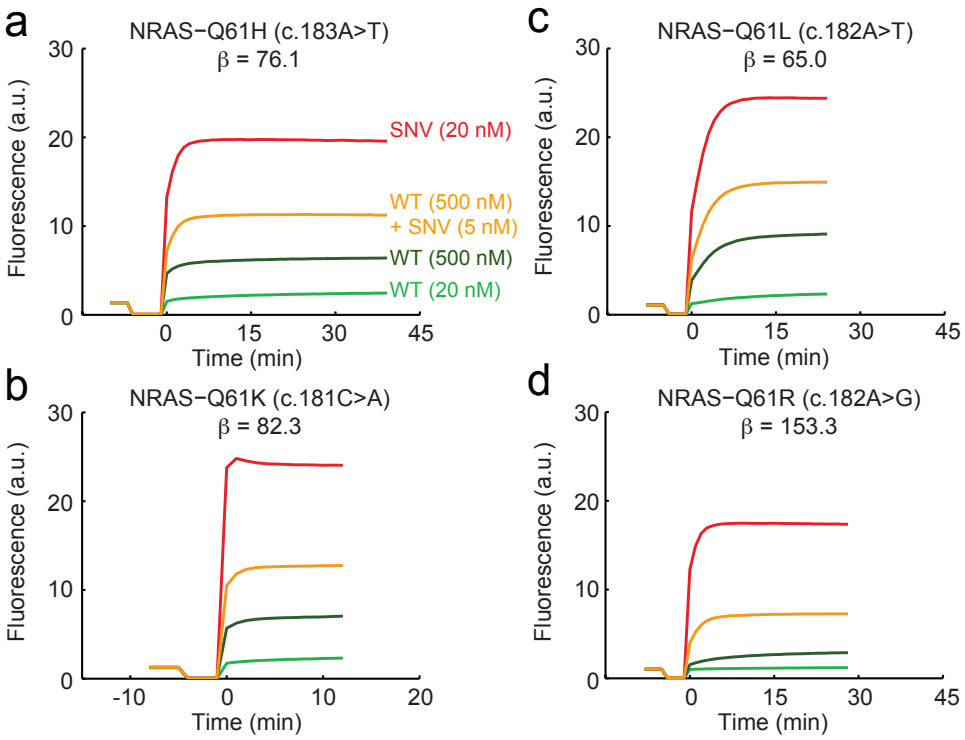

FIG. S4-9: Kinetic responses of X-Probes targeting NRAS mutations.

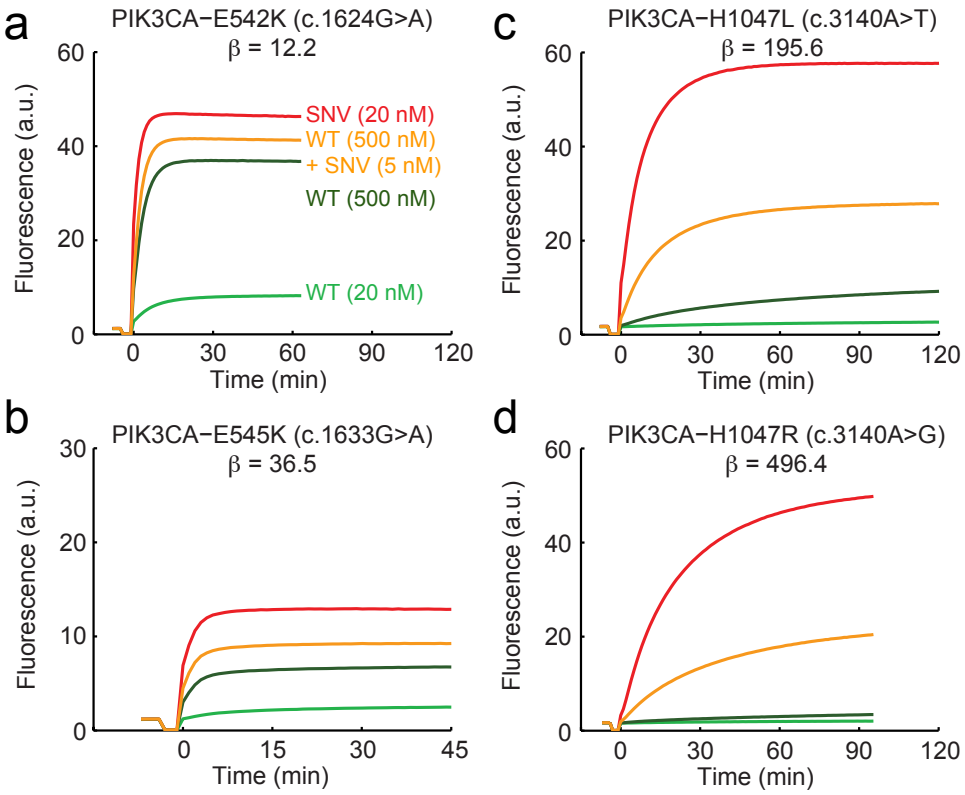

FIG. S4-10: Kinetic responses of X-Probes targeting PIK3CA mutations.

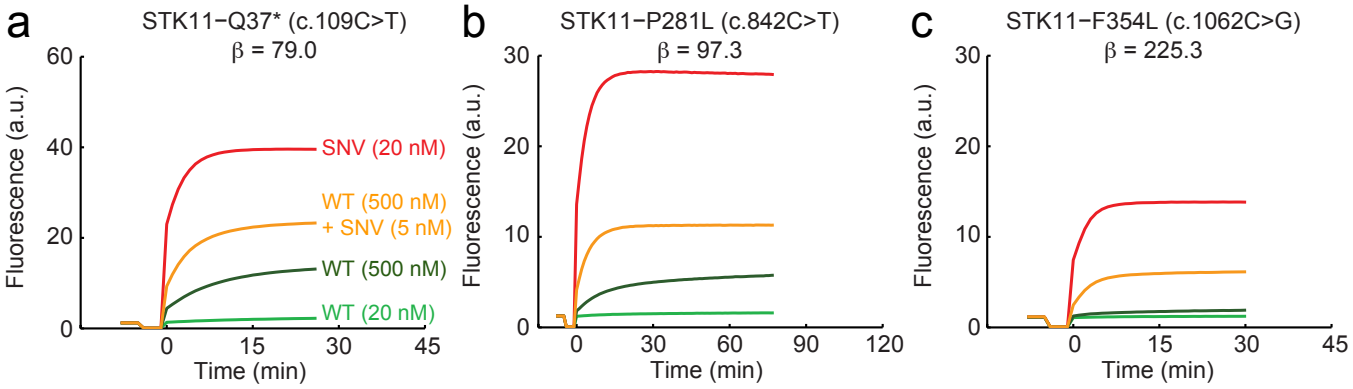

FIG. S4-11: Kinetic responses of X-Probes targeting STK11 mutations.

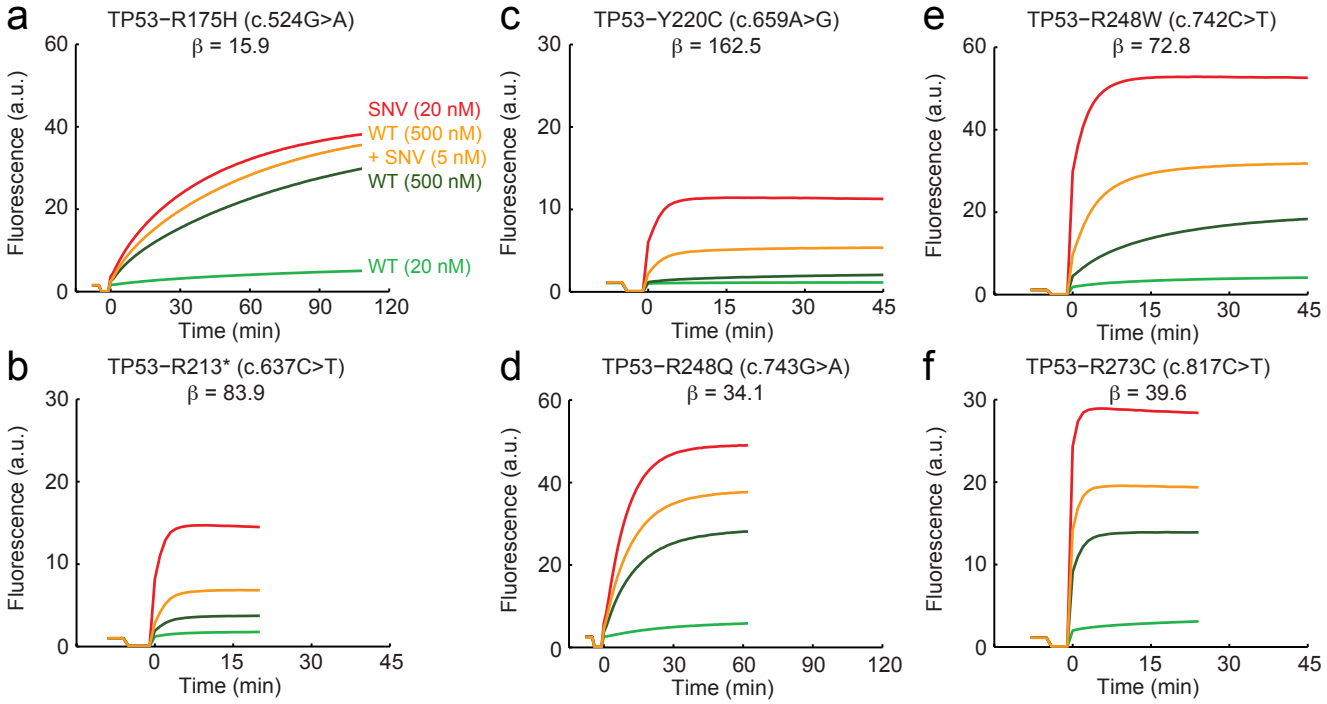

FIG. S4-12: Kinetic responses of X-Probes targeting TP53 mutations.

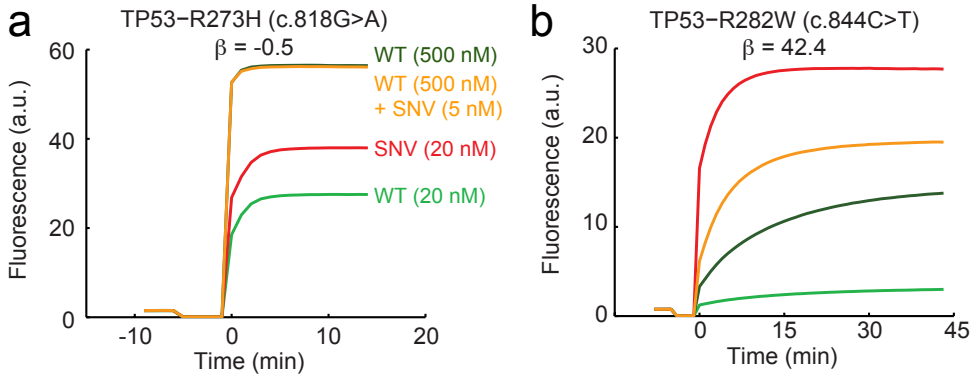

FIG. S4-13: Kinetic responses of X-Probes targeting TP53 mutations.

Text S5: Trial-to-trial Variability for X-Probes to DNA and RNA Targets.

One important metric for any assay or reagent is reproducibility of results. Given the relatively large number of experiments we performed, and the relatively long amount of time required for each experiment, we selected 6 representative X-Probe/target pairs to perform triplicate experiments on to characterize the trial-to-trial error of X-Probe reactions. These were EGFR-L858R (c.2573T>G), NRAS-Q61H (c.183A>T), KRAS-G12C (c.34G>T), KRAS-G12R (c.34G>C), PIK3CA-E545K (c.1633G>A), and PIK3CA-H1047R (c.3140A>G). In Section S4, we only reported β values calculated from the first experiment of each triplicate set. The triplicate kinetic traces, for both DNA and RNA targets, are shown in Fig. S5-1 through S5-3, and their mean and sample standard deviations are summarized in Table S5.

Target mutation	Target type	Mean β value	Std. dev.	Coeff. of variation
EGFR-L858R (c.2573T>G)	DNA	153.2	7.4	4.9%
NRAS-Q61H (c.183A>T)	DNA	75.4	1.1	1.4%
KRAS-G12C (c.34G>T)	DNA	18.5	0.4	2.4%
KRAS-G12R (c.34G>C)	DNA	105.7	0.9	0.8%
PIK3CA-E545K (c.1633G>A)	DNA	36.0	0.5	1.3%
PIK3CA-H1047R (c.3140A>G)	DNA	495.2	5.3	1.1%
EGFR-L858R (c.2573T>G)	RNA	319.5	30.3	9.5%
NRAS-Q61H (c.183A>T)	RNA	-2.5	2.4	-96.1%
KRAS-G12C (c.34G>T)	RNA	50.1	5.4	10.8%
KRAS-G12R (c.34G>C)	RNA	69.9	5.9	8.4%
PIK3CA-E545K (c.1633G>A)	RNA	53.1	9.0	16.9%
PIK3CA-H1047R (c.3140A>G)	RNA	198.2	57.0	28.7%

TABLE S5: Summary of trial-to-trial variability for triplicate experiments.

Trial-to-trial variability for DNA target experiments were low; for all experiments, the coefficient of variation (sample standard deviation divided by mean) was below 5%. For experiments involving RNA targets, trial-to-trial variability was somewhat higher, with standard deviations ranging up to 10, or coefficient of variation up to 30%.

The less consistent performance for RNA targets is likely due to our methodology as well as X-Probe design principle. In order to reduce the risk of RNA degradation due to RNAse contamination, we introduced roughly 0.1% RNAse-Zap solution into each RNA sample. One side effect of the RNAse-Zap is that it caused the solution to be more "soapy", and the pipetting volumes became less accurate due to inconsistent amounts of residue left in the pipette tips. Additionally, relatively larger difference in reaction times can also affect the consistency of performance for RNA targets. (Fig. S5-1d, Fig. S5-3d). Furthermore, $\Delta G^{\circ}_{\text{rxn1}}$ affects the reaction thermodynamics and so that the specificity sensitively. However, for RNA target, we did not redesign the X-Probe using RNA-DNA hybridization parameters. Due to the differences between DNA-DNA hybridization and RNA-DNA hybridization parameters, the real $\Delta G^{\circ}_{\text{rxn}}$ for X-Probe reacting with RNA target may deviate from the optimal ΔG° significantly. We do not believe that the higher variability for RNA is intrinsic to the X-Probe system.

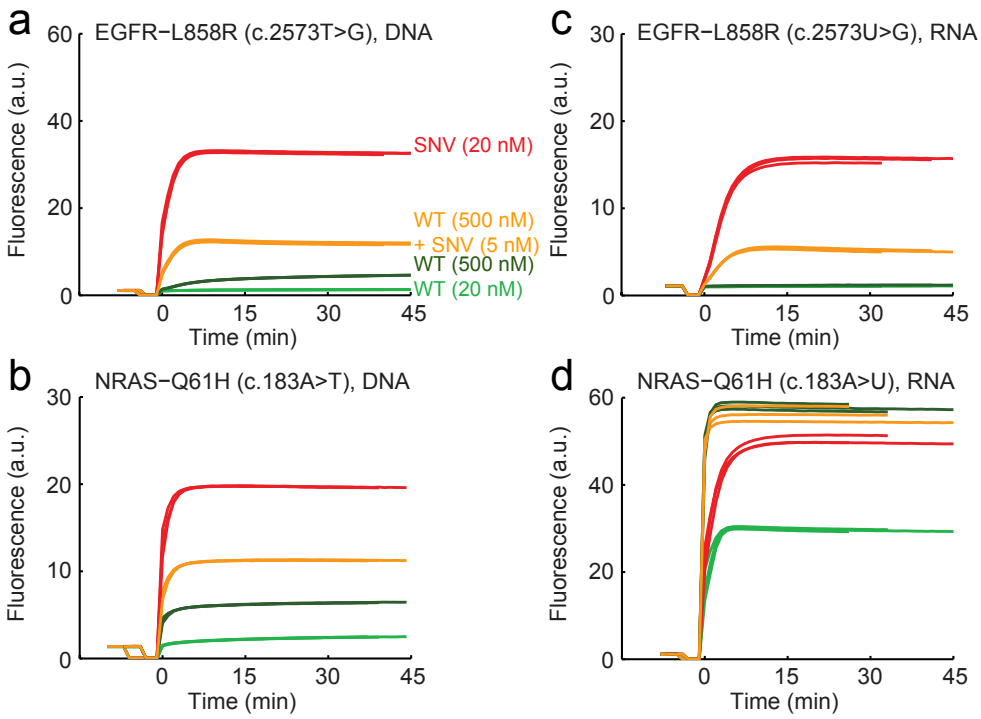

FIG. S5-1: Trial-to-trial variability for X-Probes targeting the EGFR-L858R and NRAS-Q61H mutations (both DNA and RNA targets). Three independent experiments for each set of conditions are plotted; some traces showed such good agreement that visual distinction is difficult.

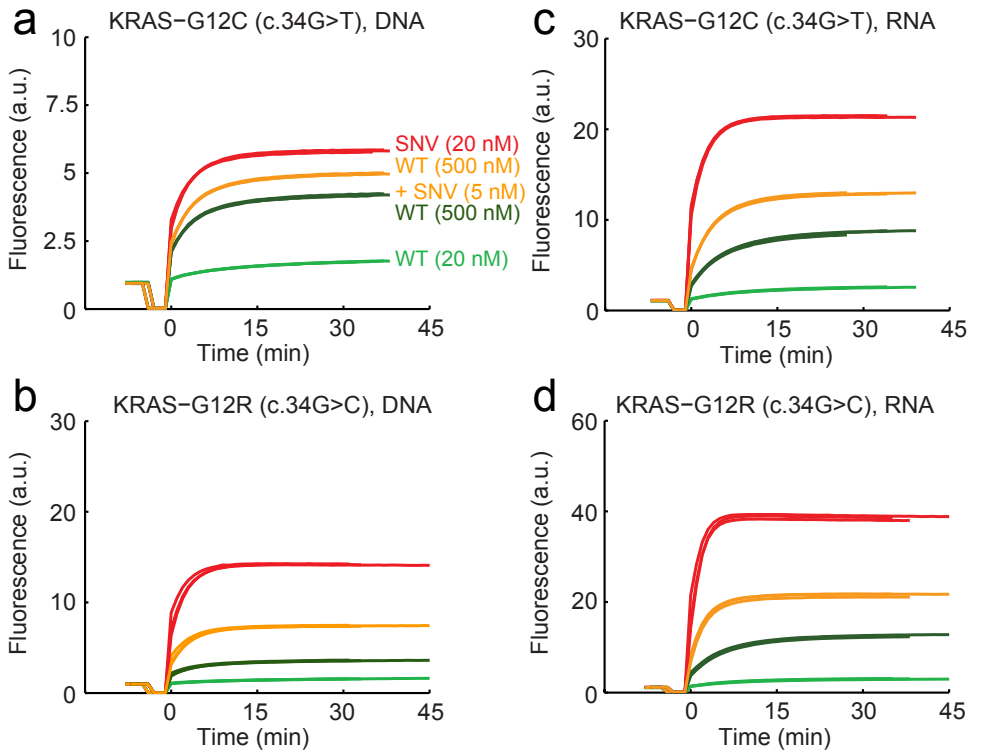

FIG. S5-2: Trial-to-trial variability for X-Probes targeting the KRAS-G12C and KRAS-G12R mutations (both DNA and RNA targets). Three independent experiments for each set of conditions are plotted; some traces showed such good agreement that visual distinction is difficult.

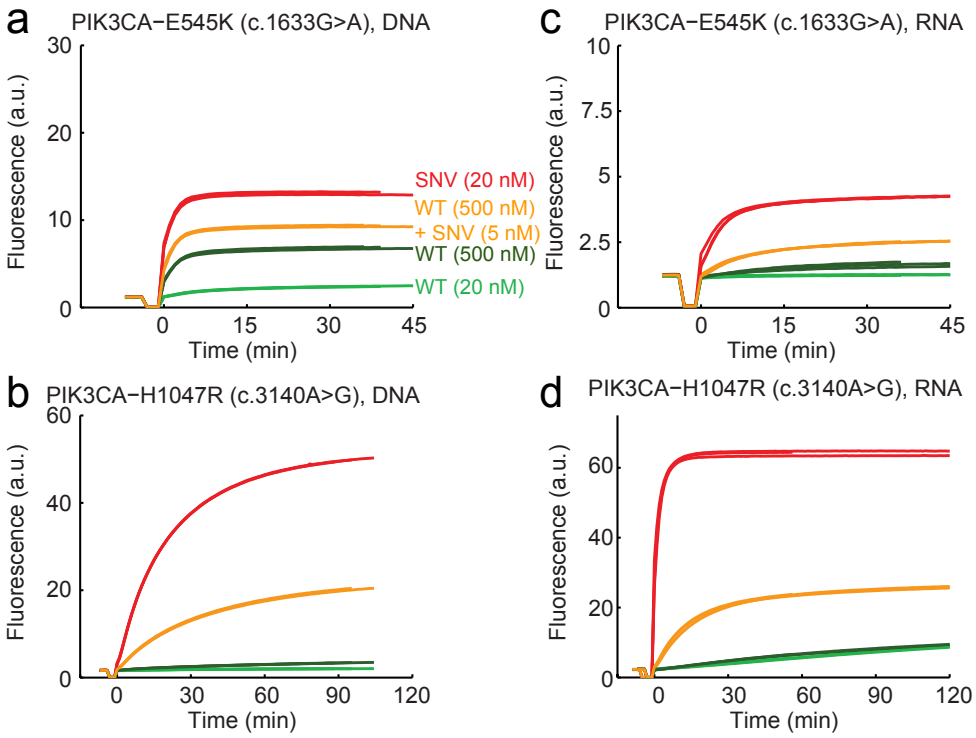

FIG. S5-3: Trial-to-trial variability for X-Probes targeting the PIK3CA-E545K and PIK3CA-H1047R mutations (both DNA and RNA targets). Three independent experiments for each set of conditions are plotted; some traces showed such good agreement that visual distinction is difficult.

Text S6: Simulations of Competitive Compositions using X-Probe and toehold Sink

Ordinary Differential Equation Simulation

We use X-Probe as the specific architecture for our probes and unlabeled toehold probe for the sinks due to X-Probes' economic advantages. To provide more accurate description to the behavior of each species in this particular system, we modified the ordinary differential equation model of dissociative Probe and Sink to include reactions between WT/SNV and unintended species QPC generated during X-Probe formation (Fig. S6-1). Another species Q is also present in the solution, but Q by itself does not react significantly with any of the other species in solution.

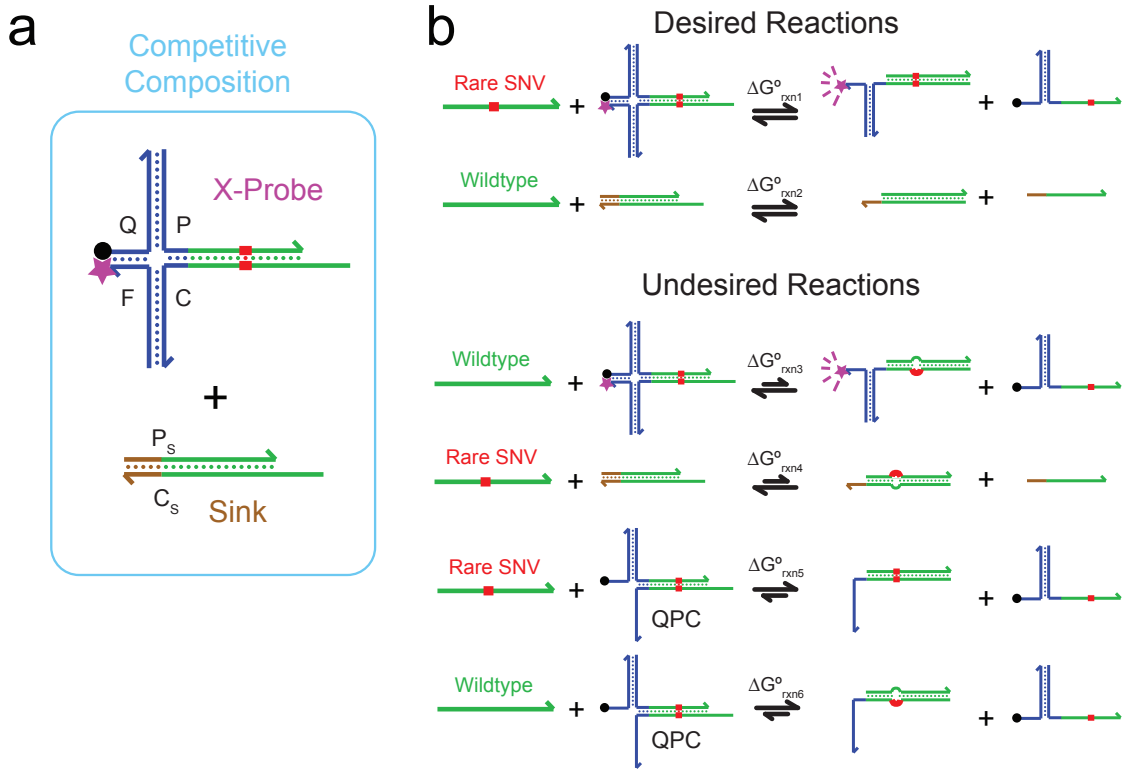

FIG. S6-1: Competitive Composition **(a)** architectures used in the work, and **b** reactions.

The chemical reactions of modified ordinary differential equation model, not including short-lived intermediates, are:

$$SNV + FQPC \underset{k_{1-}}{\overset{k_{1+}}{\rightleftharpoons}} SNV \cdot FC + PQ \qquad \Delta G^{\circ}_{\text{rxn1}}$$

$$WT + P_S C_S \underset{k_{2-}}{\overset{k_{2+}}{\rightleftharpoons}} WT \cdot C_S + P_S \qquad \Delta G^{\circ}_{\text{rxn2}}$$

$$WT + FQPC \underset{k_{3-}}{\overset{k_{3+}}{\rightleftharpoons}} WT \cdot FC + PQ \qquad \Delta G^{\circ}_{\text{rxn3}}$$

$$SNV + P_S C_S \underset{k_{4-}}{\overset{k_{4+}}{\rightleftharpoons}} SNV \cdot C_S + P_S \qquad \Delta G^{\circ}_{\text{rxn4}}$$

$$SNV + QPC \underset{k_{5-}}{\overset{k_{5+}}{\rightleftharpoons}} C \cdot SNV + PQ \qquad \Delta G^{\circ}_{\text{rxn5}}$$

$$WT + QPC \underset{k_{6-}}{\overset{k_{6+}}{\rightleftharpoons}} C \cdot WT + PQ \qquad \Delta G^{\circ}_{\text{rxn6}}$$

wherein k_+ and k_- represent the forward and the reverse rate constants. As before, the values of all forward reaction rate constants k_+ are assumed to be 3×10^5 $\text{M}^{-1}\text{s}^{-1}$; this is estimated based on previous studies [2] and

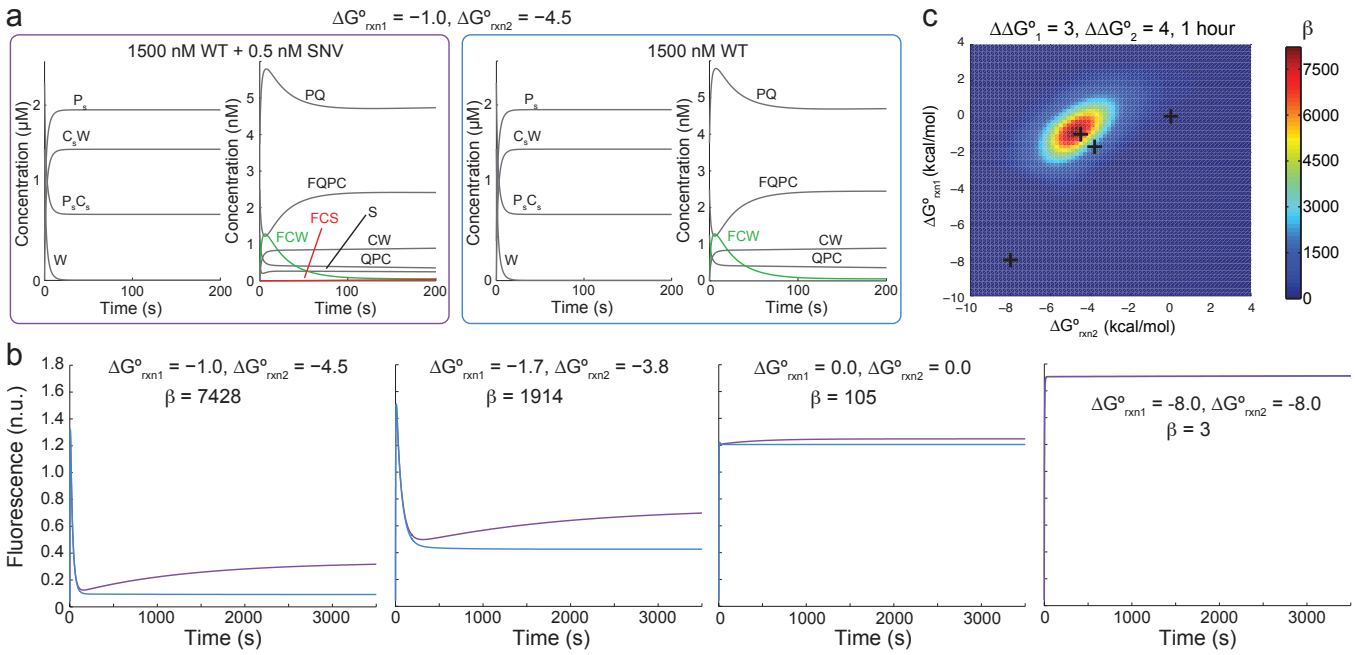

FIG. S6-2: Simulation Results and Impact of $\Delta G^\circ_{\text{rxn1}}$ and $\Delta G^\circ_{\text{rxn2}}$. **(a)** Kinetic traces for the concentrations of different species. For all simulations shown here, $\Delta\Delta G^\circ_1 = +3$ kcal/mol, $\Delta\Delta G^\circ_2 = +4$ kcal/mol, and initial concentrations are [S] = 0.5 nM, [W] = 1500 nM, [FQPC] = 2.5 nM, [QPC] = 1.25 nM, [PQ] = 3.75 nM, [P_SC_S] = 2250 nM, and [P_S] = 450 nM. High fluorescence species are shown in red (SNV bound) or green (WT bound). **(b)** Simulated fluorescence responses of the Competitive Compositions with different $\Delta G^\circ_{\text{rxn1}}$ and $\Delta G^\circ_{\text{rxn2}}$ values in reaction with a sample with WT (light blue) and WT with 0.033% SNV (purple). The initial fluorescence spike is due to the rapid but unfavorable initial reaction between the WT and the X-Probe, which is reversed over time. **(c)** Simulation summary of β after 1 hour of reaction for different values of $\Delta G^\circ_{\text{rxn1}}$ and $\Delta G^\circ_{\text{rxn2}}$.

our internal calibration experiments. The reverse rate constants can be calculated as

$$k_- = \frac{k_+}{K_{\text{eq}}} = k_+ e^{\Delta G^\circ_{\text{rxn}}/R\tau}$$

where $\Delta G^\circ_{\text{rxn}}$ denotes the standard free energy of the relevant reaction. For the reactions between WT or SNV and QPC, $\Delta G^\circ_{\text{rxn5}} \equiv \Delta G^\circ_{\text{rxn1}} + \Delta G^\circ_{\text{NH}}$ and $\Delta G^\circ_{\text{rxn6}} \equiv \Delta G^\circ_{\text{rxn1}} + \Delta\Delta G^\circ_1 + \Delta G^\circ_{\text{NH}}$, where $\Delta G^\circ_{\text{NH}}$ denotes the hybridization standard free energy of nonhomologous region missing in QPC, and has estimated value of -8 kcal/mol for the X-Probe sequences used in this work.

For convenience, we abbreviate SNV to 'S' and WT to 'WT'. The corresponding ordinary differential equations are:

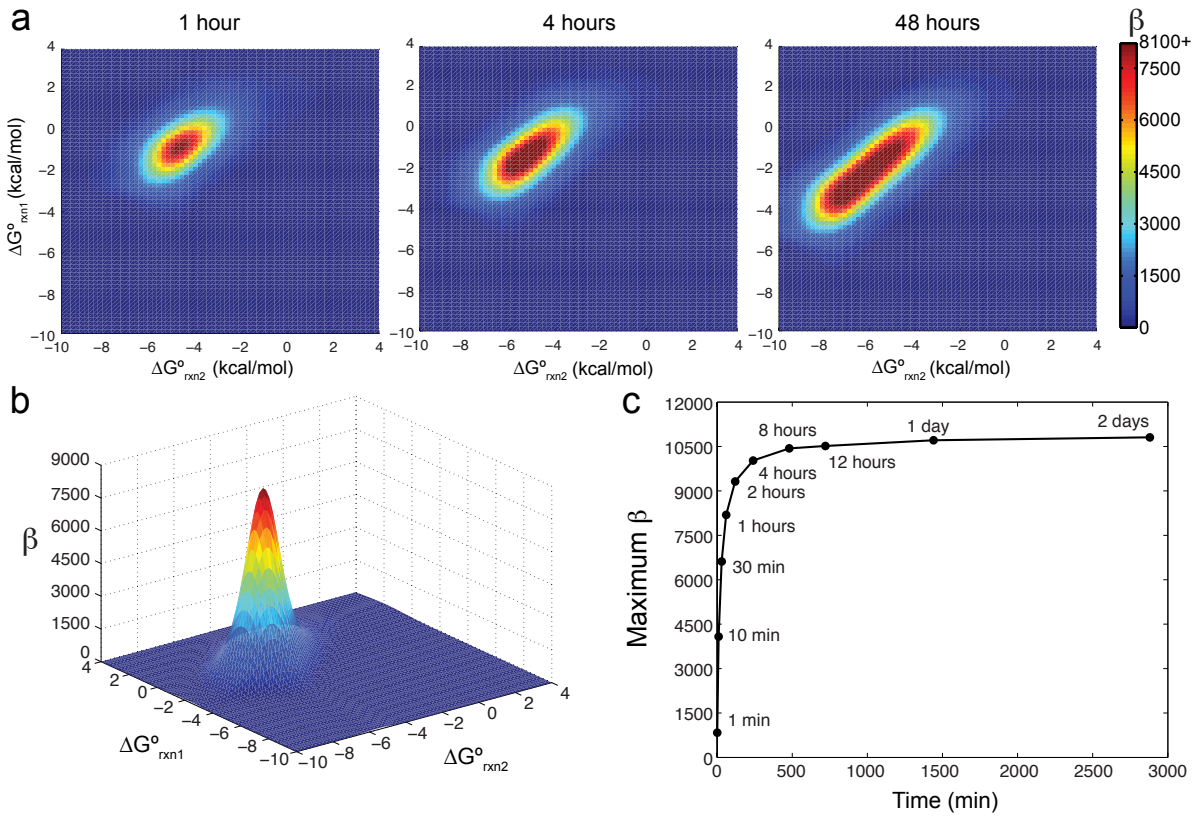

FIG. S6-3: ODE simulation result summaries for different reaction times. **(a)** Dependence of β on $\Delta G^{\circ}_{\text{rxn1}}$ and $\Delta G^{\circ}_{\text{rxn3}}$ for different duration reactions. **(b)** Three-dimensional representation of the β dependence on $\Delta G^{\circ}_{\text{rxn1}}$ and $\Delta G^{\circ}_{\text{rxn3}}$ at t= 1 hr. **(c)** Dependence of optimized β on reaction time.

$$
\begin{aligned}
\frac{d[S]}{dt} &= -k_{1+}[FQPC][S] + k_{1-}[S\cdot FC][PQ] - k_{4+}[P_SC_S][S] + k_{4-}[S\cdot C_S][P_S] - \\
&\quad k_{5+}[QPC][S] + k_{5-}[C\cdot S][PQ] \\
\frac{d[W]}{dt} &= -k_{3+}[FQPC][W] + k_{3-}[W\cdot FC][PQ] - k_{2+}[P_SC_S][W] + k_{2-}[W\cdot C_S][P_S] - \\
&\quad k_{6+}[QPC][W] + k_{6-}[C\cdot W][PQ] \\
\frac{d[PQ]}{dt} &= k_{1+}[FQPC][S] - k_{1-}[S\cdot FC][PQ] + k_{3+}[FQPC][W] - k_{3-}[W\cdot FC][PQ] + \\
&\quad k_{5+}[QPC][S] - k_{5-}[C\cdot S][PQ] + k_{6+}[QPC][W] - k_{6-}[C\cdot W][PQ] \\
\frac{d[FQPC]}{dt} &= -k_{1+}[FQPC][S] + k_{1-}[S\cdot FC][PQ] - k_{3+}[FQPC][W] + k_{3-}[W\cdot FC][PQ] \\
\frac{d[P_S]}{dt} &= k_{4+}[P_SC_S][S] - k_{4-}[S\cdot C_S][P_S] + k_{2+}[P_SC_S][W] - k_{2-}[W\cdot C_S][P_S] \\
\frac{d[P_SC_S]}{dt} &= -k_{4+}[P_SC_S][S] + k_{4-}[S\cdot C_S][P_S] - k_{2+}[P_SC_S][W] + k_{2-}[W\cdot C_S][P_S] \\
\frac{d[S\cdot FC]}{dt} &= k_{1+}[FQPC][S] - k_{1-}[S\cdot FC][PQ] \\
\frac{d[W\cdot FC]}{dt} &= k_{3+}[FQPC][W] - k_{3-}[W\cdot FC][PQ] \\
\frac{d[S\cdot C_S]}{dt} &= k_{4+}[P_SC_S][S] - k_{4-}[S\cdot C_S][P_S] \\
\frac{d[W\cdot C_S]}{dt} &= k_{2+}[P_SC_S][W] - k_{2-}[W\cdot C_S][P_S] \\
\frac{d[QPC]}{dt} &= -k_{5+}[QPC][S] + k_{5-}[C\cdot S][PQ] - k_{6+}[QPC][W] + k_{6-}[C\cdot W][PQ] \\
\frac{d[C\cdot S]}{dt} &= k_{5+}[QPC][S] - k_{5-}[C\cdot S][PQ] \\
\frac{d[C\cdot W]}{dt} &= k_{6+}[QPC][W] - k_{6-}[C\cdot W][PQ]
\end{aligned}
$$

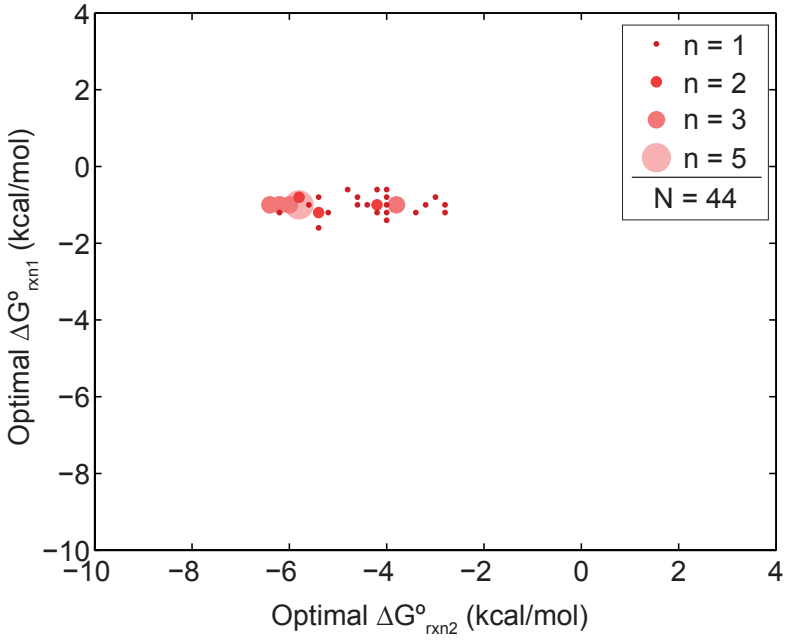

FIG. S6-4: Distribution of 44 optimal $\Delta G^\circ_{\text{rxn}}$ combinations.

The ordinary differential equation model is simulated using MATLAB's stiff "ode23s" solver, using relative tolerance of 10^{-4} and absolute tolerance of 10^{-20}.

Fig. S6-2a shows kinetic traces of various species in the system for a particular pair of $\Delta G^\circ_{\text{rxn}}$ values, and Fig. S6-2b shows time-based fluorescence response (represented as concentrations of fluorescent species) of Competitive Compositions with different $\Delta G^\circ_{\text{rxn1}}$ and $\Delta G^\circ_{\text{rxn2}}$. Fig. S6-2c summarize the predicted β after 1 hour of reaction plotted against the values of $\Delta G^\circ_{\text{rxn1}}$ and $\Delta G^\circ_{\text{rxn2}}$; shown as black "+" are different combinations of $\Delta G^\circ_{\text{rxn}}$ whose fluorescence kinetics are plotted in Fig. S6-2b. Simulations only includes reactions between WT and Probe and Sink are based on a subset of the ordinary differential equations displayed above.

As can be seen, the optimal $\Delta G^\circ_{\text{rxn}}$ values combination of this system is roughly -0.9 kcal/mol for $\Delta G^\circ_{\text{rxn1}}$ and -4.7 kcal/mol for $\Delta G^\circ_{\text{rxn2}}$. Even relatively small deviations from the optimal combination of $\Delta G^\circ_{\text{rxn1}}$ and $\Delta G^\circ_{\text{rxn2}}$ can severely reduce observed β. For example, 0.7 kcal/mol deviations in $\Delta G^\circ_{\text{rxn1}}$ and $\Delta G^\circ_{\text{rxn2}}$ results in a 4-fold reduction of β (from 7428 to 1914). A naive design, such as by designing both Probe and Sink to have $\Delta G^\circ_{\text{rxn}} = -8$ kcal/mol (as in the case of ref. [9]), will result in observed β that is more than 1000-fold lower than optimal.

Although we have done our best to design the X-Probe and Sink based on simulation guidance, errors in literature parameters for DNA hybridization may lead to about 1 kcal/mol deviation in $\Delta G^\circ_{\text{rxn}}$ values from the intended of all X-Probe and Sink designs. Thus, our experimental results, while encouraging at being able to reliably detect rare alleles down to 0.1%, are a factor of 10 below that which is attainable through optimized knowledge-driven design.

Competitive Composition performance is sensitive to reaction time (Fig. S6-3). As reaction time increases, the range of high-performing $\Delta G^\circ_{\text{rxn1}}$ and $\Delta G^\circ_{\text{rxn2}}$ broadens to the lower-left (more negative $\Delta G^\circ_{\text{rxn}}$ values). Fig. S6-3c plots the dependence of optimal β on reaction time; optimal β initially increases sharply, but plateaus after roughly 4 hours.

Additionally, the optimal $\Delta G^\circ_{\text{rxn}}$ values shift for different $\Delta\Delta G^\circ$ values. For the 44 SNV/WT pairs we have tested, optimal $\Delta G^\circ_{\text{rxn1}}$ and $\Delta G^\circ_{\text{rxn2}}$ values can vary from -1.6 to -0.6 kcal/mol and -6.4 to -2.8 kcal/mol according to simulations for 1 hour (Fig. S6-4).

Definition and Calculation Method of $\Delta\Delta G^\circ$

The values of $\Delta\Delta G^\circ_1$ and $\Delta\Delta G^\circ_2$ in this manuscript are defined as thermodynamic penalties of unpreferred reactions as compared to corresponding preferred energies:

$$\begin{aligned}\Delta\Delta G^\circ_1 &\equiv E_3 - E_1 = \Delta G^\circ_{\text{rxn3}} - \Delta G^\circ_{\text{rxn1}} \\ \Delta\Delta G^\circ_2 &\equiv E_4 - E_2 = \Delta G^\circ_{\text{rxn4}} - \Delta G^\circ_{\text{rxn2}}\end{aligned}$$

For Competitive Composition with X-Probes and toehold Sinks, the values of $\Delta G^\circ_{\text{rxn}}$ in turn are defined as:

$$\begin{aligned}\Delta G^\circ_{\text{rxn1}} &= \Delta G^\circ(S \cdot FC) + \Delta G^\circ(PQ) - \Delta G^\circ(FQPC) - \Delta G^\circ(S) \\ \Delta G^\circ_{\text{rxn2}} &= \Delta G^\circ(W \cdot C_S) + \Delta G^\circ(P_S) - \Delta G^\circ(P_S C_S) - \Delta G^\circ(W) \\ \Delta G^\circ_{\text{rxn3}} &= \Delta G^\circ(W \cdot FC) + \Delta G^\circ(PQ) - \Delta G^\circ(FQPC) - \Delta G^\circ(W) \\ \Delta G^\circ_{\text{rxn4}} &= \Delta G^\circ(S \cdot C_S) + \Delta G^\circ(P_S) - \Delta G^\circ(P_S C_S) - \Delta G^\circ(S)\end{aligned}$$

Substituting $\Delta G^\circ_{\text{rxn}}$ into $\Delta\Delta G^\circ$ expressions, we obtain:

$$\begin{aligned}\Delta\Delta G^\circ_1 &= \Delta G^\circ(W \cdot FC) - \Delta G^\circ(S \cdot FC) + \Delta G^\circ(S) - \Delta G^\circ(W) \\ \Delta\Delta G^\circ_2 &= \Delta G^\circ(S \cdot C_S) - \Delta G^\circ(W \cdot C_S) + \Delta G^\circ(W) - \Delta G^\circ(S)\end{aligned}$$

We define $\Delta\Delta G^\circ_{1m} \equiv (\Delta G^\circ(W \cdot FC) - \Delta G^\circ(S \cdot FC))$ and $\Delta\Delta G^\circ_{2m} \equiv (\Delta G^\circ(S \cdot C_S) - \Delta G^\circ(W \cdot C_S))$. Because the only difference between FC·W and FC·S is the polymorphic nucleotide, $\Delta\Delta G^\circ_{1m}$ can be computed solely based on the relative thermodynamics of the single-base mismatch bubble formed by the WT bound to the X-Probe. For example, if the WT sequence near the polymorphic nucleotide is 'CTG' and the SNV sequence near the polymorphic nucleotide is 'CGG', then $\Delta\Delta G^\circ_{1m}$ can be computed as:

$$\begin{aligned}\Delta\Delta G^\circ_{1m} &= \Delta G^\circ\begin{pmatrix}CTG\\GCC\end{pmatrix} - \Delta G^\circ\begin{pmatrix}CGG\\GCC\end{pmatrix} \\ &= \left(\Delta G^\circ\begin{pmatrix}CT\\GC\end{pmatrix} + \Delta G^\circ\begin{pmatrix}TG\\CC\end{pmatrix}\right) - \left(\Delta G^\circ\begin{pmatrix}CG\\GC\end{pmatrix} + \Delta G^\circ\begin{pmatrix}GG\\CC\end{pmatrix}\right) = 4.9 \text{ kcal/mol (at 37 °C in 1 M Na}^+\text{)}\end{aligned}$$

Similarly, $\Delta\Delta G^\circ_{2m}$ for the same WT/SNV sequences can be computed as:

$$\begin{aligned}\Delta\Delta G^\circ_{2m} &= \Delta G^\circ\begin{pmatrix}CGG\\GAC\end{pmatrix} - \Delta G^\circ\begin{pmatrix}CTG\\GAC\end{pmatrix} \\ &= \left(\Delta G^\circ\begin{pmatrix}CG\\GA\end{pmatrix} + \Delta G^\circ\begin{pmatrix}GG\\AC\end{pmatrix}\right) - \left(\Delta G^\circ\begin{pmatrix}CT\\GA\end{pmatrix} + \Delta G^\circ\begin{pmatrix}TG\\AC\end{pmatrix}\right) = 2.8 \text{ kcal/mol(at 37 °C in 1 M Na}^+\text{)}\end{aligned}$$

According to nearest neighbor model of nucleic acid hybridization, right and left neighboring bases influence the also affect $\Delta\Delta G^\circ_{1m}$ and $\Delta\Delta G^\circ_{2m}$ values. Therefore, there are a total of 192 different $\Delta\Delta G^\circ_m$ values due to a single-base mismatch (4 possibilities for each neighboring base, 4 possibilities for the WT nucleotide, and 3 possibilities for the SNV nucleotide). The distribution of $\Delta\Delta G^\circ$ values for DNA-DNA interaction is summarized in Fig. S6-5a.

It is important to note that the values of $\Delta\Delta G^\circ_{1m}$ and $\Delta\Delta G^\circ_{2m}$ for any given SNV/WT pair exists a strong anti-correlation ($R^2 = 0.56$) (Fig. S6-5b). Thus, the sum of $\Delta\Delta G^\circ_{1m}$ and $\Delta\Delta G^\circ_{2m}$ has a smaller standard deviation (0.73 kcal/mol) than the individual $\Delta\Delta G^\circ_m$ values (1.0 kcal/mol), despite having doubled the mean (Fig. S6-5c). Another important observation is that $\Delta\Delta G^\circ_{1m} + \Delta\Delta G^\circ_{2m} = \Delta\Delta G^\circ_1 + \Delta\Delta G^\circ_2$, because the secondary structures of WT and SNV act in opposite direction on $\Delta\Delta G^\circ_1$ and $\Delta\Delta G^\circ_2$. The aggregated result is that, in addition to significant improvement in performance, Competitive Composition is expected to exhibit much less variation than X-Probe alone among different mismatch identities, consistent with our experimental observations (Fig. 5bc).

Finally, we address the question of whether the sum $\Delta\Delta G^\circ_1 + \Delta\Delta G^\circ_2$ is an appropriate metric for estimating the β performance of the Competitive Composition system. To do so, we performed a large number of simulations to obtain the maximum β values for different combinations of $\Delta\Delta G^\circ_1$ and $\Delta\Delta G^\circ_2$, in each case discovering the optimal $\Delta G^\circ_{\text{rxn1}}$ and $\Delta G^\circ_{\text{rxn2}}$ values through systematic simulation. We noticed a strong linear relationship between the maximum observed β_{MAX} value and a linear combination of the two $\Delta\Delta G^\circ$ values, $(\Delta\Delta G^\circ_1 + \gamma\Delta\Delta G^\circ_2)$ (Fig. S6-6a). Surprisingly, $\gamma = 1$ (equal weighting of the two $\Delta\Delta G^\circ$) was not the best predictor of β_{MAX}; instead, $\gamma = 0.931$ yielded the maximum correlation with β_{MAX}, with $R^2 = 0.997$ (Fig. S6-6b).

Thus, $\Delta\Delta G^\circ_1$ and $\Delta G^\circ_{\text{rxn1}}$ is marginally more important in rare allele detection performance.

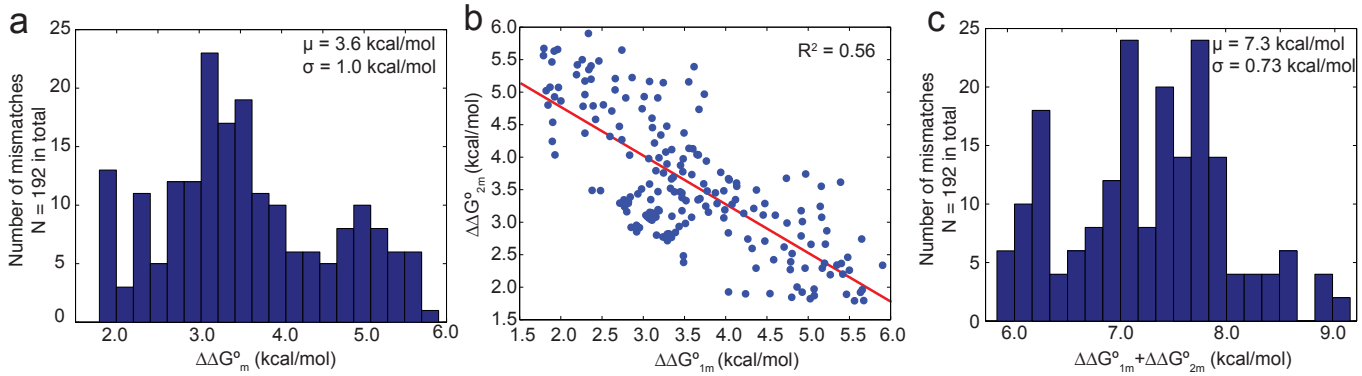

FIG. S6-5: Analysis of single-base mismatch $\Delta\Delta G^\circ$ values. **(a)** $\Delta\Delta G^\circ$ distribution at 37 °C in 1M Na^+. **(b)** Anti-correlation between $\Delta\Delta G^\circ_{1m}$ and $\Delta\Delta G^\circ_{2m}$ values. **(c)** Distribution of $(\Delta\Delta G^\circ_{1m} + \Delta\Delta G^\circ_{2m})$.

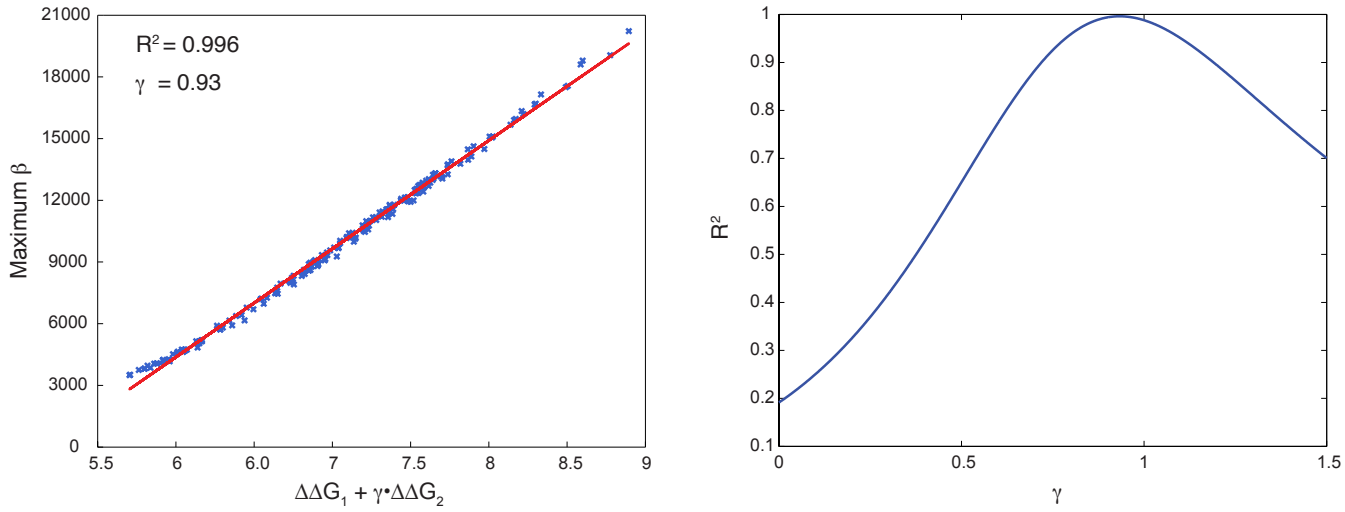

FIG. S6-6: Effects of $\Delta\Delta G^\circ_1$ and $\Delta\Delta G^\circ_2$ on maximum achievable value of β for a 0.033% SNV load. **(a)** Maximum observed β (based on optimized values of $\Delta G^\circ_{\text{rxn1}}$ and $\Delta G^\circ_{\text{rxn2}}$) possesses strong correlation with a linear combination of $\Delta\Delta G^\circ_1$ and $\Delta\Delta G^\circ_2$, with a scaling constant of γ on the latter. **(b)** Different values of γ lead to different correlation constants R^2, with a maximum $R^2 = 0.997$ at $\gamma = 0.931$.

Text S7: Competitive Composition experiments with labeled Sink

Shown in this section are experimental results of Competitive Composition with both Probe and Sink being labeled. Considering the cost of testing such Competitive Composition on many different sequences, we showcase capability of using labeled Sink as a self-calibration of the assay only on one Competitive Composition system, targeting EGFR L858R (c.2573>G)/EGFR WT pair.

Sink protector (with RQ at the 5′ end) and complement (with Alexa 647 at the 3′ end) were ordered at the 1 umole scale with HPLC purification from IDT. The sequences and the formulations of the X-Probe and the Sink remain preserved (see also Method and Section S12). Based on our internal calibration experiment, the optimal excitation and emission wavelength of Alexa 647 fluorophore is 646 nm/663 nm. However, Sink concentration is 300-fold higher than that of X-Probe concentration, so using optimal excitation/emission wavelengths for would cause significant detection (photodetector saturation). Therefore, we decide to use suboptimal ex/em wavelength for Alexa 647 fluorophore to compensate for its higher concentration. We chose 685 nm as excitation and 710 nm as emission wavelength for Alexa 647 fluorophore to minimize fluorescence bleed-through, and to ensure fluorescence signal elicited by Sink is comparable with that by X-Probe.

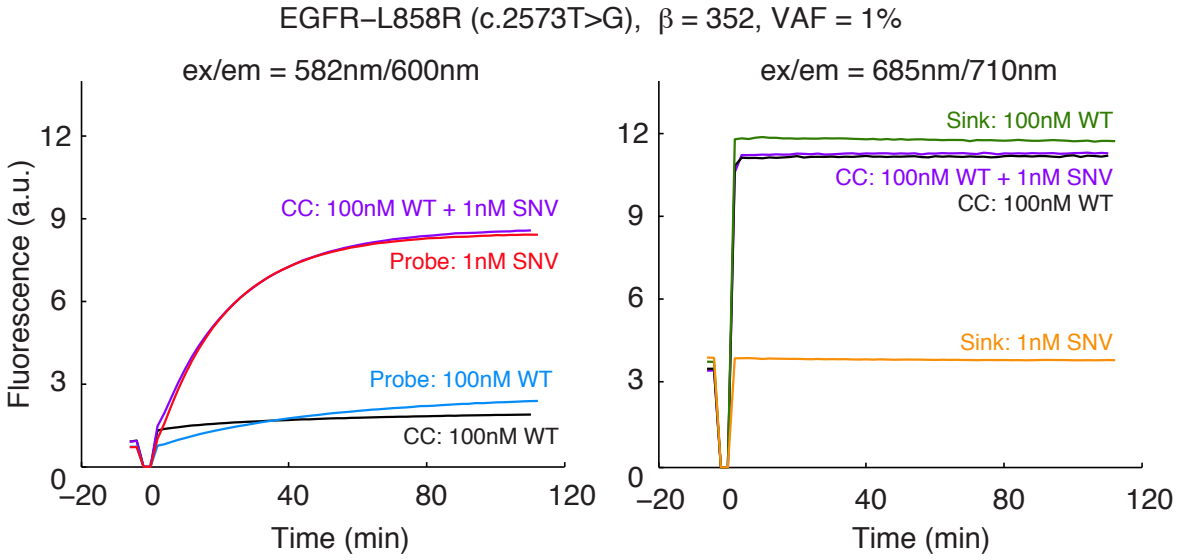

FIG. S7: Fluorescent response of Competitive Composition experiments with labeled Sink. The Competitive Composition is designed to target EGFR-L858R (c.2573>G) mutation, with X-Probe functionalized with ROX fluorophore and Sink functionalized with Alexa 647 fluorophore (Section S12). Both excitation and emission channels are monitored simultaneously via a multi-group assay. Left panel: fluorescence responses of X-Probe only and Competitive Composition to WT, SNV and sample mixture at 1% VAF. Right panel: fluorescence responses of Sink only and Competitive Composition experiments.

Fig. S7 shows fluorescence response of Competitive Composition with labeled Sink, X-Probe only, and Sink only to 100 nM WT, 1nM SNV, and a mixture of 100 nM WT and 1 nM SNV. Here, X-Probe and Sink concentrations are 0.5 nM and 150 nM, respectively.

As can be seen, 100 nM WT with Competitive Composition (right panel, purple), WT/SNV mixture with Competitive Composition (right panel, black), and 100 nM WT with Sink (right panel, green) yield similar fluorescence signal in Alexa 647 channel, while 1 nM SNV with Sink shows insignificant signal increase as compared to background. In contrast, in ROX channel, 1 nM SNV elicits more than 3-fold additional fluorescence signal as compared to the 100 nM of WT, resulting in a background-constrained discrimination factor β over 300.

The aggregated conclusion from the above results is that in reactions between Competitive Composition and a mixed sample, most of interference between the dominant allele (WT) and rare-allele specific detection mechanism (Probe) can be suppressed by the Sink. The Probe and Sink are functioning as intended.

Text S8: Competitive Composition experiments with various SNV concentrations in WT background

Shown in this section are experimental results for 6 representative Competitive Compositions with varying Target (SNV) concentrations. Fig. S8-1 summarizes these results for SNV concentrations ranging 3.5 logs, from 0.1 nM to 300 nM, while the WT concentration remained constant (100 nM).

To maintain reasonable signal to noise ratio, X-Probe concentrations need to be comparable with SNV concentrations. Assuming the quenching ratio between ROX and RQ is 50, SNV molecule at 1/50 of the concentration of the Probe will result in the same fluorescence level as the background, if the reaction achieves 100% yield. To be conservative, we decided SNV concentrations should not be lower than 1/10 of the Probe concentration. Simultaneously, if SNVs are in large excess of the Probe, the fluorescence signal will be saturated and cannot provide either quantitative or qualitative information on target concentrations. Consequently, experiments are performed in two groups: a high concentration group and a low concentration group, with the former using 20 nM X-Probe concentration, and the latter using 0.5 nM (see also Methods Section).

As can be seen, the fluorescence signal monotonically (but not linearly) increases with SNV concentrations, showing semi-quantitative feature of the Competitive Composition reactions. The raw fluorescence traces for each experiment are shown in Fig. S8-2 and Fig. S8-3.

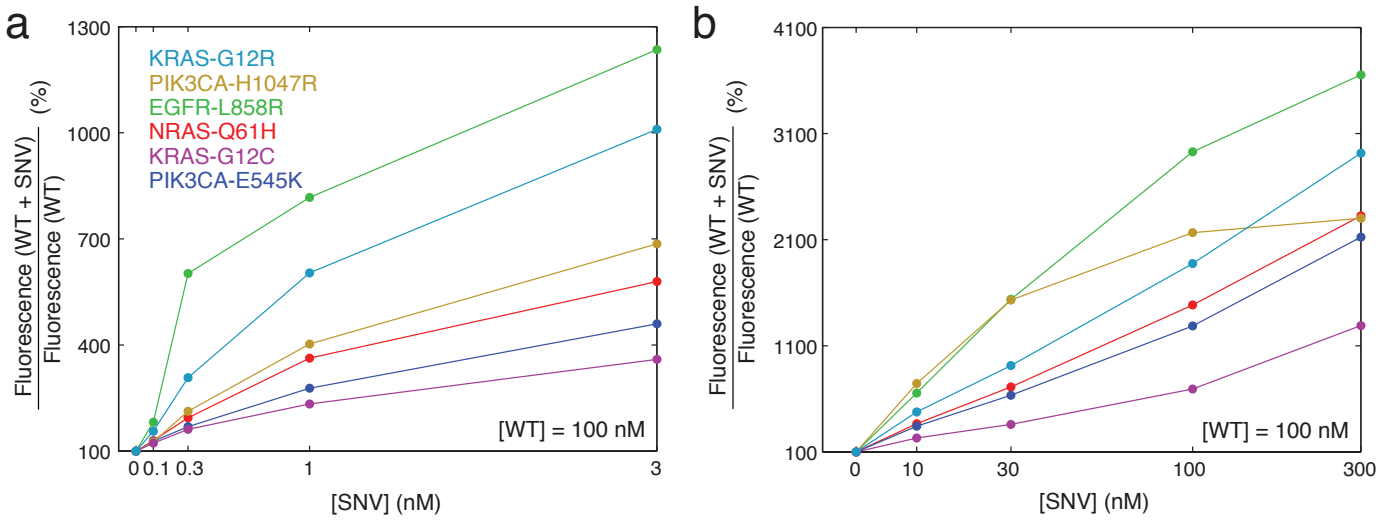

FIG. S8-1: Summary of signal increases observed for 6 Competitive Composition reactions with different concentrations of SNV, in a background of WT.

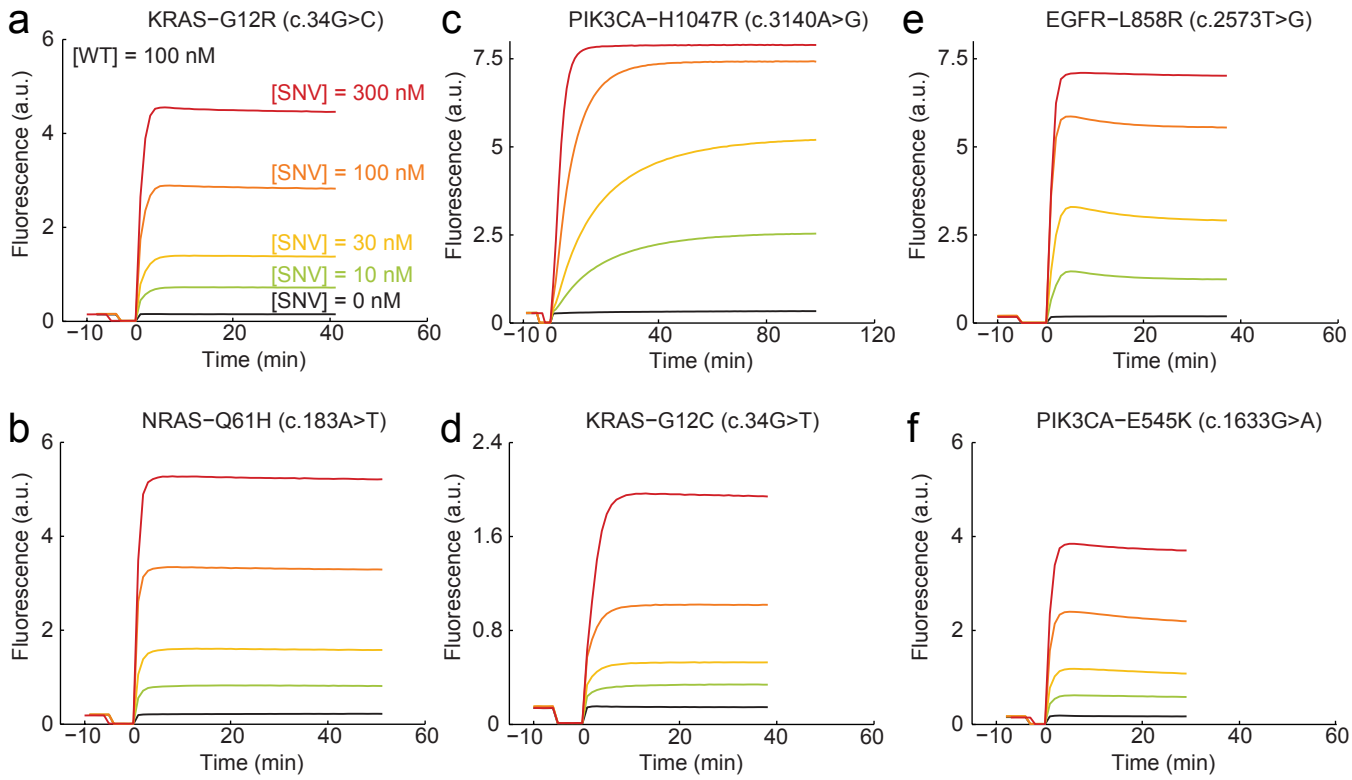

FIG. S8-2: Kinetic responses of Competitive Composition reactions with 10 to 300 nM SNV.

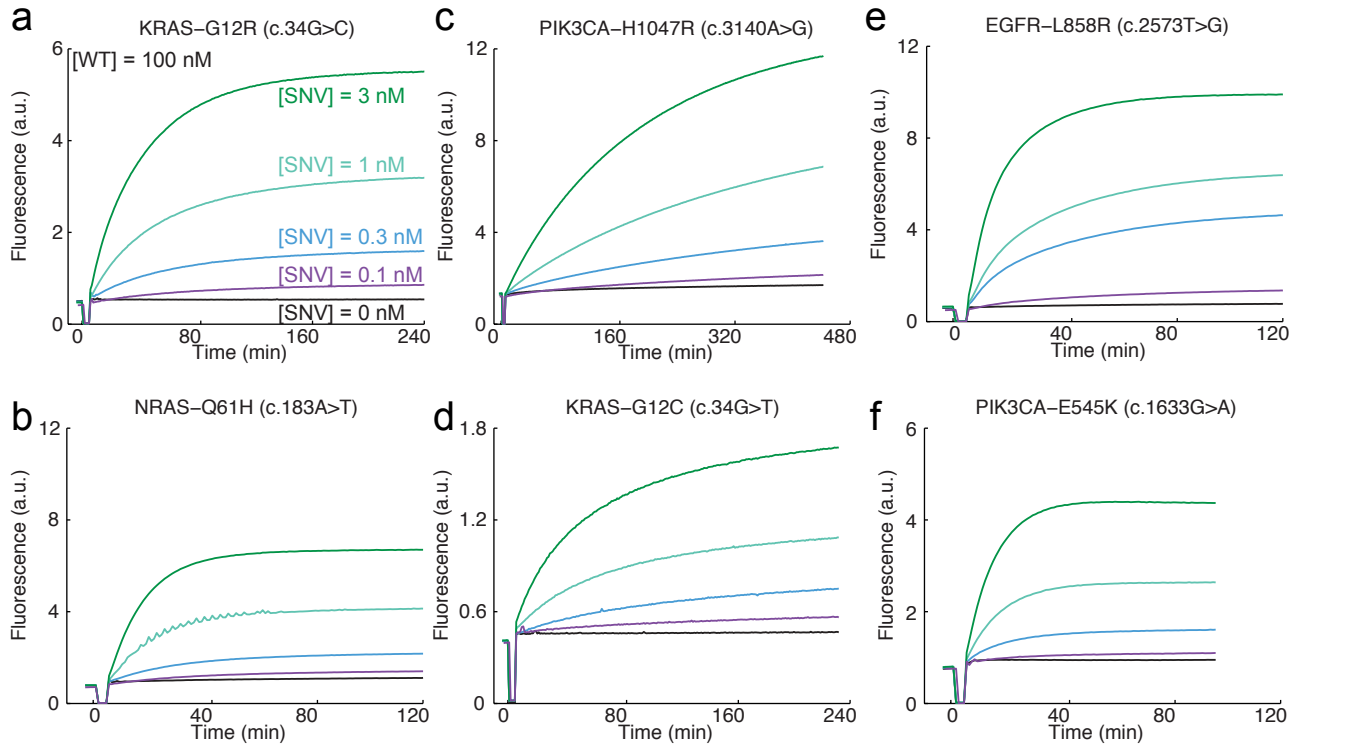

FIG. S8-3: Kinetic responses of Competitive Composition reactions with 0.1 to 3 nM SNV.

Text S9: Kinetic traces for 44 Competitive Compositions to DNA targets at 0.1% SNV Load.

Shown in this section are the experimental results of 44 different Competitive Compositions, each designed against one frequently observed point mutation in COSMIC. These 44 target sequences are the same as the ones tested for X-Probes (Section S4), and utilize the X-Probes designs earlier as one component of the Competitive Composition. Thus, results here are highly comparable to the results of the X-Probe system alone, because the reactions include the same target and X-Probe and only have Sink as an additional component.

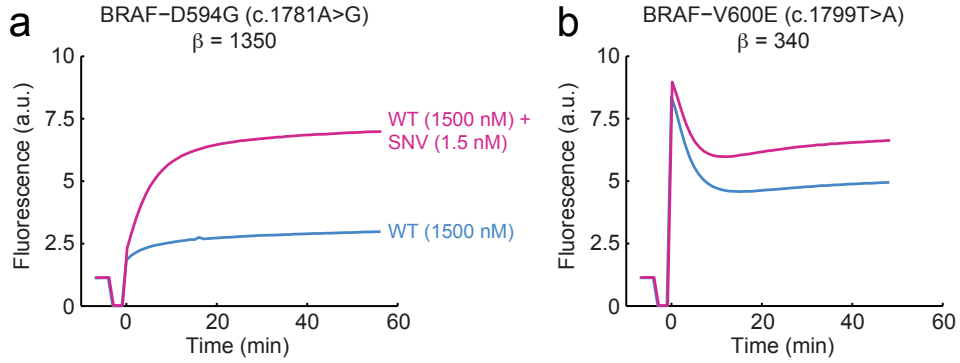

FIG. S9-1: Kinetic responses of Competitive Compositions targeting BRAF mutations, 0.1% SNV load.

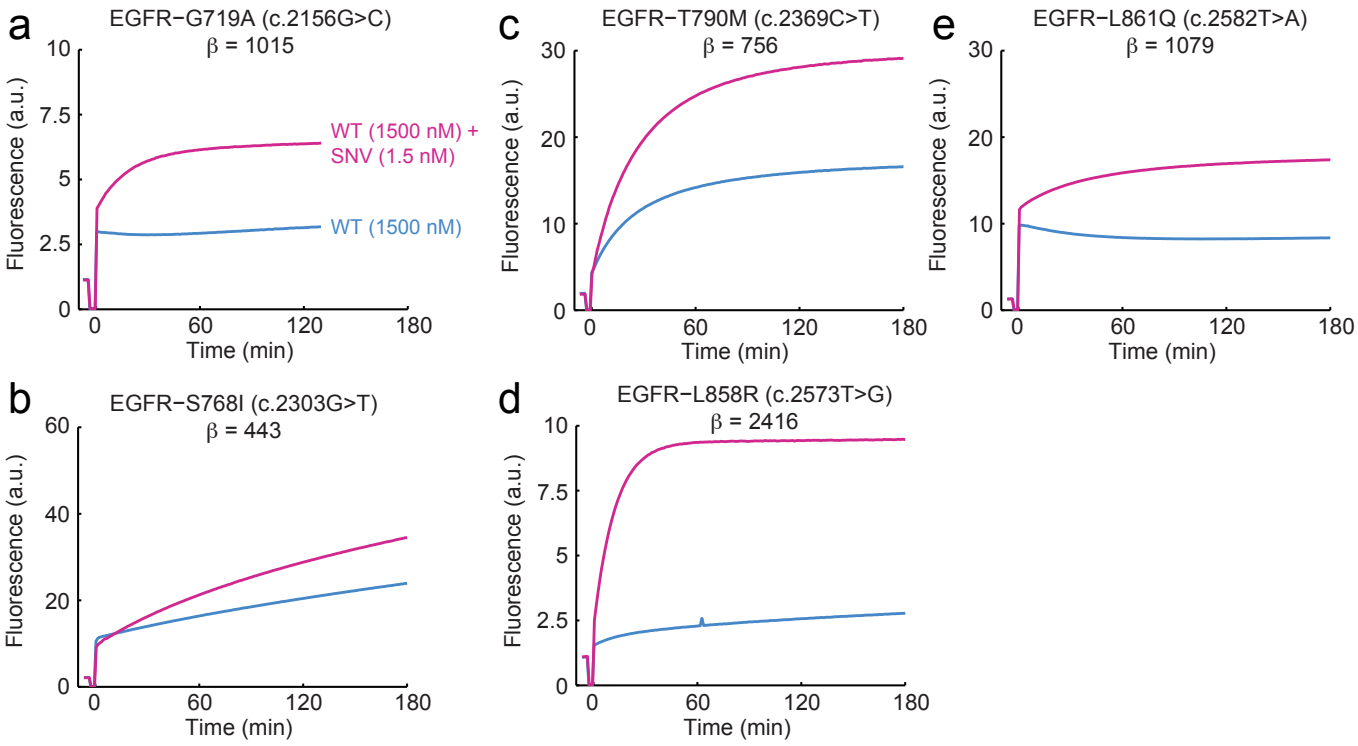

FIG. S9-2: Kinetic responses of Competitive Compositions targeting EGFR mutations, 0.1% SNV load.

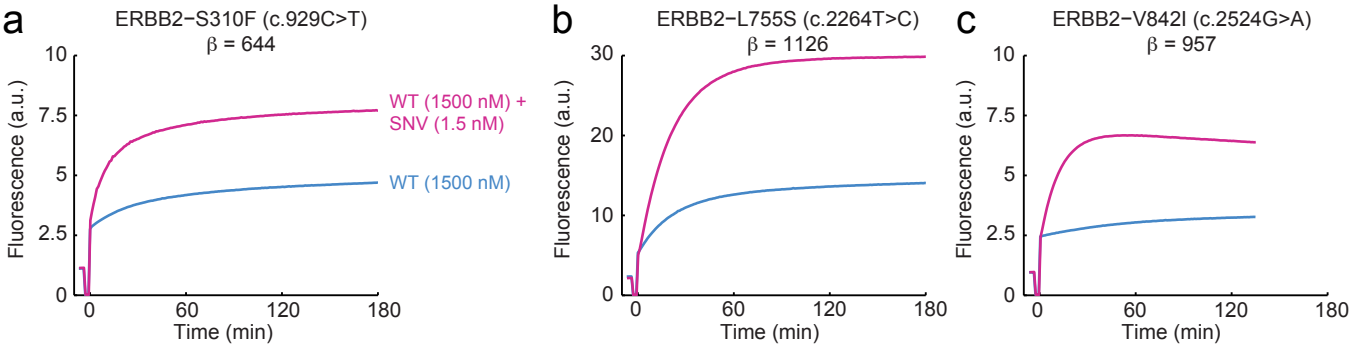

FIG. S9-3: Kinetic responses of Competitive Compositions targeting ERBB2 mutations, 0.1% SNV load.

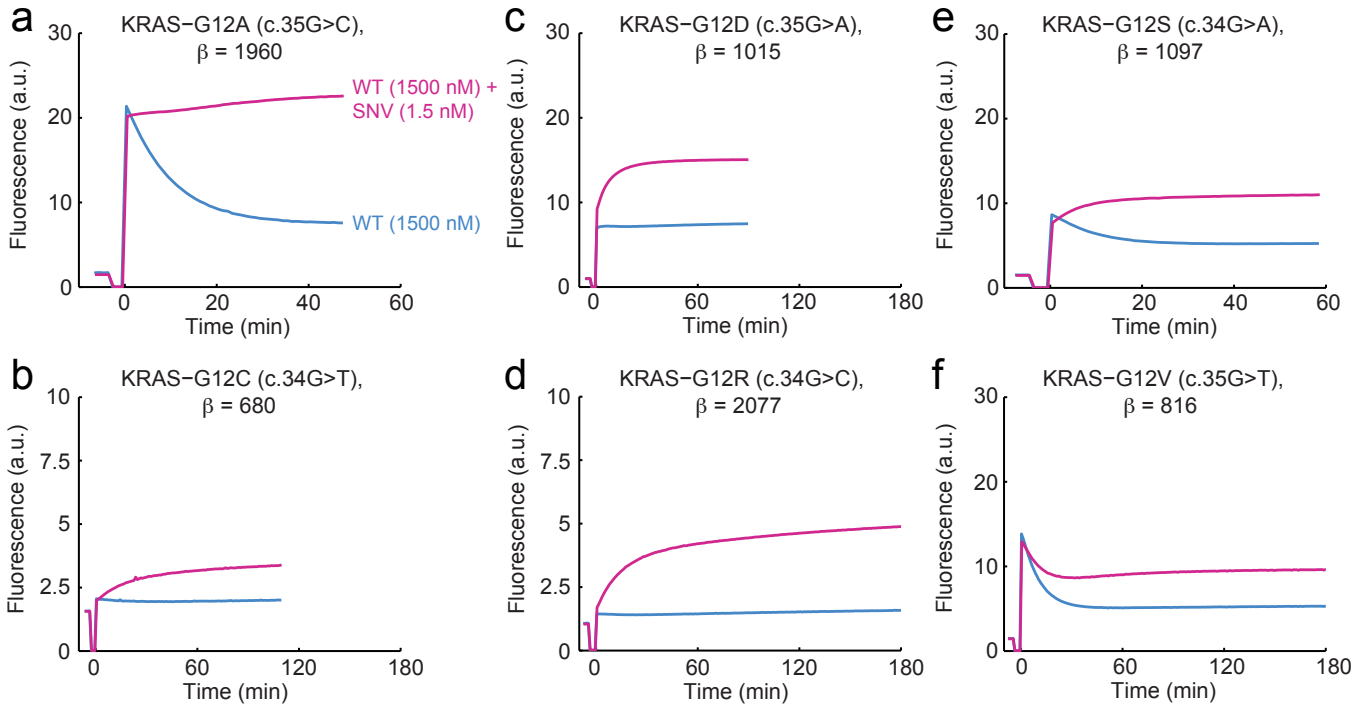

FIG. S9-4: Kinetic responses of Competitive Compositions targeting KRAS mutations, 0.1% SNV load.

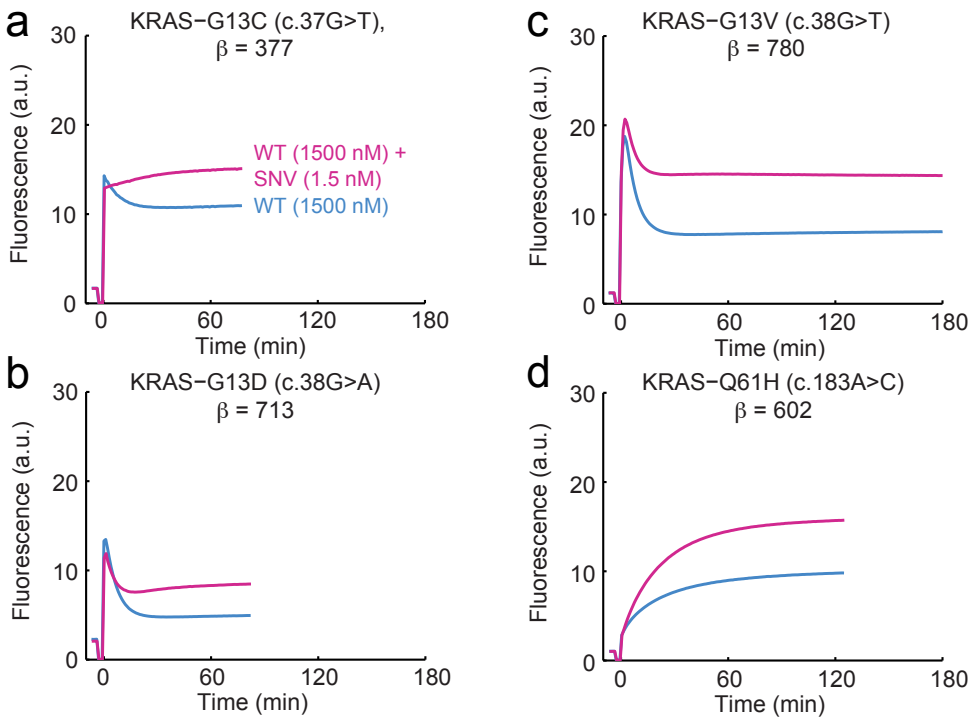

FIG. S9-5: Kinetic responses of Competitive Compositions targeting KRAS mutations, 0.1% SNV load.

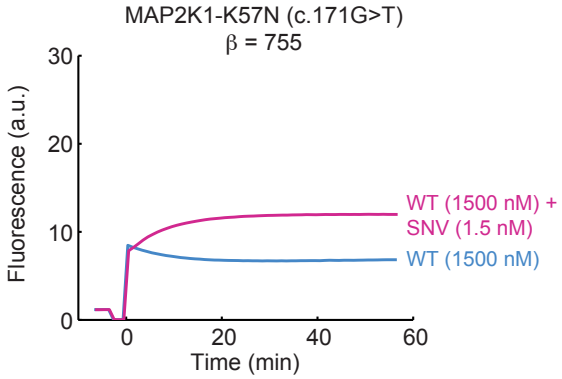

FIG. S9-6: Kinetic responses of a Competitive Composition targeting a MAP2K mutation.

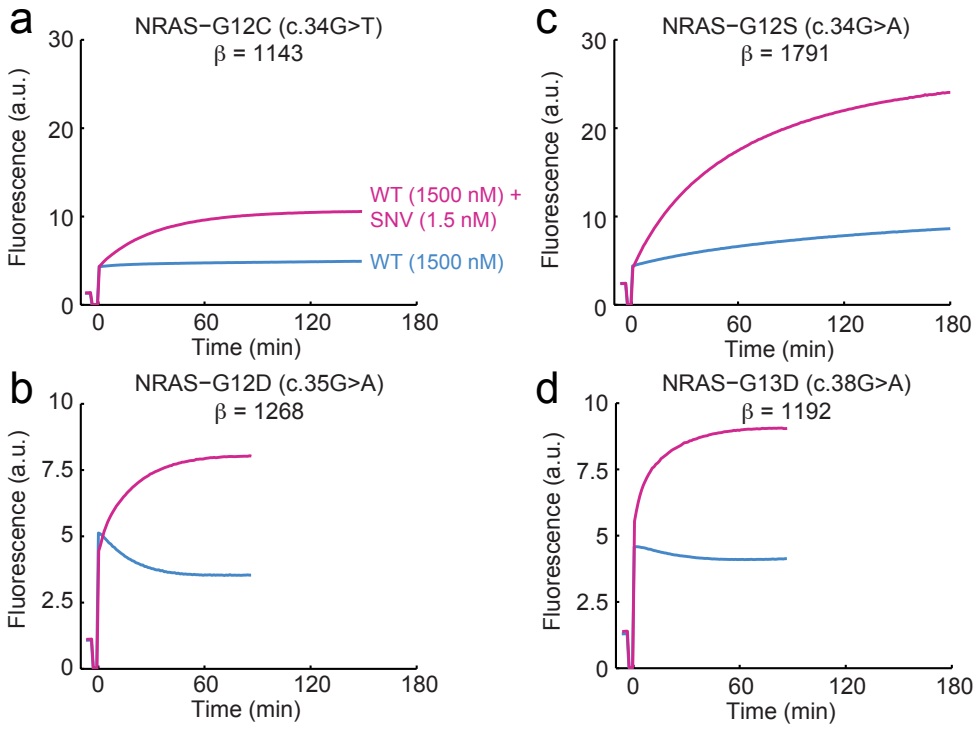

FIG. S9-7: Kinetic responses of Competitive Compositions targeting NRAS mutations, 0.1% SNV load.

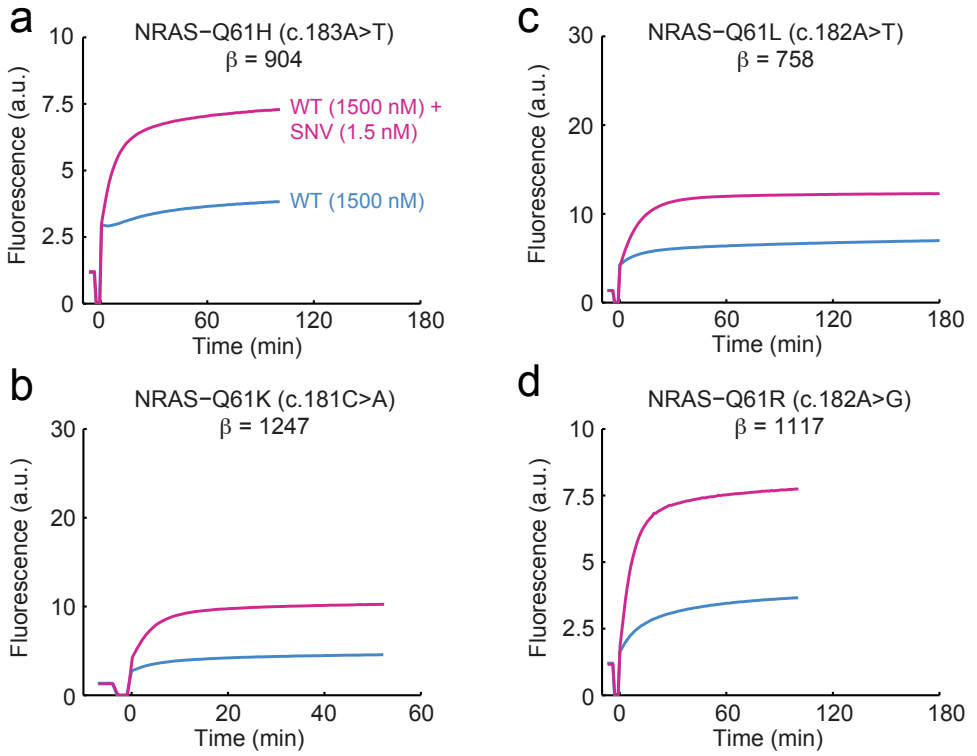

FIG. S9-8: Kinetic responses of Competitive Compositions targeting NRAS mutations, 0.1% SNV load.

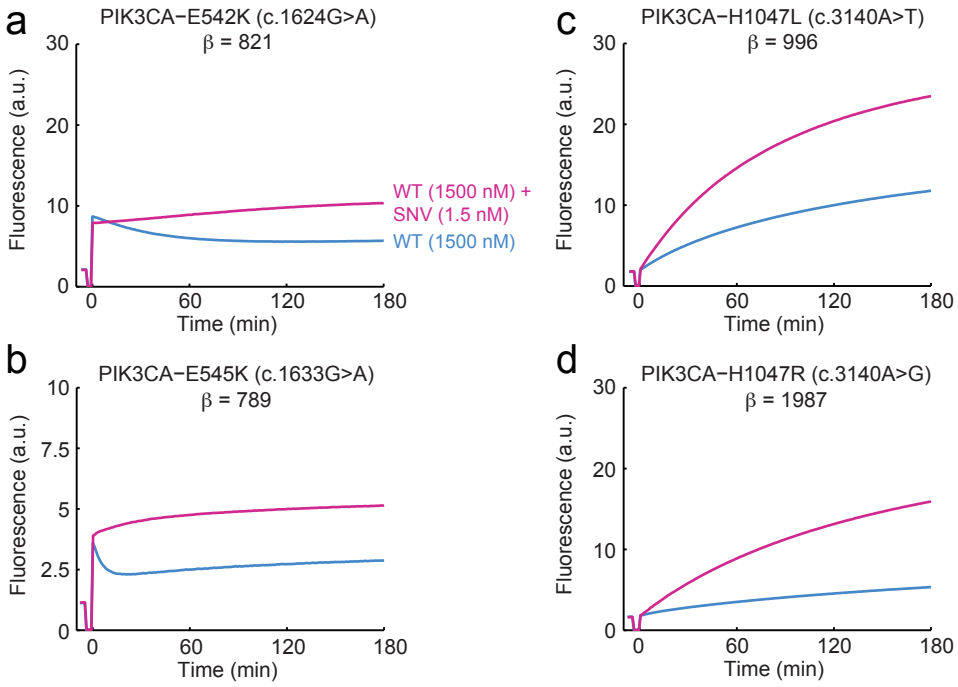

FIG. S9-9: Kinetic responses of Competitive Compositions targeting PIK3CA mutations, 0.1% SNV load.

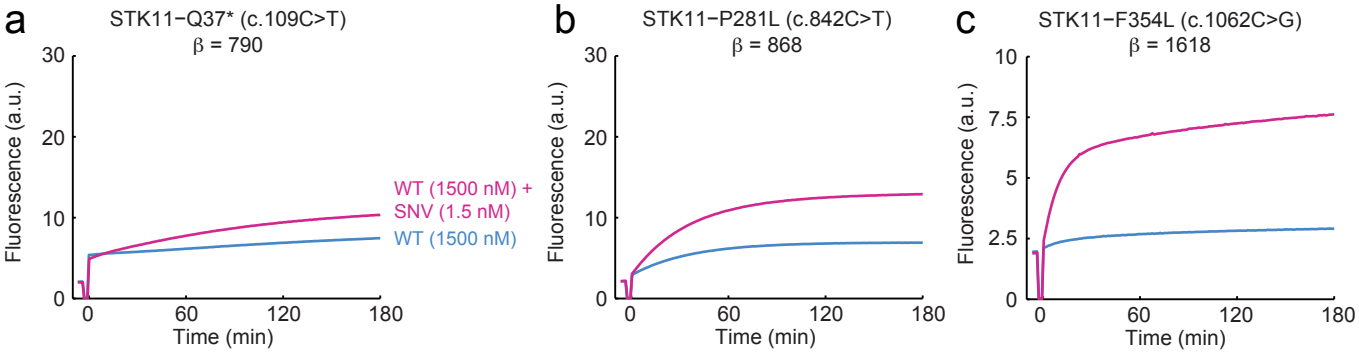

FIG. S9-10: Kinetic responses of Competitive Compositions targeting STK11 mutations, 0.1% SNV load.

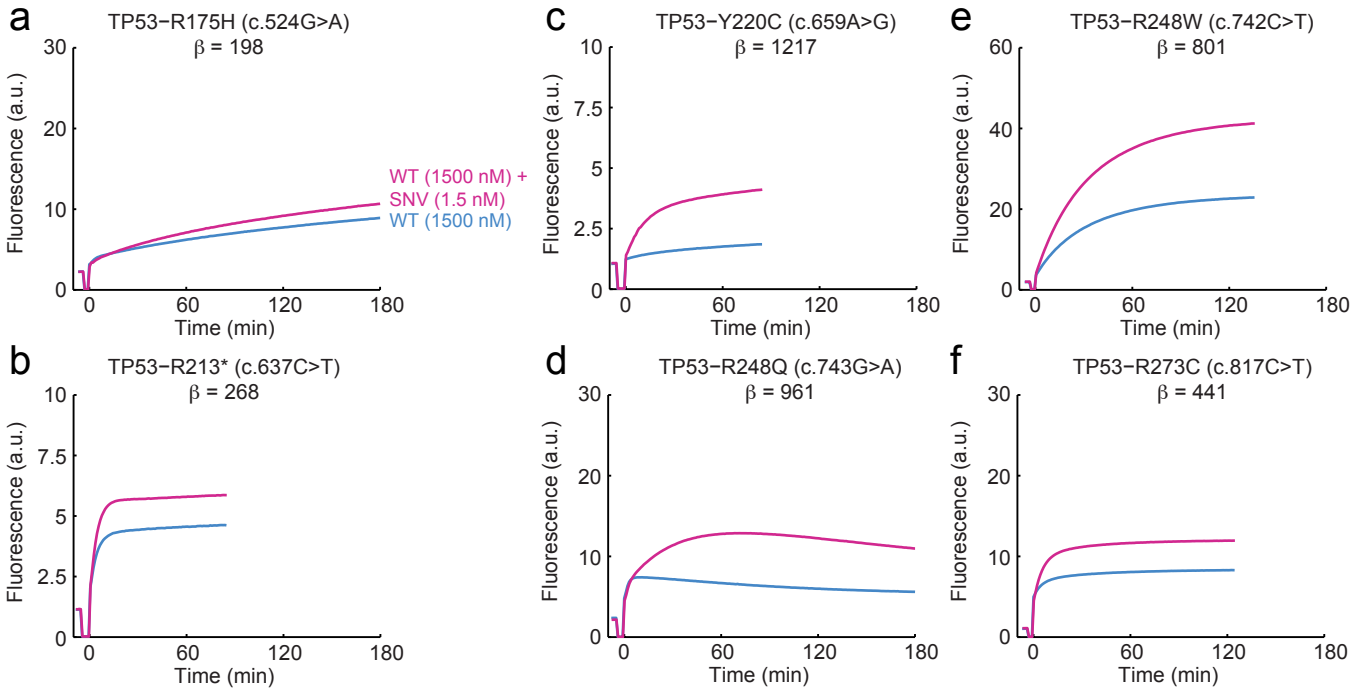

FIG. S9-11: Kinetic responses of Competitive Compositions targeting TP53 mutations, 0.1% SNV load.

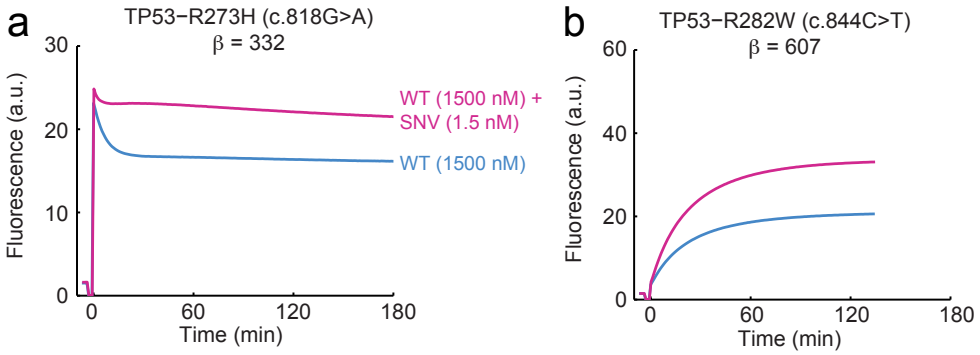

FIG. S9-12: Kinetic responses of Competitive Compositions targeting TP53 mutations, 0.1% SNV load.

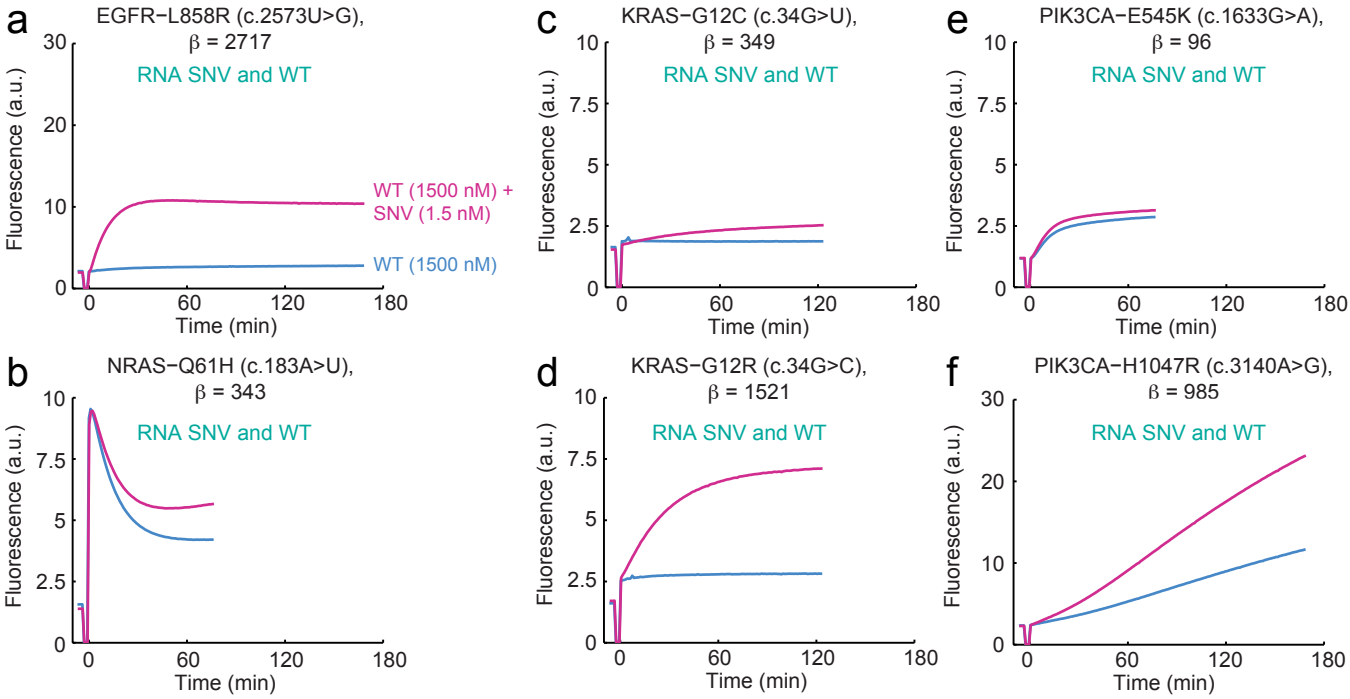

FIG. S9-13: Kinetic responses of Competitive Compositions targeting RNA SNV and WT sequences.

Text S10: Kinetic traces for 40 Competitive Compositions to DNA targets at 0.033% SNV Load.

Shown in this section are the experimental results of 40 different Competitive Compositions, each designed against one frequently observed point mutation in COSMIC. Four of the Competitive Compositions tested in Section S9 were not tested here at 0.033% load, due to low expectations for significant β based on their 0.1% load performance.

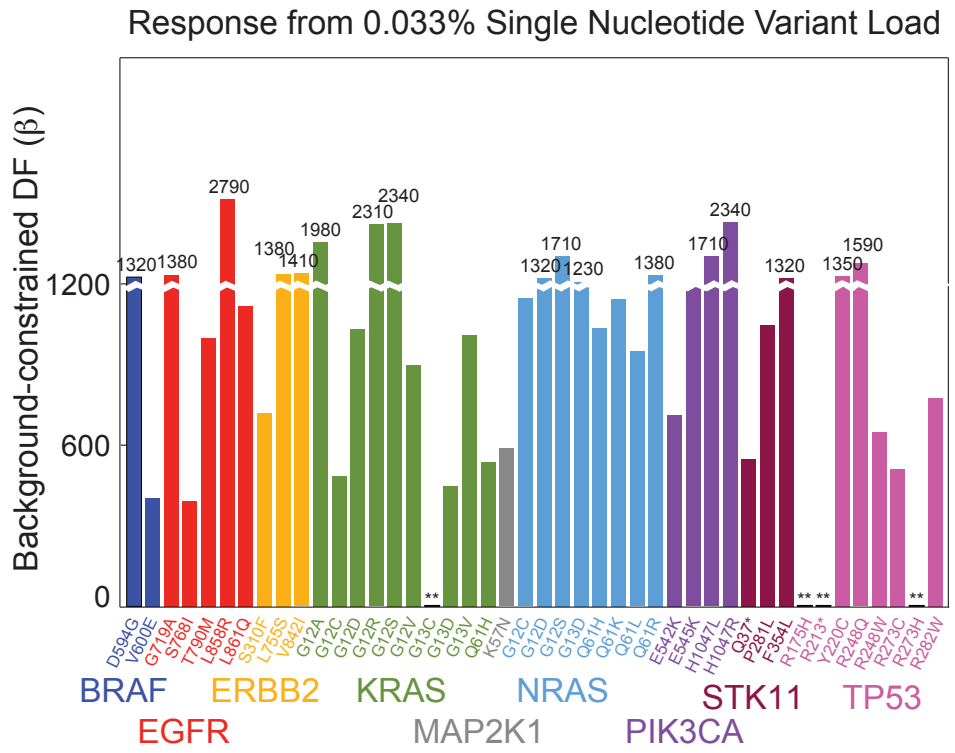

FIG. S10-1: Summary of β observed for Competitive Compositions with 0.033% SNV Load. Double asterisk (**) denotes that the experiment was not performed, due to low expectations of β from the 0.01% load experiments.

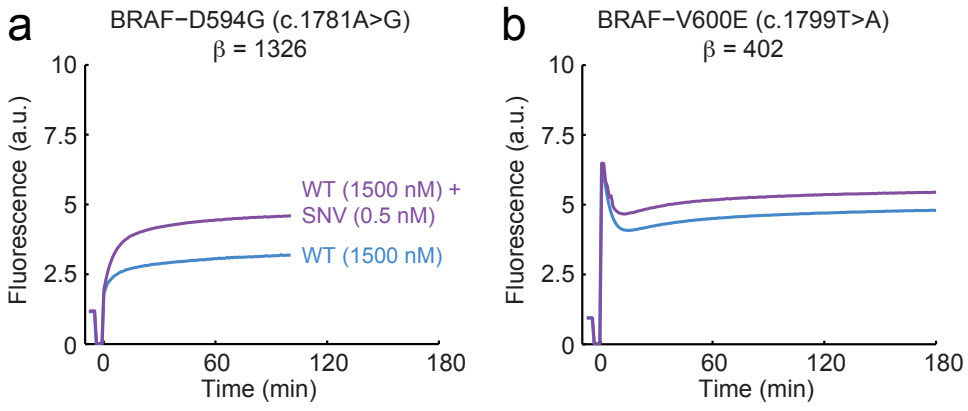

FIG. S10-2: Kinetic responses of Competitive Compositions targeting BRAF mutations, 0.033% SNV load.

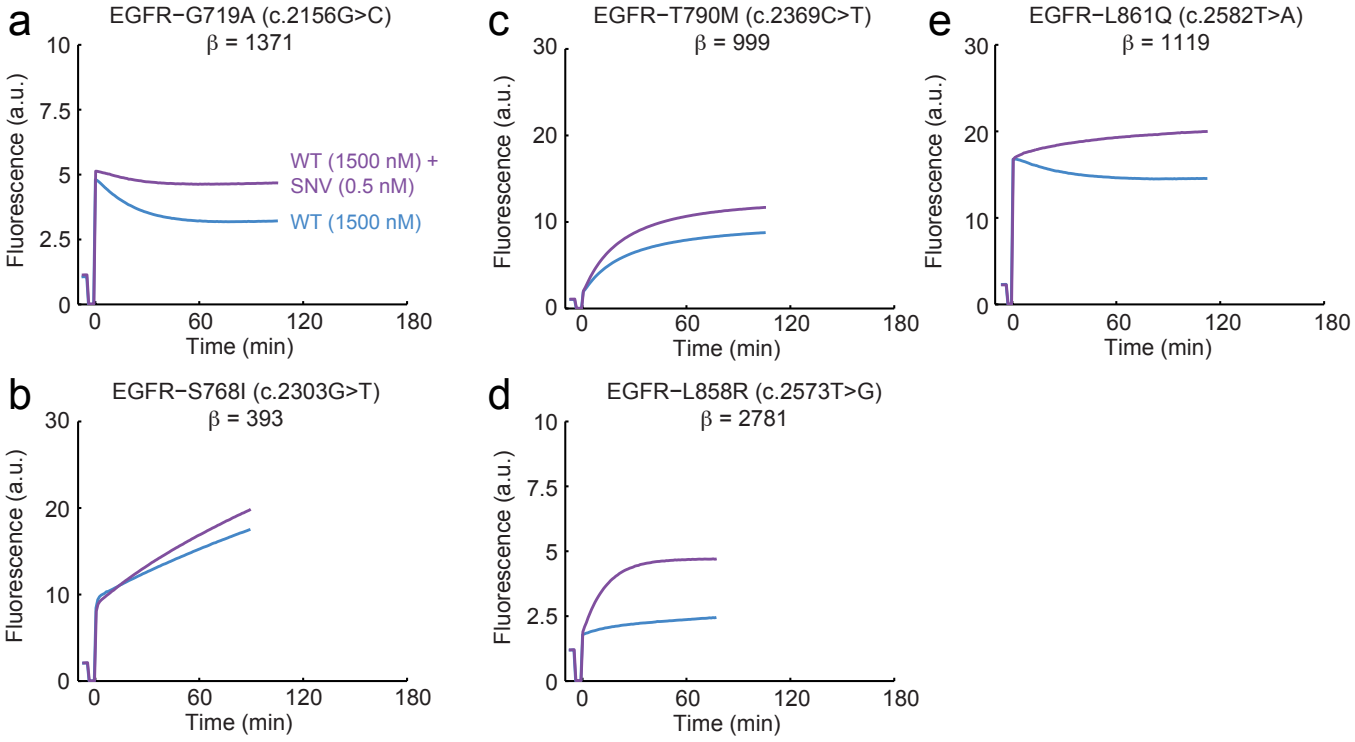

FIG. S10-3: Kinetic responses of Competitive Compositions targeting EGFR mutations, 0.033% SNV load.

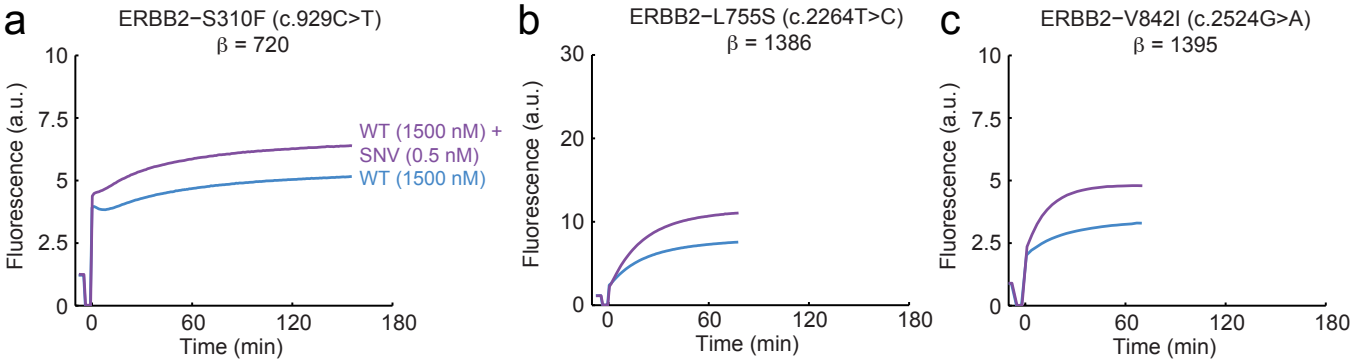

FIG. S10-4: Kinetic responses of Competitive Compositions targeting ERBB2 mutations, 0.033% SNV load.

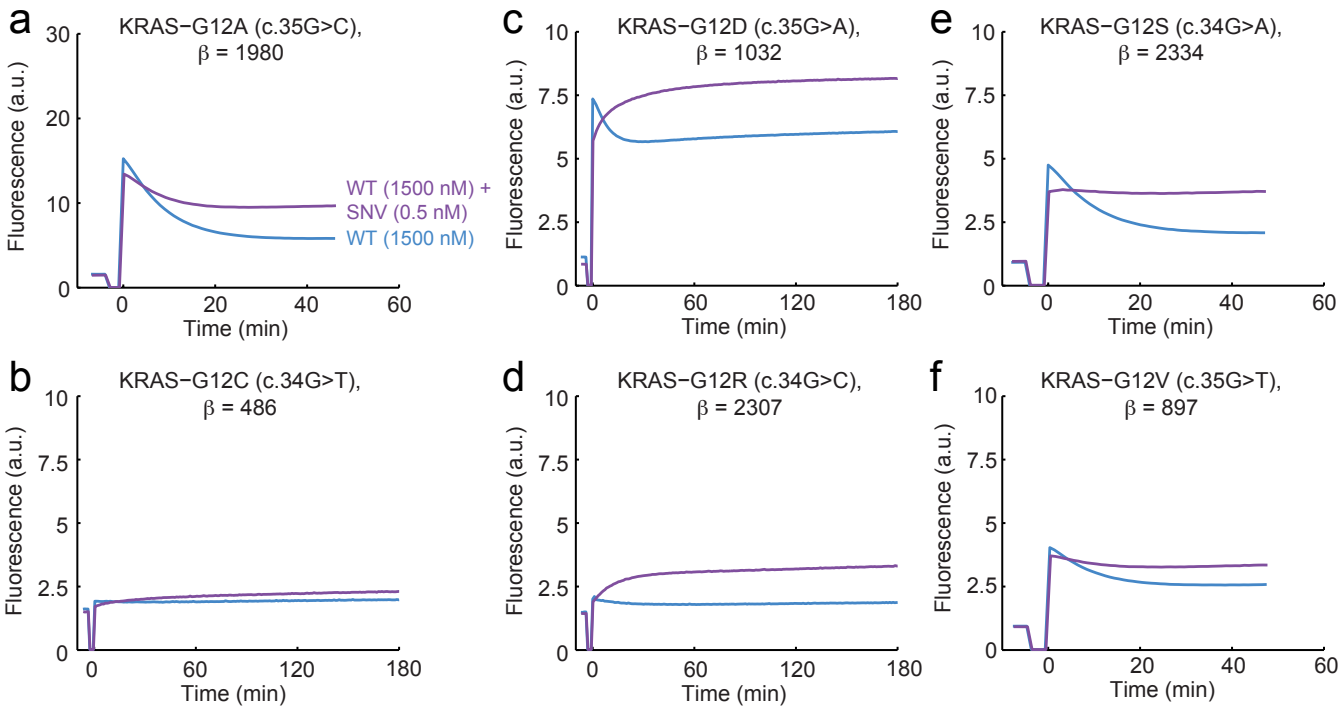

FIG. S10-5: Kinetic responses of Competitive Compositions targeting KRAS mutations, 0.033% SNV load.

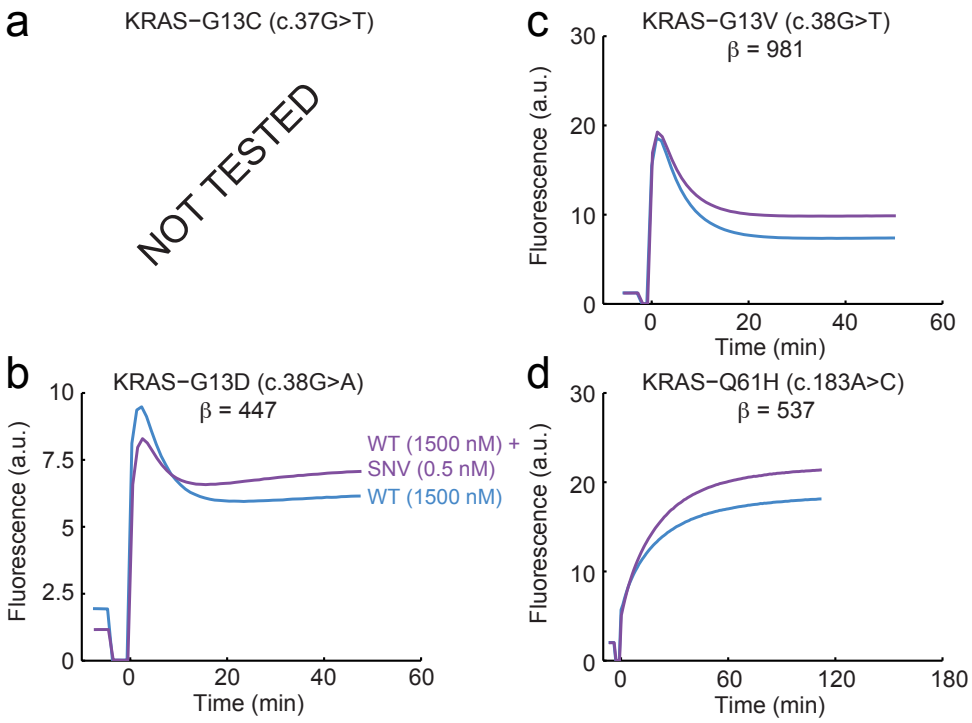

FIG. S10-6: Kinetic responses of Competitive Compositions targeting KRAS mutations, 0.033% SNV load.

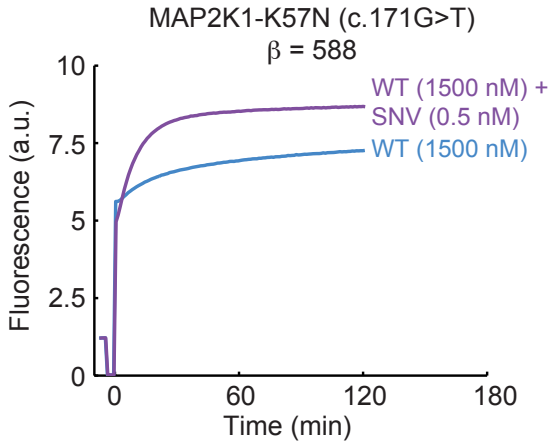

FIG. S10-7: Kinetic responses of a Competitive Composition targeting a MAP2K mutation.

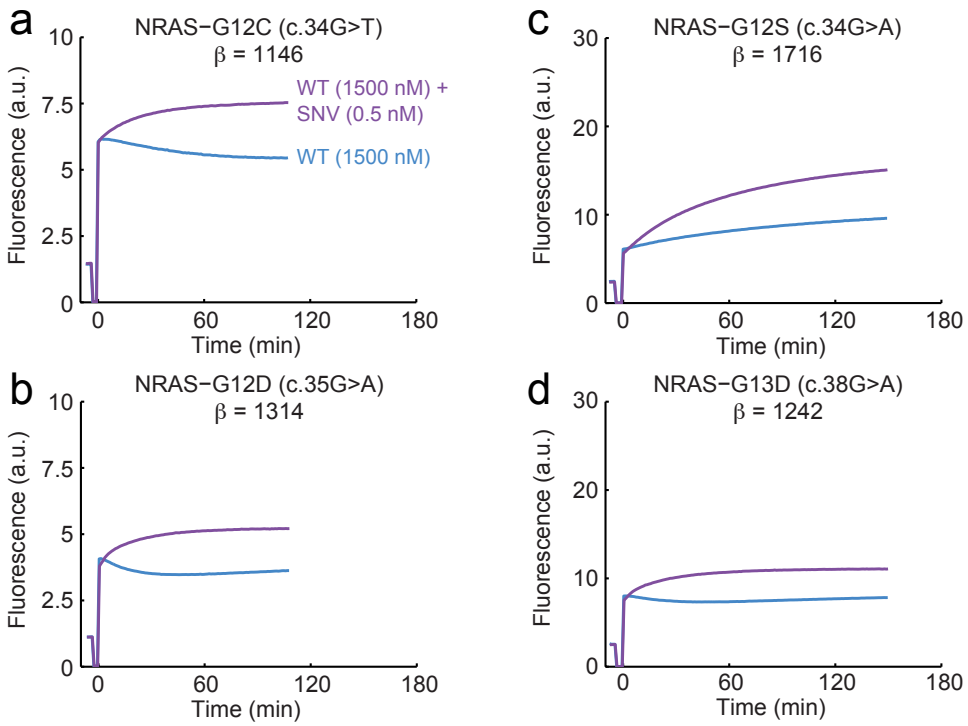

FIG. S10-8: Kinetic responses of Competitive Compositions targeting NRAS mutations, 0.033% SNV load.

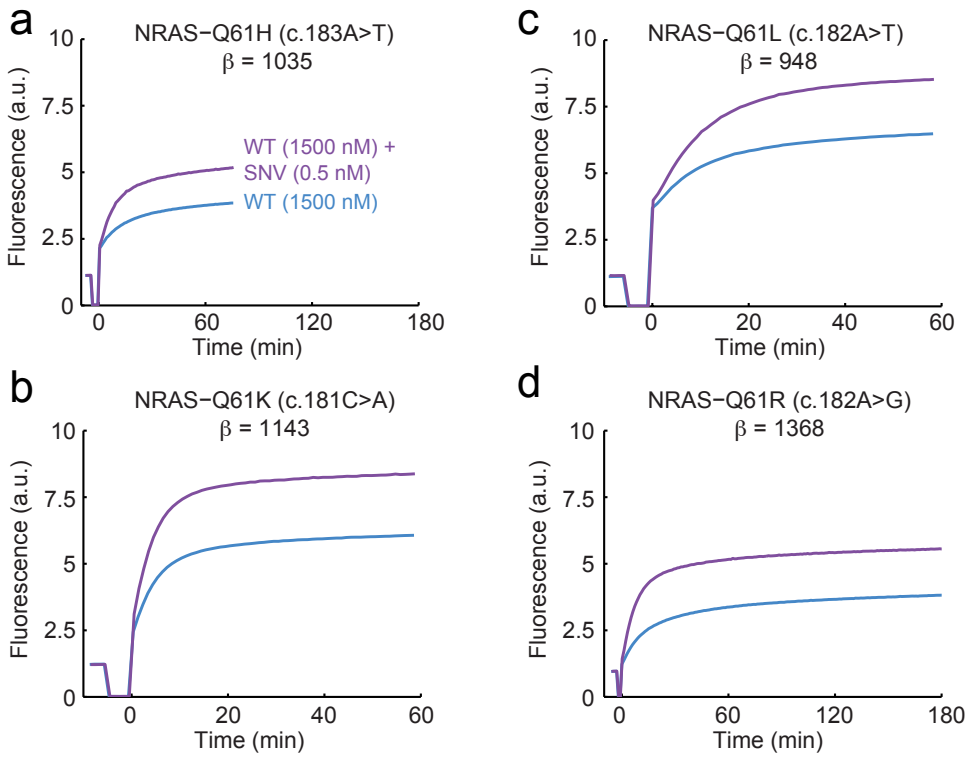

FIG. S10-9: Kinetic responses of Competitive Compositions targeting NRAS mutations, 0.033% SNV load.

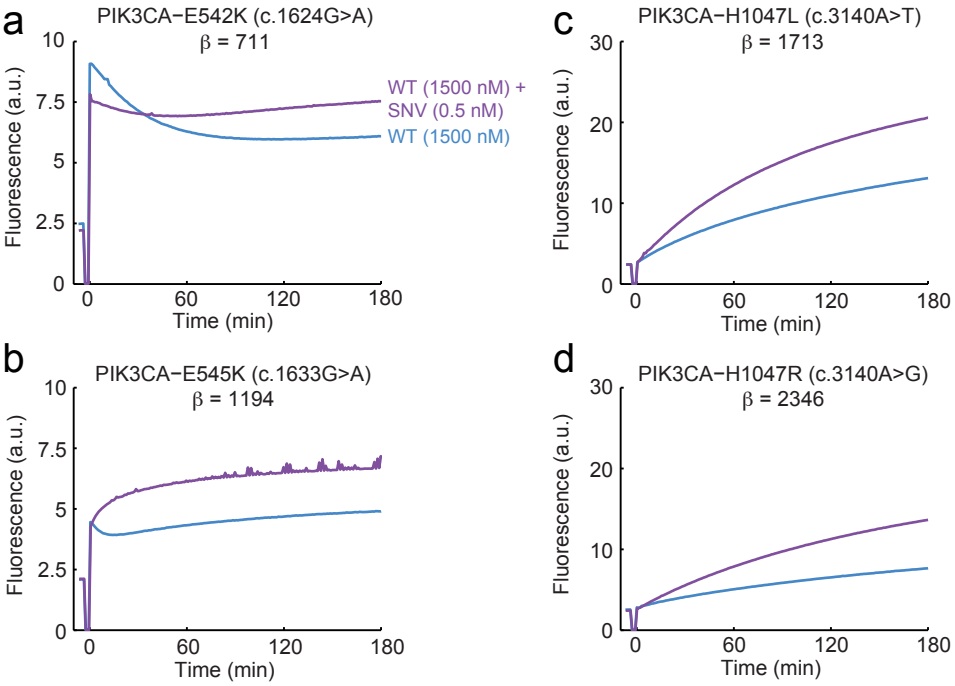

FIG. S10-10: Kinetic responses of Competitive Compositions targeting PIK3CA mutations, 0.033% SNV load.

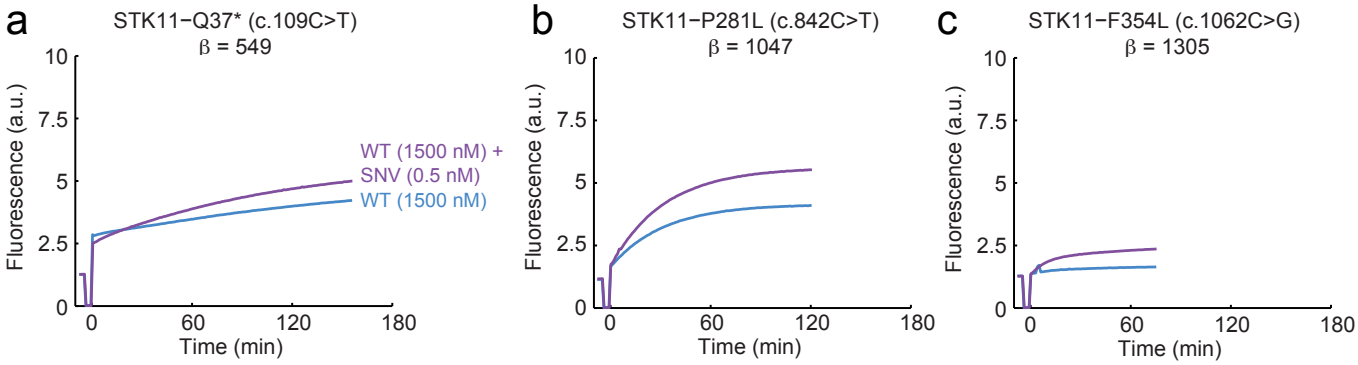

FIG. S10-11: Kinetic responses of Competitive Compositions targeting STK11 mutations, 0.033% SNV load.

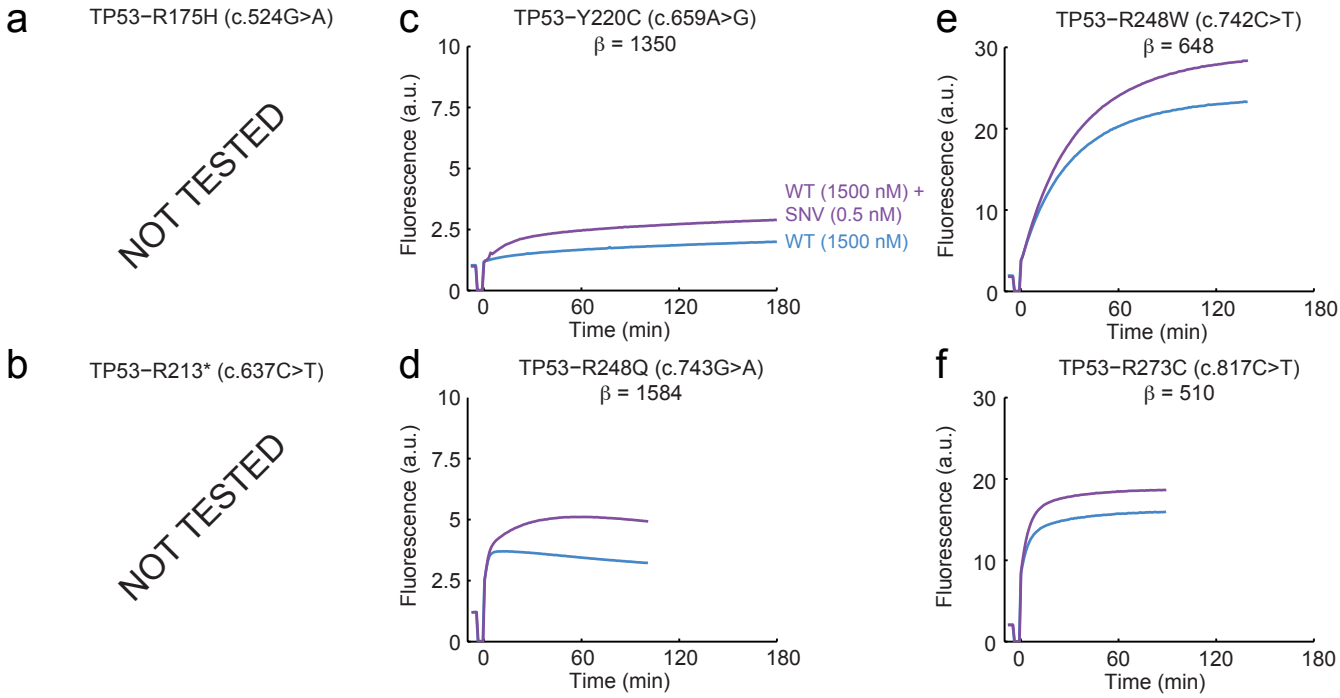

FIG. S10-12: Kinetic responses of Competitive Compositions targeting TP53 mutations, 0.033% SNV load.

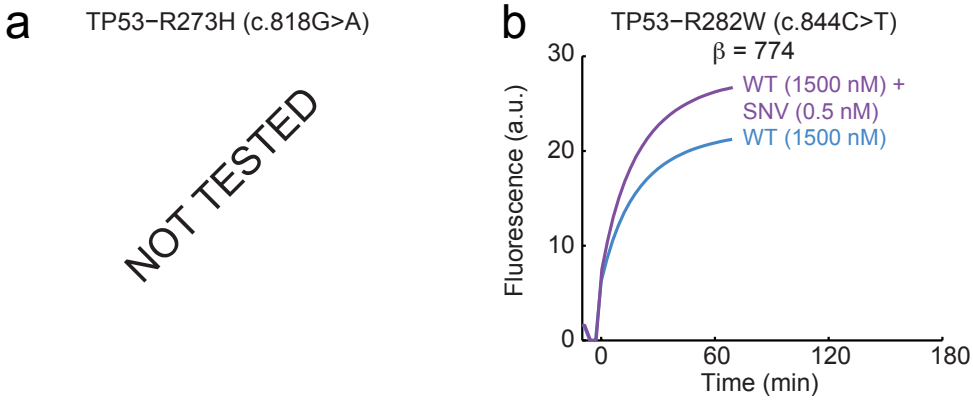

FIG. S10-13: Kinetic responses of Competitive Compositions targeting TP53 mutations, 0.033% SNV load.

Text S11: Kinetic traces for 6 Competitive Compositions to DNA targets at 0.01% SNV Load.

Given the relatively consistent background-constrained discrimination factor β we observed for the 40 different Competitive compositions at the 0.1% load level and the 0.033% load level, we believed that only 6 Competitive Compositions would yield statistically significant signal increase at 0.01% load levels (i.e. signal increase due to 0.01% SNV $>$ 15% over WT). These six experiments are shown in Fig. S11.

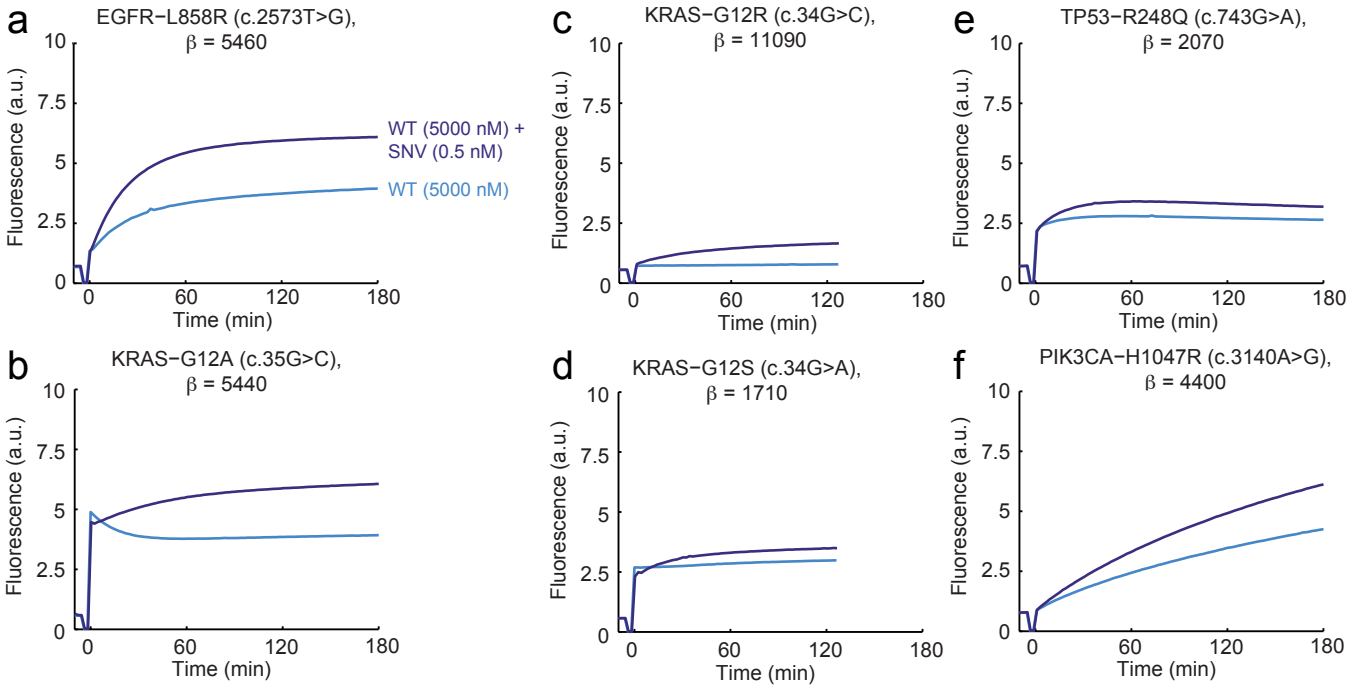

FIG. S11: Kinetic responses of Competitive Compositions at 0.01% SNV load.

Text S12: Sequences of Oligonucleotides Used

The DNA sequences of all oligonucleotides used are shown here in tabular form. RNA sequences for SNV and WT are the analogs of the DNA sequences (with T's replaced by U's) and are not explicitly shown. All functionalized strands were post-synthesis HPLC purified by IDT; all other strands were ordered with standard desalt and not purified. In functionalized sequences, /3Rox_N/ denotes the IDT entry code for the 3′ ROX fluorophore functionalized by NHS ester chemistry, /5IAbRQ/ the IDT entry code for the 5′ Iowa Black Red Quencher group, and /5IABkFQ/ the IDT code for the 5′ Iowa Black Fluorescence Quencher group.

Length of NH* (nt)	Species	Sequence
7 (default)	F	GTTAAATCGTGGATAGTAGAC TTCGCAC /3Rox_N/
	Q	/5IAbRQ/ GTGCGAA CAGGTACATTTGCTCGTCCTT

* Length of region 10.

TABLE S12-1: Sequences of universal X-Probe strands.

Species	Sequence
P_S	/5IAbRQ/ TGTTAATAGTCAAGATCACAGATTTTGG
C_S	GCCAGCCCAAAATCTGTGATCTTGACTATTAACA /3AlexF647N/

TABLE S12-2: Sequences of labeled Sink strands targeting EGFR-L858 wildtype.

Primer	Sequence
Forward Primer	CCATGCTCACAGCCTCATC
Reverse Primer	TGTTTCCTGAGGAGTCTGAGG

TABLE S12-3: Sequences non-allele specific primers at SMAD7 gene locus.

Allele	Species	Sequence
SMAD7-C	P	AAGGACGAGCAAATGTACCTG CACTCATCCAAAAGAGGAAA
	C	GGGTCCTGTTTCCTCTTTTGGATGAGTG GTCTACTATCCACGATTTAAC
	P_s	CGACTCTCATCCAAAAGAGGAA
	C_s	GGGTCCTATTTCCTCTTTTGGATGAGAGTCG
SMAD7-T	P	AAGGACGAGCAAATGTACCTG CACTCATCCAAAAGAGGAA
	C	GGGTCCTATTTCCTCTTTTGGATGAGTG GTCTACTATCCACGATTTAAC
	P_s	ACACACTCATCCAAAAGAGGAAA
	C_s	GGGTCCTGTTTCCTCTTTTGGATGAGTGTGT

TABLE S12-4: Sequences of target-specific X-Probe components and Sink targeting SMAD7-T allele and SMAD7-C allele.

Mutation	Species	Sequence
BRAF-D594G (c.1781A>G)	SNV	ATAGGTG**G**TTTTGGTCTAGCTACAGTGAAA
	WT	ATAGGTG**A**TTTTGGTCTAGCTACAGTGAAA
	P	AAGGACGAGCAAATGTACCTG CAAGGTGGTTTTGGTCTAGC
	C	TTCACTGTAGCTAGACCAAAACCACCTTG GTCTACTATCCACGATTTAAC
	P_s	TGTTAATAAGGTGATTTTGGTCTAGC
	C_s	TCACTGTAGCTAGACCAAAATCACCTTATTAACA
BRAF-V600E (c.1799T>A)	SNV	ATAGGTGATTTTGGTCTAGCTACAG**A**GAAA
	WT	ATAGGTGATTTTGGTCTAGCTACAG**T**GAAA
	P	AAGGACGAGCAAATGTACCTG CAAGGTGATTTTGGTCTAG
	C	TCTCTGTAGCTAGACCAAAATCACCTTG GTCTACTATCCACGATTTAAC
	P_s	CGCAGGTGATTTTGGTCTAGC
	C_s	TCACTGTAGCTAGACCAAAATCACCTGCG

TABLE S12-5: Sequences of SNV, WT, target-specific X-Probe components, and Sink for BRAF mutations.

Mutation	Species	Sequence
EGFR-G719A (c.2156G>C)	SNV	TTCAAAAAGATCAAAGTGCTGGCCTCCGGT
	WT	TTCAAAAAGATCAAAGTGCTGGGCTCCGGT
	P	AAGGACGAGCAAATGTACCTG CACAAAAAGATCAAAGTGCTGG
	C	CGGAGGCCAGCACTTTGATCTTTTTGTG GTCTACTATCCACGATTTAAC
	P_s	AGGCAAAAAGATCAAAGTGCTGG
	C_s	CGGAGCCCAGCACTTTGATCTTTTTGCCT
EGFR-S768I (c.2303G>T)	SNV	GCCTACGTGATGGCCATCGTGGACAACCCC
	WT	GCCTACGTGATGGCCAGCGTGGACAACCCC
	P	AAGGACGAGCAAATGTACCTG CACTACGTGATGGCCATCGT
	C	GGTTGTCCACGATGGCCATCACGTAGTG GTCTACTATCCACGATTTAAC
	P_s	AGTTCTACGTGATGGCCAGCGTG
	C_s	GGTTGTCCACGCTGGCCATCACGTAGAACT
EGFR-T790M (c.2369C>T)	SNV	GTGCAGCTCATCATGCAGCTCATGCCCTTC
	WT	GTGCAGCTCATCACGCAGCTCATGCCCTTC
	P	AAGGACGAGCAAATGTACCTG CAGCAGCTCATCATGCAGCTC
	C	AGGGCATGAGCTGCATGATGAGCTGCTG GTCTACTATCCACGATTTAAC
	P_s	TGTTAATAGCAGCTCATCACGCAGCTC
	C_s	AGGGCATGAGCTGCGTGATGAGCTGCTATTAACA
EGFR-L858R (c.2573T>G)	SNV	ATGTCAAGATCACAGATTTTGGGCGGGCCA
	WT	ATGTCAAGATCACAGATTTTGGGCTGGCCA
	P	AAGGACGAGCAAATGTACCTG CAGTCAAGATCACAGATTTTGG
	C	GCCCGCCCAAAATCTGTGATCTTGACTG GTCTACTATCCACGATTTAAC
	P_s	TGTTAATAGTCAAGATCACAGATTTTGG
	C_s	GCCAGCCCAAAATCTGTGATCTTGACTATTAACA
EGFR-L861Q (c.2582T>A)	SNV	TGGCCAAACAGCTGGGTGCGGAAGAGAAAG
	WT	TGGCCAAACTGCTGGGTGCGGAAGAGAAAG
	P	AAGGACGAGCAAATGTACCTG CAGCCAAACAGCTGGGTGCG
	C	TTTCTCTTCCGCACCCAGCTGTTTGGCTG GTCTACTATCCACGATTTAAC
	P_s	TAGTTGCCAAACTGCTGGGTGCG
	C_s	TTCTCTTCCGCACCCAGCAGTTTGGCAACTA

TABLE S12-6: Sequences of SNV, WT, target-specific X-Probe components, and Sink for EGFR mutations.

Mutation	Species	Sequence
ERBB2-S310F (c.929C>T)	SNV	ACTACCTTTCTACGGACGTGGGATTCTGCA
	WT	ACTACCTTTCTACGGACGTGGGATCCTGCA
	P	AAGGACGAGCAAATGTACCTG CATACCTTTCTACGGACGTG
	C	CAGAATCCCACGTCCGTAGAAAGGTATG GTCTACTATCCACGATTTAAC
	P_s	TGTTAATATACCTTTCTACGGACGTG
	C_s	CAGGATCCCACGTCCGTAGAAAGGTATATTAACA
ERBB2-L755S (c.2264T>C)	SNV	TTCCAGTGGCCATCAAAGTGTCGAGGGAAA
	WT	TTCCAGTGGCCATCAAAGTGTTGAGGGAAA
	P	AAGGACGAGCAAATGTACCTG CACCAGTGGCCATCAAAGTG
	C	TCCCTCGACACTTTGATGGCCACTGGTG GTCTACTATCCACGATTTAAC
	P_s	GTTAATACCAGTGGCCATCAAAGTG
	C_s	TCCCTCAACACTTTGATGGCCACTGGTATTAAC
ERBB2-V842I (c.2524G>A)	SNV	GGATGTGCGGCTCATACACAGGGACTTGGC
	WT	GGATGTGCGGCTCGTACACAGGGACTTGGC
	P	AAGGACGAGCAAATGTACCTG CAATGTGCGGCTCATACACA
	C	CAAGTCCCTGTGTATGAGCCGCACATTG GTCTACTATCCACGATTTAAC
	P_s	GTTAATAATGTGCGGCTCGTACACA
	C_s	CAAGTCCCTGTGTACGAGCCGCACATTATTAAC

TABLE S12-7: Sequences of SNV, WT, target-specific X-Probe components, and Sink for ERBB2 mutations.

Mutation	Species	Sequence
KRAS-G12A (c.35G>C)	SNV	CTTGTGGTAGTTGGAGCTG**C**TGGC
	WT	CTTGTGGTAGTTGGAGCTG**G**TGGC
	P	AAGGACGAGCAAATGTACCTG CAACTTGTGGTAGTTGGAG
	C	GCCAGCAGCTCCAACTACCACAAGTTG GTCTACTATCCACGATTTAAC
	P_s	CCGCTGTGGTAGTTGGA
	C_s	CACCAGCTCCAACTACCACAGCGC
KRAS-G12C (c.34G>T)	SNV	CTTGTGGTAGTTGGAGCT**T**GTGGC
	WT	CTTGTGGTAGTTGGAGCT**G**GTGGC
	P	AAGGACGAGCAAATGTACCTG CAACTTGTGGTAGTTGGAGC
	C	GCCACAAGCTCCAACTACCACAAGTTG GTCTACTATCCACGATTTAAC
	P_s	CCGCTGTGGTAGTTGGA
	C_s	CACCAGCTCCAACTACCACAGCGC
KRAS-G12D (c.35G>A)	SNV	CTTGTGGTAGTTGGAGCTG**A**TGGC
	WT	CTTGTGGTAGTTGGAGCTG**G**TGGC
	P	AAGGACGAGCAAATGTACCTG CAACTTGTGGTAGTTGGAG
	C	GCCATCAGCTCCAACTACCACAAGTTG GTCTACTATCCACGATTTAAC
	P_s	GCATCTGTGGTAGTTGGA
	C_s	CACCAGCTCCAACTACCACAGATGC
KRAS-G12R (c.34G>C)	SNV	CTTGTGGTAGTTGGAGCT**C**GTGGC
	WT	CTTGTGGTAGTTGGAGCT**G**GTGGC
	P	AAGGACGAGCAAATGTACCTG CAACTTGTGGTAGTTGGAGC
	C	GCCACGAGCTCCAACTACCACAAGTTG GTCTACTATCCACGATTTAAC
	P_s	CCGCTGTGGTAGTTGGA
	C_s	CACCAGCTCCAACTACCACAGCGC
KRAS-G12S (c.34G>A)	SNV	CTTGTGGTAGTTGGAGCT**A**GTGGC
	WT	CTTGTGGTAGTTGGAGCT**G**GTGGC
	P	AAGGACGAGCAAATGTACCTG CAACTTGTGGTAGTTGGAG
	C	GCCACTAGCTCCAACTACCACAAGTTG GTCTACTATCCACGATTTAAC
	P_s	CCGCTGTGGTAGTTGGA
	C_s	CACCAGCTCCAACTACCACAGCGC
KRAS-G12V (c.35G>T)	SNV	CTTGTGGTAGTTGGAGCTG**T**TGGC
	WT	CTTGTGGTAGTTGGAGCTG**G**TGGC
	P	AAGGACGAGCAAATGTACCTG CAACTTGTGGTAGTTGGAG
	C	GCCAACAGCTCCAACTACCACAAGTTG GTCTACTATCCACGATTTAAC
	P_s	CCGCTGTGGTAGTTGGA
	C_s	CACCAGCTCCAACTACCACAGCGC
KRAS-G13C (c.37G>T)	SNV	CTTGTGGTAGTTGGAGCTGGT**T**GC
	WT	CTTGTGGTAGTTGGAGCTGGT**G**GC
	P	AAGGACGAGCAAATGTACCTG CAACTTGTGGTAGTTGGAG
	C	GCAACCAGCTCCAACTACCACAAGTTG GTCTACTATCCACGATTTAAC
	P_s	CAGGCTGTGGTAGTTGGA
	C_s	CACCAGCTCCAACTACCACAGCCTG
KRAS-G13D (c.38G>A)	SNV	CTTGTGGTAGTTGGAGCTGGTG**A**CGTAGGC
	WT	CTTGTGGTAGTTGGAGCTGGTG**G**CGTAGGC
	P	AAGGACGAGCAAATGTACCTG CATGTGGTAGTTGGAGCTGG
	C	CTACGTCACCAGCTCCAACTACCACATG GTCTACTATCCACGATTTAAC
	P_s	TTAATATGTGGTAGTTGGAGCTGGT
	C_s	CTACGCCACCAGCTCCAACTACCACATATTAA
KRAS-G13V (c.38G>T)	SNV	CTTGTGGTAGTTGGAGCTGGTG**T**CGTAGGC
	WT	CTTGTGGTAGTTGGAGCTGGTG**G**CGTAGGC
	P	AAGGACGAGCAAATGTACCTG CATGTGGTAGTTGGAGCTGG
	C	CTACGACACCAGCTCCAACTACCACATG GTCTACTATCCACGATTTAAC
	P_s	AGGTGTGGTAGTTGGAGCTGGT
	C_s	CTACGCCACCAGCTCCAACTACCACACCT
KRAS-Q61H (c.183A>C)	SNV	GCAGGTCA**C**GAGGAGTACAGTGCAATGAGG
	WT	GCAGGTCA**A**GAGGAGTACAGTGCAATGAGG
	P	AAGGACGAGCAAATGTACCTG CAAGGTCACGAGGAGTACAG
	C	TCATTGCACTGTACTCCTCGTGACCTTG GTCTACTATCCACGATTTAAC
	P_s	TGTTAATAAGGTCAAGAGGAGTACAG
	C_s	TCATTGCACTGTACTCCTCTTGACCTTATTAACA

TABLE S12-8: Sequences of SNV, WT, target-specific X-Probe components, and Sink for KRAS mutations.

Mutation	Species	Sequence
MAP2K1-K57N (c.171G>T)	SNV	ACCCAGAA**T**CAGAAGGTGGGAGAACTGAAG
	WT	ACCCAGAA**G**CAGAAGGTGGGAGAACTGAAG
	P	AAGGACGAGCAAATGTACCTG CACCAGAATCAGAAGGTGGG
	C	TTCAGTTCTCCCACCTTCTGATTCTGGTG GTCTACTATCCACGATTTAAC
	P_s	AGGCCAGAAGCAGAAGGTGGG
	C_s	TCAGTTCTCCCACCTTCTGCTTCTGGCCT

TABLE S12-9: Sequences of SNV, WT, target-specific X-Probe components, and Sink for MAP2K1 mutation.

Mutation	Species	Sequence
NRAS-G12C (c.34G>T)	SNV	GTGGTTGGAGCATGTGGTGTTGGGAAAAGC
	WT	GTGGTTGGAGCAGGTGGTGTTGGGAAAAGC
	P	AAGGACGAGCAAATGTACCTG CAGGTTGGAGCATGTGGTGTT
	C	CTTTTCCCAACACCACATGCTCCAACCTG GTCTACTATCCACGATTTAAC
	P_s	AGGGGTTGGAGCAGGTGGTGT
	C_s	TTTTCCCAACACCACCTGCTCCAACCCCT
NRAS-G12D (c.35G>A)	SNV	GTGGTTGGAGCAGATGGTGTTGGGAAAAGC
	WT	GTGGTTGGAGCAGGTGGTGTTGGGAAAAGC
	P	AAGGACGAGCAAATGTACCTG CAGGTTGGAGCAGATGGTGTT
	C	CTTTTCCCAACACCATCTGCTCCAACCTG GTCTACTATCCACGATTTAAC
	P_s	AGGGGTTGGAGCAGGTGGTGT
	C_s	TTTTCCCAACACCACCTGCTCCAACCCCT
NRAS-G12S (c.34G>A)	SNV	TACAAACTGGTGGTGGTTGGAGCAAGTGGT
	WT	TACAAACTGGTGGTGGTTGGAGCAGGTGGT
	P	AAGGACGAGCAAATGTACCTG CTCAAACTGGTGGTGGTTGGA
	C	CACTTGCTCCAACCACCACCAGTTTGAG GTCTACTATCCACGATTTAAC
	P_s	CGATCAAACTGGTGGTGGTTGGA
	C_s	CACCTGCTCCAACCACCACCAGTTTGATCG
NRAS-G13D (c.38G>A)	SNV	GTGGTTGGAGCAGGTGATGTTGGGAAAAGC
	WT	GTGGTTGGAGCAGGTGGTGTTGGGAAAAGC
	P	AAGGACGAGCAAATGTACCTG CAGGTTGGAGCAGGTGATGTT
	C	CTTTTCCCAACATCACCTGCTCCAACCTG GTCTACTATCCACGATTTAAC
	P_s	AGGGGTTGGAGCAGGTGGTGT
	C_s	TTTTCCCAACACCACCTGCTCCAACCCCT
NRAS-Q61H (c.183A>T)	SNV	ATACTGGATACAGCTGGACATGAAGAGTAC
	WT	ATACTGGATACAGCTGGACAAGAAGAGTAC
	P	AAGGACGAGCAAATGTACCTG CAACTGGATACAGCTGGAC
	C	ACTCTTCATGTCCAGCTGTATCCAGTTG GTCTACTATCCACGATTTAAC
	P_s	TGTTAATAACTGGATACAGCTGGAC
	C_s	ACTCTTCTTGTCCAGCTGTATCCAGTTATTAACA
NRAS-Q61K (c.181C>A)	SNV	ATACTGGATACAGCTGGAAAAGAAGAGTAC
	WT	ATACTGGATACAGCTGGACAAGAAGAGTAC
	P	AAGGACGAGCAAATGTACCTG CAACTGGATACAGCTGGAA
	C	ACTCTTCTTTTCCAGCTGTATCCAGTTG GTCTACTATCCACGATTTAAC
	P_s	TGTTAATAACTGGATACAGCTGGAC
	C_s	ACTCTTCTTGTCCAGCTGTATCCAGTTATTAACA
NRAS-Q61L (c.182A>T)	SNV	GGACATACTGGATACAGCTGGACTAGAAGA
	WT	GGACATACTGGATACAGCTGGACAAGAAGA
	P	AAGGACGAGCAAATGTACCTG CAACATACTGGATACAGCT
	C	TTCTAGTCCAGCTGTATCCAGTATGTTG GTCTACTATCCACGATTTAAC
	P_s	GTTAATAACATACTGGATACAGCTG
	C_s	TTCTTGTCCAGCTGTATCCAGTATGTTATTAAC
NRAS-Q61R (c.182A>G)	SNV	ATACTGGATACAGCTGGACGAGAAGAGTAC
	WT	ATACTGGATACAGCTGGACAAGAAGAGTAC
	P	AAGGACGAGCAAATGTACCTG CAACTGGATACAGCTGGACG
	C	TACTCTTCTCGTCCAGCTGTATCCAGTTG GTCTACTATCCACGATTTAAC
	P_s	GTGTTAATAACTGGATACAGCTGGAC
	C_s	ACTCTTCTTGTCCAGCTGTATCCAGTTATTAACAC

TABLE S12-10: Sequences of SNV, WT, target-specific X-Probe components, and Sink for NRAS mutations.

Mutation	Species	Sequence
PIK3CA-E542K (c.1624G>A)	SNV	CTCTCTAAAATCACTGAGCAGGAGAAAGAT
	WT	CTCTCTGAAATCACTGAGCAGGAGAAAGAT
	P	AAGGACGAGCAAATGTACCTG CACTCTAAAATCACTGAGCA
	C	TCTTTCTCCTGCTCAGTGATTTTAGAGTG GTCTACTATCCACGATTTAAC
	P_s	AGGCTCTGAAATCACTGAGCA
	C_s	CTTTCTCCTGCTCAGTGATTTCAGAGCCT
PIK3CA-E545K (c.1633G>A)	SNV	AGATCCTCTCTCTGAAATCACTAAGCAGGA
	WT	AGATCCTCTCTCTGAAATCACTGAGCAGGA
	P	AAGGACGAGCAAATGTACCTG CAATCCTCTCTCTGAAATCAC
	C	CCTGCTTAGTGATTTCAGAGAGAGGATTG GTCTACTATCCACGATTTAAC
	P_s	TTAATAATCCTCTCTCTGAAATCAC
	C_s	CTGCTCAGTGATTTCAGAGAGAGGATTATTAA
PIK3CA-H1047L (c.3140A>T)	SNV	TGATGCACTTCATGGTGGCTGGACAACAAA
	WT	TGATGCACATCATGGTGGCTGGACAACAAA
	P	AAGGACGAGCAAATGTACCTG CAATGCACTTCATGGTGGCT
	C	TGTTGTCCAGCCACCATGAAGTGCATTG GTCTACTATCCACGATTTAAC
	P_s	TGTTAATAATGCACATCATGGTGGCT
	C_s	TGTTGTCCAGCCACCATGATGTGCATTATTAACA
PIK3CA-H1047R (c.3140A>G)	SNV	TGATGCACGTCATGGTGGCTGGACAACAAA
	WT	TGATGCACATCATGGTGGCTGGACAACAAA
	P	AAGGACGAGCAAATGTACCTG CAATGCACGTCATGGTGGCT
	C	TGTTGTCCAGCCACCATGACGTGCATTG GTCTACTATCCACGATTTAAC
	P_s	GTGTTAATAATGCACATCATGGTGGCT
	C_s	TGTTGTCCAGCCACCATGATGTGCATTATTAACAC

TABLE S12-11: Sequences of SNV, WT, target-specific X-Probe components, and Sink for PIK3CA mutations.

Mutation	Species	Sequence
STK11-Q37* (c. 109C>T)	SNV	ATCGACTCCACCGAGGTCATCTACTAGCCG
	WT	ATCGACTCCACCGAGGTCATCTACCAGCCG
	P	AAGGACGAGCAAATGTACCTG CACGACTCCACCGAGGTCAT
	C	GCTGGTAGATGACCTCGGTGGAGTCGTG GTCTACTATCCACGATTTAAC
	P_s	CACCACGACTCCACCGAGGTCAT
	C_s	GCTGGTAGATGACCTCGGTGGAGTCGTGGTG
STK11-P281L (c.842C>T)	SNV	ATCCCGGGCGACTGTGGCCCCCTGCTCTCT
	WT	ATCCCGGGCGACTGTGGCCCCCCGCTCTCT
	P	AAGGACGAGCAAATGTACCTG CACCCGGGCGACTGTGGCCCC
	C	AGAGCAGGGGGCCACAGTCGCCCGGGTG GTCTACTATCCACGATTTAAC
	P_s	TGTTAATACCCGGGCGACTGTGGCCCC
	C_s	AGAGCGGGGGGCCACAGTCGCCCGGGTATTAACA
STK11-F354L (c.1062C>G)	SNV	AGGACCTCTTGGACATCGAGGATGACATCA
	WT	AGGACCTCTTCGACATCGAGGATGACATCA
	P	AAGGACGAGCAAATGTACCTG CAGACCTCTTGGACATCGAG
	C	ATGTCATCCTCGATGTCCAAGAGGTCTG GTCTACTATCCACGATTTAAC
	P_s	GTTAATAGACCTCTTCGACATCGAG
	C_s	ATGTCATCCTCGATGTCGAAGAGGTCTATTAAC

TABLE S12-12: Sequences of SNV, WT, target-specific X-Probe components, and Sink for STK11 mutations.

Mutation	Species	Sequence
TP53-R175H (c.524G>A)	SNV	GTTGTGAGGCGCTGCCCCCACCATGAGCGC
	WT	GTTGTGAGGCACTGCCCCCACCATGAGCGC
	P	AAGGACGAGCAAATGTACCTG CATGTGAGGCACTGCCCCCAC
	C	GCTCATGGTGGGGGCAGTGCCTCACATG GTCTACTATCCACGATTTAAC
	P_s	GTCGAGGCGCTGCCCCCACCATG
	C_s	AGCGCTCATGGTGGGGGCAGCGCCTCGAC
TP53-R213*(c.637C>T)	SNV	ACTTTTTGACATAGTGTGGTGGTGCCCTAT
	WT	ACTTTTCGACATAGTGTGGTGGTGCCCTAT
	P	AAGGACGAGCAAATGTACCTG CATTTTTGACATAGTGTGGTG
	C	AGGGCACCACCACACTATGTCAAAAATG GTCTACTATCCACGATTTAAC
	P_s	AAGACAATTTTCGACATAGTGTGGTG
	C_s	AGGGCACCACCACACTATGTCGAAAATTGTCTT
TP53-Y220C (c.659A>G)	SNV	CGACATAGTGTGGTGGTGCCCTGTGAGCCG
	WT	CGACATAGTGTGGTGGTGCCCTATGAGCCG
	P	AAGGACGAGCAAATGTACCTG CAACATAGTGTGGTGGTGCCC
	C	GCTCACAGGGCACCACCACACTATGTTG GTCTACTATCCACGATTTAAC
	P_s	TGTTAATAACATAGTGTGGTGGTGCC
	C_s	GCTCATAGGGCACCACCACACTATGTTATTAACA
TP53-R248Q (c.743G>A)	SNV	TTCCTGCATGGGCGGCATGAACCAGAGGCC
	WT	TTCCTGCATGGGCGGCATGAACCGGAGGCC
	P	AAGGACGAGCAAATGTACCTG CACCTGCATGGGCGGCATGA
	C	CCTCTGGTTCATGCCGCCCATGCAGGTG GTCTACTATCCACGATTTAAC
	P_s	GCCCTGCATGGGCGGCATGAAC
	C_s	CCTCCGGTTCATGCCGCCCATGCAGGGC
TP53-R248W (c.742C>T)	SNV	ATGAACTGGAGGCCCATCCTCACCATCATC
	WT	ATGAACCGGAGGCCCATCCTCACCATCATC
	P	AAGGACGAGCAAATGTACCTG CAGAACTGGAGGCCCATCCT
	C	TGATGGTGAGGATGGGCCTCCAGTTCTG GTCTACTATCCACGATTTAAC
	P_s	TGTTAATAGAACCGGAGGCCCATCCT
	C_s	TGATGGTGAGGATGGGCCTCCGGTTCTATTAACA
TP53-R273C (c.817C>T)	SNV	ACGGAACAGCTTTGAGGTGTGTGTTTGTGC
	WT	ACGGAACAGCTTTGAGGTGCGTGTTTGTGC
	P	AAGGACGAGCAAATGTACCTG CAGGAACAGCTTTGAGGTGT
	C	ACAAACACACACCTCAAAGCTGTTCCTG GTCTACTATCCACGATTTAAC
	P_s	TGTTAATAGGAACAGCTTTGAGGTGC
	C_s	ACAAACACGCACCTCAAAGCTGTTCCTATTAACA
TP53-R273H (c.818G>A)	SNV	AGGTGCATGTTTGTGCCTGTCCTGGGAGAG
	WT	AGGTGCGTGTTTGTGCCTGTCCTGGGAGAG
	P	AAGGACGAGCAAATGTACCTG CAGTGCATGTTTGTGCCTGT
	C	CTCCCAGGACAGGCACAAACATGCACTG GTCTACTATCCACGATTTAAC
	P_s	TCGTACGGAACAGCTTTGAGGTG
	C_s	AAACACGCACCTCAAAGCTGTTCCGTACGA
TP53-R282W (c.844C>T)	SNV	GGGAGAGACTGGCGCACAGAGGAAGAGAAT
	WT	GGGAGAGACCGGCGCACAGAGGAAGAGAAT
	P	AAGGACGAGCAAATGTACCTG CAGAGAGACTGGCGCACAGA
	C	TCTCTTCCTCTGTGCGCCAGTCTCTCTG GTCTACTATCCACGATTTAAC
	P_s	GTTAATAGAGAGACCGGCGCACAGA
	C_s	TCTCTTCCTCTGTGCGCCGGTCTCTCTATTAAC

TABLE S12-13: Sequences of SNV, WT, target-specific X-Probe components, and Sink for TP53 mutations.

[1] Zhang, D.Y. & Winfree, E. Control of DNA Strand Displacement Kinetics Using Toehold Exchange. *J. Am. Chem. Soc.* **131,** 17303-17314 (2009).
[2] Radding, C. M., Beattie, K. L., Holloman W. K. & Wiegand, R. C. Uptake of homologous single-stranded fragments by superhelical DNA. *J. Mol. Biol.* **116,** 859-839 (1977).
[3] Zhang, D. Y., Chen, S. X. & Yin, P. Optimizing the specificity of nucleic acid hybridization, *Nature Chemistry* **4**, 208-214 (2012).
[4] SantaLucia, J. & Hicks, D. The Thermodynamics of DNA Structural Motifs. *Ann. Rev. Biochem.* **33,** 415-440 (2004).
[5] Zuker, M. Mfold web server for nucleic acid folding and hybridization prediction. *Nucleic Acids Res.* **31,** 3406-15, (2003).
[6] Tyagi, S. & Kramer, F.R. Molecular beacons: probes that fluoresce upon hybridization. *Nature Biotechnology* **14,** 303-308 (1996).
[7] Tyagi, S. Imaging intracellular RNA distribution and dynamics in living cells. *Nature Methods* **6,** 331-338 (2009).
[8] Zhang, D.Y. & Winfree, E. Robustness and modularity properties of a non-covalent DNA catalytic reaction. *Nucleic Acids Res.* **38,** 4182-4197 (2010).
[9] Li, Q., Luan G., Guo, Q. & Liang, J. A new class of homogeneous nucleic acid probe based on specific displacement hybridization, *Nucleic Acids Research* **30,** e5 (2002).
[10] Zhang, D. Y. Towards Domain-Based Sequence Design for DNA Strand Displacement Reactions. *Lecture Notes in Computer Science* **6518,** 162-175 (2011).